Best Available
Copy
for all Pictures

AD-768 968

THE PHYSICS OF INTERFACE INTERACTIONS RELATED TO RELIABILITY OF FUTURE ELECTRONIC DEVICES

Thomas H. DiStefano, et al

IBM Thomas J. Watson Research Center

Prepared for:

Air Force Cambridge Research Laboratories
Defense Advanced Research Projects Agency

31 January 1973

DISTRIBUTED BY:

NTIS
National Technical Information Service
U. S. DEPARTMENT OF COMMERCE
5285 Port Royal Road, Springfield Va. 22151

ARPA Order No. 2180

Program Code No. 2D1

Contractor: IBM Corporation

Effective Date of Contract: 1 August 1972

Contract No. F19628-73-C-0006

Co-Principal Investigator and Phone No.
Dr. Thomas H. DiStefano/914 945-2215
Dr. King-Ning Tu

AFCRL Project Scientist and Phone No.
Dr. John C. Garth/617 861-4051

Contract Expiration Date: 31 January 1974

BY

DISTRIBUTION/AVAILABILITY CODES

A

Qualified requestors may obtain additional copies from the Defense Documentation Center. All others should apply to the National Technical Information Service.

UNCLASSIFIED
Security Classification

AD 768968

DOCUMENT CONTROL DATA - R & D

(Security classification of title, body of abstract and indexing annotation must be entered when the overall report is classified)

1. ORIGINATING ACTIVITY (Corporate author) IBM Thomas J. Watson Research Center International Business Machines Corporation P.O. Box 218, Yorktown Heights, New York 10598	2a. REPORT SECURITY CLASSIFICATION UNCLASSIFIED 2b.

3. REPORT TITLE

THE PHYSICS OF INTERFACE INTERACTIONS RELATED TO RELIABILITY OF FUTURE ELECTRONIC DEVICES

4. DESCRIPTIVE NOTES (Type of report and inclusive dates)

Scientific. Interim.

5. AUTHOR(S) (First name, middle initial, last name)

Thomas H. DiStefano
King-Ning Tu

6. REPORT DATE	7a. TOTAL NO. OF PAGES	7b. NO. OF REFS
31 January 1973	~~128~~ 136	94

8a. CONTRACT OR GRANT NO. ARPA Order No. 2180 F19628-73-C-0006	9a. ORIGINATOR'S REPORT NUMBER(S)
b. PROJECT ~~xx~~ Task, Work Unit Nos. q180 n/a n/a	Semi-Annual Technical Report No. 1
c. DoD Element 61101D	9b. OTHER REPORT NO(S) (Any other numbers that may be assigned this report)
d. Dod Sub-element 678100	AFCRL-TR-73-0483

10. DISTRIBUTION STATEMENT

A - Approved for public release; distribution unlimited.

11. SUPPLEMENTARY NOTES This research was supported by the Defense Advanced Research Projects Agency.	12. SPONSORING MILITARY ACTIVITY Air Force Cambridge Research Laboratories (LQ) L. G. Hanscom Field Bedford, Massachusetts 01730

13. ABSTRACT

Photoemission and thermionic emission results show that the Si-SiO_2 energy barrier can be reduced from 4.2 eV to about 2.5 eV by a monolayer coverage of sodium. Scanning Internal Photoemission maps were made of the SiO_2 interface which was "stained" by a small amount of sodium. We obtained images of the contact barrier which show microscopic imperfections such as phosphorus precipitates on the interface as well as microscratches. The resulting high local sodium concentration can cause enhanced electron injection and dielectric breakdown of the SiO_2 at relatively low electric fields.

In the area of transition metal oxides, we have made progress in understanding the mechanism of switching found in thin films of Nb_2O_5. In a Scanning Internal Photoemission study, we found no correlation between the contact barrier and formation of a switching filament. The formation of a conductive filament in Nb_2O_5, observed directly in an electron microscope, is initiated at an irregularity on the contract. Briefly stated, a conduction and switching in these materials is determined by the gross physical structure, and not by an electronic process.

In another area, involving structural instabilities of thin glass films, we find that a small phosphorus impurity is able to recrystallize SiO_2 at the relatively low temperature of 525°C. Phosphorus is commonly used to dope the SiO_2 used in MOS transistors. Also, we have found a destructive interface reaction between SiO_2 and vanadium. This is significant because of an active metal such as vanadium is often used to increase the adhesion of a second metal to the surface of SiO_2.

DD FORM 1 NOV 65 1473

Reproduced by
NATIONAL TECHNICAL INFORMATION SERVICE
U S Department of Commerce
Springfield VA 22151

UNCLASSIFIED
Security Classification

14. KEY WORDS	LINK A		LINK B		LINK C	
	ROLE	WT	ROLE	WT	ROLE	WT
Glass-metal reaction						
Denitrification of SiO_2						
Crystallization of SiO_2						
Vanadium silicide						
Diffusion of P in glass						
Interfaces, $Si-SiO_2$						
Internal photoemission						
Dielectric breakdown						
SiO_2						

ic

AFCRL-TR-73-0483

THE PHYSICS OF INTERFACE INTERACTIONS RELATED TO RELIABILITY OF FUTURE ELECTRONIC DEVICES

by

Thomas H. DiStefano and King-Ning Tu

IBM Thomas J. Watson Research Center
International Business Machines Corporation
P. O. Box 218
Yorktown Heights, New York 10598

Contract No. F19628-73-C-0006
Project No. 2180

Semi-Annual Technical Report No. 1

31 January 1973

Contract Monitor: John C. Garth
Solid State Sciences Laboratory

Approved for public release; distribution unlimited.

Sponsored by
Defense Advanced Research Projects Agency
ARPA Order No. 2180
Monitored by
AIR FORCE CAMBRIDGE RESEARCH LABORATORIES
AIR FORCE SYSTEMS COMMAND
UNITED STATES AIR FORCE
BEDFORD, MASSACHUSETTS 01730

THE PHYSICS OF INTERFACE INTERACTIONS RELATED TO RELIABILITY OF FUTURE ELECTRONIC DEVICES

Photoemission and thermionic emission results show that the Si-SiO_2 energy barrier can be reduced from 4.2 eV to about 2.5 eV by a monolayer coverage of sodium. Scanning Internal Photoemission maps were made of the SiO_2 interface which was "stained" by a small amount of sodium. We obtained images of the contact barrier which show microscopic imperfections such as phosphorus precipitates on the interface as well as microscratches. The resulting high local sodium concentration can cause enhanced electron injection and dielectric breakdown of the SiO_2 at relatively low electric fields.

In the area of transition metal oxides, we have made progress in understanding the mechanism of switching found in thin films of Nb_2O_5. In a Scanning Internal Photoemission study, we found no correlation between the contact barrier and formation of a switching filament. The formation of a conductive filament in Nb_2O_5, observed directly in an electron microscope, is initiated at an irregularity on the contract. Briefly stated, conduction and switching in these materials is determined by the gross physical structure, and not by an electronic process.

In another area, involving structural instabilities of thin glass films, we find that a small phosphorus impurity is able to recrystallize SiO_2 at the relatively low temperature of 525°C. Phosphorus is commonly used to dope the SiO_2 used in MOS transistors. Also, we have found a destructive interface reaction between SiO_2 and vanadium. This is significant because of an active metal such as vanadium is often used to increase the adhesion of a second metal to the surface of SiO_2.

TABLE OF CONTENTS

INTRODUCTION 1

I. The Reliability of Semiconductor-Insulator Interfaces 3

A. Interface Imaging by Scanning Internal Photoemission 5

B. The Influence of Sodium on the Si-SiO_2 Interface 27

II. Band Structure and Switching in Transition Metal Oxides 50

A. Direct Observation of Field-Induced Crystallization in Niobium Oxide Films 53

B. Photoemission Study of Filament Formation in Nb_2O_5 61

C. Quasi-Elastic Electron Scattering in EuO; A Possible Explanation for Observed "Paramagnetic" Spin Polarized Photoemission 67

III. Instabilities Associated with Metal-Glass Interactions 77

A. Catalyzed Crystallization and Transformation in SiO_2 Thin Films 80

B. Phosphorus Diffusion in Partially Crystallized Films of SiO_2 95

C. Interaction of V with Bare and Oxidized Si Wafers 118

Preceding page blank

THE PHYSICS OF INTERFACE INTERACTIONS RELATED TO RELIABILITY OF FUTURE ELECTRONIC DEVICES

Reproduced from best available copy.

INTRODUCTION

The electronic structure of simple interfaces has been characterized to some extent in the past, but important factors which modify the interface and possibly degrade the structure have been almost entirely neglected. A new effort was begun at IBM Research to investigate carrier injection at a semiconductor-insulator interface as well as the physical structure of the interface, particularly for the system Si-SiO_2. The emphasis of this study is upon the reliability implications of changes and imperfections which occur at the dielectric interfaces of an MOS transistor device. It has become apparent that several types of modern devices (such as MOS transistors, charge coupled structures, charge storage transistors, etc.) are sensitive to conditions at the semiconductor surface. It is the object of this study to identify and characterize the critical phenomena which determine interface reliability at both metal-insulator and semiconductor-insulator interfaces. Several recent findings are mentioned below.

- Dielectric breakdown is the principal reliability problem in the integrated circuit industry. We have found that microscratches and microsplits on the Si-SiO_2 interface cause any residual sodium to accumulate in them to produce a "weak spot" in the insulation. Since these very fine microscratches are formed during polishing of the silicon wafer, they can be eliminated by better polishing techniques.

- We have found widespread phosphorus precipitation on Si-SiO_2 interfaces formed on n^+ silicon, such as that usually found in MOS devices, by using Scanning Internal Photoemission. The reliability implications of this precipitate involve de-vitrification of the SiO_2 and dielectric breakdown. We are studying methods of eliminating this precipitation.

● Sodium was found to reduce the barrier for electron injection from silicon into SiO_2. This low barrier produces charge leakage into the insulator, a serious degradation mechanism in the newer "floating gate" (FAMOS) transistors. Photoemission and thermionic emission results show that the energy barrier can be reduced from 4.2 eV to about 2.5 eV by a monolayer coverage of sodium at the interface. Even at a coverage of about 1/100 monolayer, the barrier can be reduced appreciably.

● Switching in transition metal oxide capacitors held some promise for use in logic circuitry because of the speed and small size of the device. However, the progress we have made in understanding the switching mechanism shows that the switching is structural and not electronic, and thus unsuitable for use as a reliable device. The basic switching mechanism, studied by the Scanning Internal Photoemission technique and electron microscopy, involves the formation and destruction of a conductive metallic bridge in the grain boundaries of a small crystallized region. The formation of a conductive filament in Nb_2O_5 was observed directly in an electron microscope. The formation of the microcrystalline conductive filament is initiated by breakdown at an irregularity on the contact. These observations, along with the photoemission results, indicate that the formation of the conductive filament is not controlled by the electronic barrier.

● In another area, involving structural instabilities of thin glass films, we find that a small phosphorus impurity is able to recrystallize SiO_2 at the relatively low temperature of 525°C. This is important because the phosphorus commonly used to dope both the silicon and the SiO_2 in the MOS transistors can cause crystallization and destruction of the SiO_2 insulation in typical devices.

● Also, we have found a destructive interface reaction between SiO_2 and vanadium. This is significant because a layer of an active metal such as vanadium or chromium is often used to increase the adhesion of a second metal to the surface of SiO_2. However this reaction can be put to use in reliably making Schottky barriers; this reaction can be used to remove any SiO_2 remaining between silicon and a metal during the formation of the Schottky constant.

I. THE RELIABILITY OF SEMICONDUCTOR-INSULATOR INTERFACES

Recently, we have shown that the contact interface on a dielectric can determine the conditions for electrical breakdown of thin films. The breakdown voltage of a thin capacitor is reduced at points where the contact barrier is low, presumably because the lowered barrier leads to a greatly increased electron injection current at those points. We have used several photoemission techniques to study the technologically important $Si-SiO_2$ interface as well at the influence of a common impurity, sodium, upon that interface.

A technique of scanning internal photoemission was developed to the point where it can produce an image of a contact barrier with a resolution of one micron. This technique was used to image $Si-SiO_2$ interface barriers which were covered with a layer of sodium ions; the sodium greatly increases the photoyield from the interface. In effect, the photoemission image maps the local sodium concentration on the interface. By using sodium to "stain" the interface, we were able to observe microscopic defects at the interface which are inaccessable to other types of measurement. In the photoemission maps, we have seen microscratches, microsplits, and precipitates at the $Si-SiO_2$ interface.

By scanning photoemission, we have found that microscratches and microsplits induce a local accumulation of sodium which far exceeds the background density. In an MOS type of device, these interface defects can cause a local concentration of sodium to build up over a period of time. An important implication of this sodium accumulation is that a nominally low level of alkali contamination ($\sim 10^{11}/cm^2$) can give rise to a destructively

high local concentration of alkali ions ($\sim 10^{13}/cm^2$). It follows that the effects of sodium and perhaps the other alkalis, cannot be ignored in an MOS type of device even at relatively low concentration levels. As a result, the dielectric strength of the SiO_2 is reduced with time. Clearly, such defects should be minimized by careful processing.

A photoemission and thermionic emission study of sodium coated $Si-SiO_2$ interfaces confirms the fact that a sub-monolayer coverage of the interface will produce a large barrier reduction at the contact. Both emission techniques determine contact barrier which are consistent with one another. The lowest barrier measured was for 1.3×10^{15} Na/cm^2, where the photoemission threshold is 2.5 eV and the thermionic emission barrier is 2.7 eV.

A. INTERFACE IMAGING BY SCANNING INTERNAL PHOTOEMISSION

by

T. H. DiStefano
J. M. Viggiano

IBM Thomas J. Watson Research Center
Yorktown Heights, New York 10598

Scanning Internal Photoemission Technique

Many techniques are available for microscopically imaging material surfaces but surprisingly little has been done in imaging the interface between two materials. Scanning Internal Photoemission (SIP) is a recently developed technique[1-3] for probing interfaces with a light beam to produce a direct microscopic image of an interfacial contact barrier. Maps produced by the SIP measurement display the lateral inhomogenities along a two dimensional dielectric interface. This allows an image or photograph to be made of the microscopic electronic structure of the interface, something which has previously been inaccessible to measurement. The technique is somewhat analogous to scanning electron microscopy, except that in this case a light beam is used to excite electron emission into a dielectric. Since the photoemission current increases rapidly as the electronic barrier at the interface is reduced, particularly for photon energies near threshold, local variations in the barrier are detected sensitively in the measured photocurrent. As in the scanning electron microscope, the emitted

current is displayed on a CRT screen as a function of the beam position to produce an image of the interface. The SIP images presented here exhibit striking local inhomogenities which are related to structural variations, impurities, and defects on the interface.

The spacial resolution of SIP, limited by the wavelength of the light beam, is on the order of a micron. This is sufficient to resolve many of the structural variations and defects which occur at a typical interface. The resolution of SIP could be further improved by a de-convolution technique,[4] but our preliminary measurements indicate that little would be gained by a several fold increase in resolution. In order to obtain a reasonable signal to noise ratio in the photocurrent from a resolution limited light spot, it was necessary to use laser radiation,[3] which can be focused onto a diffraction limited scanning light spot. A power level of about $10^8 W/cm^2$ will produce a measurable photocurrent from the resolution limited spot without thermally damaging the sample. This power level is sufficient to produce an image of a specimen $250\mu \times 250\mu$ in less than ten minutes.

We have used SIP to study several dielectric interfaces including $Si-SiO_2$ and $Bi-Nb_2O_5$. Although the $Si-SiO_2$ interface is quite uniform in the absence of impurities, a small amount of sodium ion coverage on the interface was found to reduce the contact barrier in localized areas.[1] The dielectric strength of SiO_2 films was found to be reduced in those areas where the contact barrier is lowered by sodium,[2] a common impurity in this system. A uniform layer of sodium added to a clean interface was found to decorate or accumulate at certain types of

interface defects, which can then be viewed directly by SIP measurements. In effect, sodium will "stain" certain defects such as microscratches, growth steps, and microcracks on the interface so that they are detected directly in an SIP image. Interface microstructure, which is inaccessible to other techniques, can be observed directly by SIP in conjunction with this sodium staining technique.

In the case of the Bi-Nb_2O_5 system, nonuniformities have been found in pure, uncountaminated specimens. Here, the variations in the contact barrier are the result of a physical reaction which takes place at the interface. Surprisingly, SIP has shown that many metal-insulator systems display a very inhomogeneous contact barrier quite unlike the simple, uniform barrier which was assumed in earlier work. It has become apparent that any study of metal-insulator interfaces should also involve an investigation of the barrier on a local scale since large area measurements only yield averaged results on an inhomogeneous system. The SIP technique seems well suited for investigations of dielectric interfaces on a scale of 1 micron or larger.

Measurement Methods

The success of the Scanning Internal Photoemission technique depends upon the sensitivity of photocurrent near threshold to small variations in the interface contact barrier. Photocurrent produced by a scanning spot of light will change considerably as the beam moves over a surface with a slightly nonuniform barrier. For a metal-insulator system near threshold Φ, the photoyield is[5]

$$Y = \eta(\hbar\omega - \Phi)^2.$$

The fractional change in photoyield (Y) or photocurrent (i) is

$$\frac{\Delta Y}{Y} = \frac{\Delta i}{i} = \frac{2\Delta\Phi}{(\hbar\omega - \Phi)}$$

which becomes quite sensitive to $\Delta\Phi$ as the photon energy $\hbar\omega \rightarrow \Phi$. As one might expect, the highest contrast is obtained with light which is slightly above the threshold Φ.

A simple system utilizing mechanically rotated mirrors was used to scan the light spot over a 250μ square area of the sample. The optical system is outlined schematically in Fig. 1. Radiation at 3250 Å from an RCA He-Cd laser was focused through a 50μ pinhole to elliminate the widely divergent light from the laser. Light from the pinhole is reflected from two front surface mirrors which are rotated through the angles ϕ and Θ respectively. The aperture of the microscope objective (f = 0.54 cm) is filled by this reflected light so that the focused spot scans the sample as ϕ and Θ are varied. A spot velocity of 3000μ/sec was obtained with Θ swept at 15Hz and ϕ at 0.008 Hz. The total spot size of about 0.43μ is determined theoretically by two nearly equal factors, laser beam divergence and lens diffraction. Of course, the optical resolution deteriorates at points away from the center of the field because of the curvature of the lens focal plane. However, this degradation of resolution away from the center of the image is barely discernable over a total field of 250μ x 250μ.

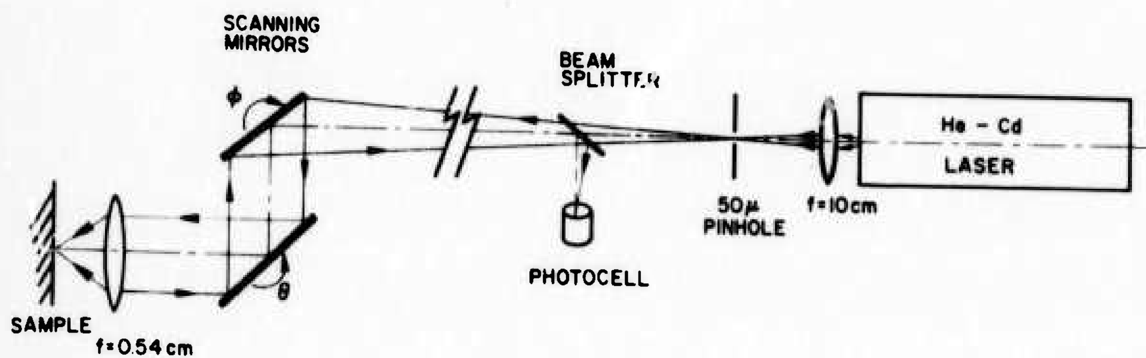

Figure 1: Optical system for the Scanning Internal Photoemission Measurements. The system is brought to focus by adjusting the sample position to minimize the size of the light spot reflected onto the luminescent screen on the back of the 50μ pinhole.

The problem of positioning and focusing the sample in the UV beam was solved by detecting the light which is reflected back from the sample. In order to understand this focusing technique, consider first the general linear system in Fig. 2a. Here, a point source on the object plane is focused onto a point in the image plane. Then, by time reversal symmetry, any light radiated from the point at this image will be focused back onto the point at the original object. By placing a reflecting surface at the image, we have the configuration shown in Fig. 2b. Here, light from a point source at the object is focused into a point on the reflector which then re-radiates the light back through the optical system. As before, light from a point on the reflector will be focused by the system onto the original object point. Light from the object point is returned back to this same point only if the reflecting surface is in focus. We use this principle to focus the system outlined in Fig. 1. Light from the pinhole is focused onto the sample which then reflects part of the light back through the system. When the sample is in focus, the reflected light returns to the pinhole, independent of the mirror positions θ and ϕ. However, if the sample is out of focus, the reflected light strikes a fluorescent screen around the pinhole where it is seen as a disc of visible light. The system is brought into focus simply by adjusting the sample position until all of the reflected light is refocused back onto the pinhole.

In order to position the light spot on the sample, an image of the sample is obtained from the reflected light. Part of the light reflected from the sample is directed onto a photocell by a beam splitter, as

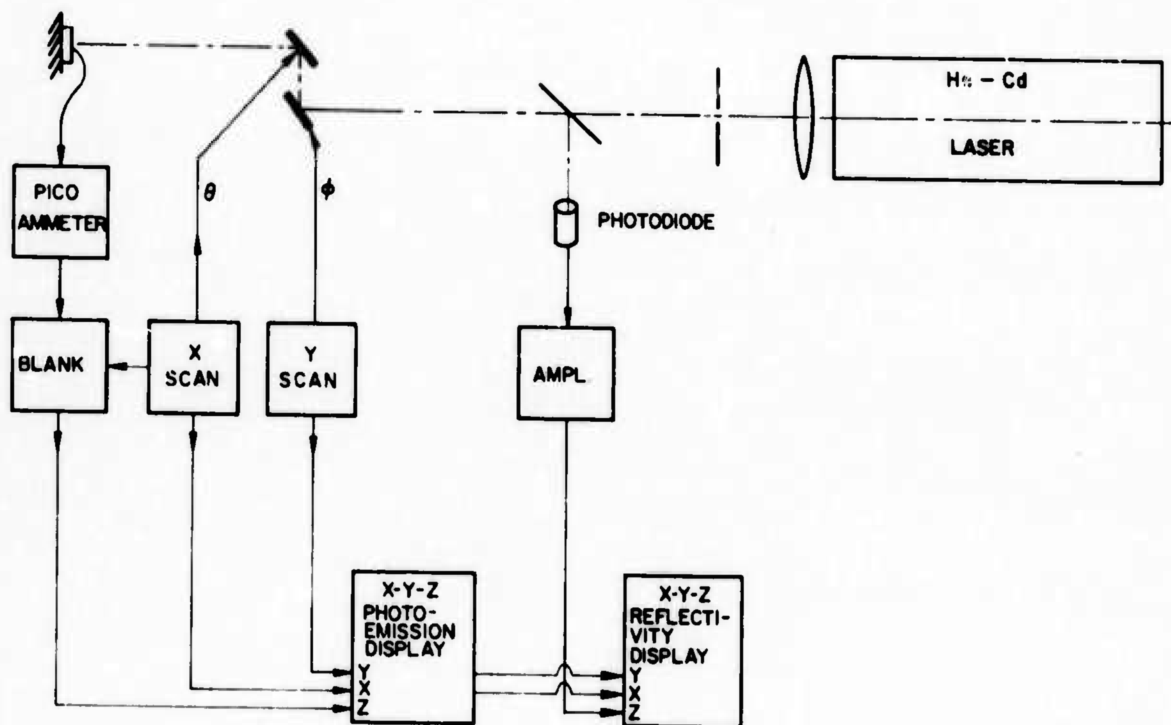

Figure 3: Measurement apparatus for the SIP system. Photocurrent produced by a scanning light spot is detected and displayed as a function of X and Y on a display CRT.

shown in Fig. 1. The light falling on the photocell comes to focus at a point which is equivalent to the position of the pinhole source and which is independent of mirror angles θ and ϕ. Current from the photocell, when displayed on an intensity modulated CRT as a function of X and Y, forms an image of the sample corresponding to optical reflectivity at the wavelength of the source laser. This reflectivity image is essential for locating the sample in the beam and for examining the surface conditions of the sample during measurement.

Both the photocurrent and the reflected light from a sample are detected and displayed on CRT screens by circuitry shown in Fig. 3. The two scanning mirrors are mounted on galvanometer movements which are driven by the nonsynchronous sawtooth generators "X Scan" and "Y Scan". These generators also drive the X and Y axes on the CRT displays. An image of the internal photoemission is formed on a CRT with Z axis modulation by the detected photocurrent from a Keithley 18000 picoammeter. The retrace scan is blanked by pulses from the X scan generator. Images of the Z axis modulated CRT display of photocurrent are produced photographically. In a similar way, sample reflectivity is displayed on a CRT with Z axis modulation by the current from a photodetector which senses the reflected light. An advantage of this technique is that both the photoemission image and the reflectivity image appear on the same coordinate system, so that direct comparisons can easily be made between the two.

Photoemission and Reflectivity Images

Photoemission and reflectivity images were obtained of $Si-SiO_2$

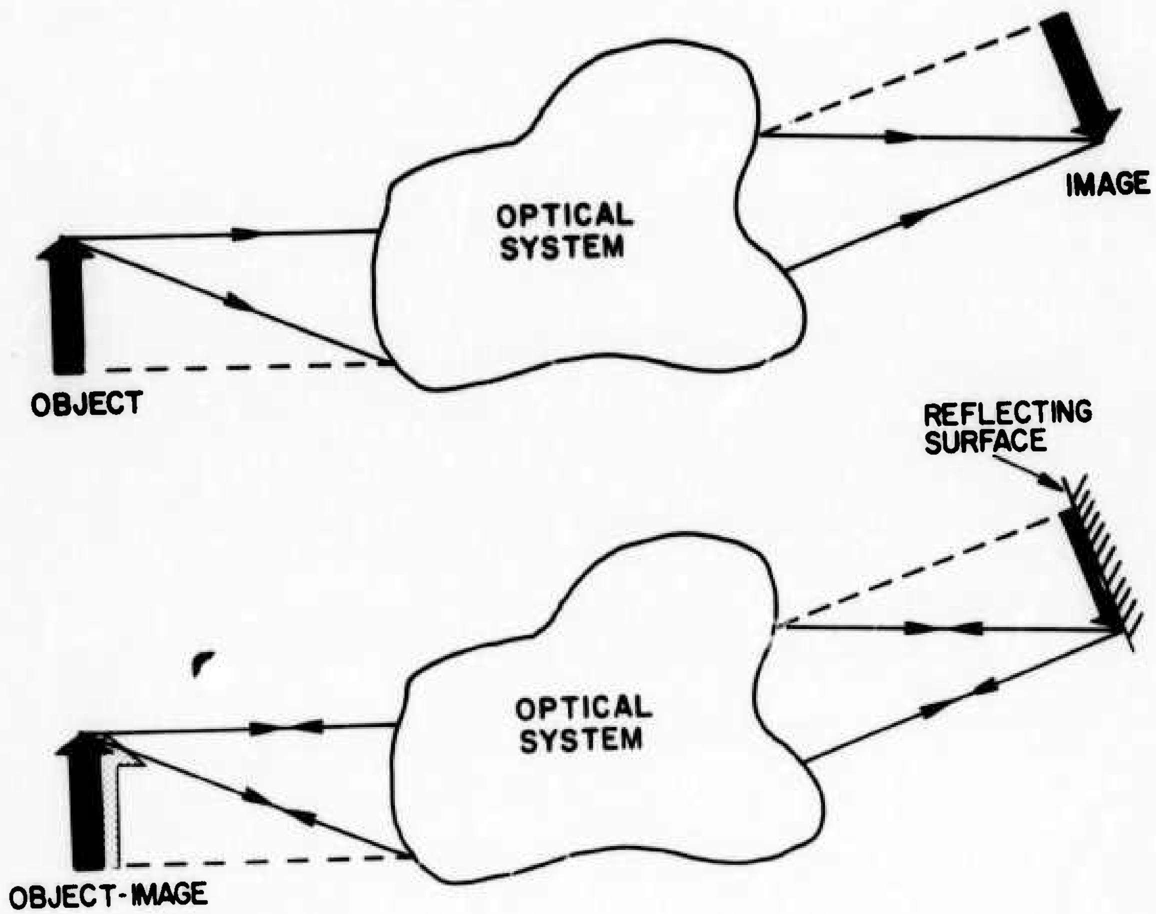

Figure 2: Schematic representation of the linear optical system outlining the time reversal principal. a. A point object is brought to focus at the image position. b. A reflecting surface at the image will return the light through the system and back to the object point.

interfaces at λ = 3250 Å and of Bi-Nb_2O_5 interfaces at λ = 6328 Å. In each case, the Scanning Internal Photoemission images show spacial inhomogeneities which can be related to physical structure. Several representative SIP images are presented, along with one typical reflectivity image, each of which covers a field of about 250μ x 250μ on the respective sample.

SIP maps were obtained from a Si-SiO_2 interface on which sodium has been deposited to an average density of $4 \times 10^{12}/cm^2$. The sodium was initially distributed uniformly over the interface, as measured by radiographic techniques with a spacial resolution of about 50μ.[6] After a period of time, about 100 hours at 150°C, the sodium is found to be redistributed over the interface in an inhomogeneous way. It is known that the sodium at the interface will produce a monotonic increase in photoyield with increasing sodium concentration.[7] Therefore, an SIP map of the interface mirrors the inhomogeneous distribution of sodium on the Si-SiO_2 interface. For the SIP maps in Figs. 4-6, the photocurrent is shown as intensity vs X and Y. The bright areas correspond to regions of high sodium concentration on the interface, because of the direct relationship between high photoyield and high sodium concentration.

The SIP maps in Figs. 4-6 were measured on a Si-SiO_2 interface with an average sodium concentration of $4 \times 10^{12}/cm^2$, and with a silicon substrate doped to $10^{20}/cm^3$ of phosphorus atoms. Each of the SIP maps displays several features in common including microscratches, sodium rich spots about 1μ in diameter, and dark regions about 10μ in

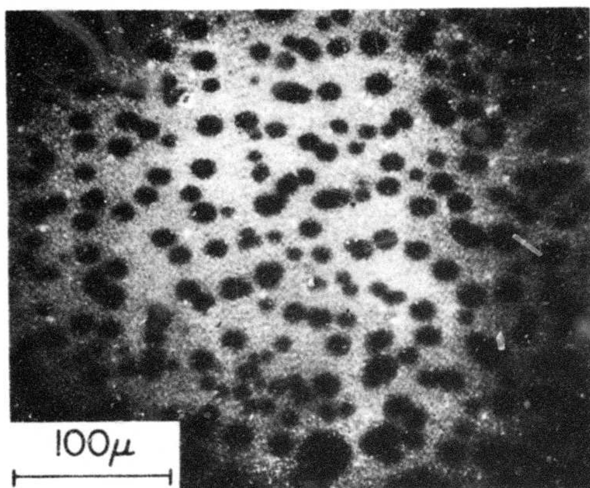

Figure 4: Scanning Internal Photoemission map of an Si-SiO_2 interface covered with $4 \times 10^{12}/cm^2$ sodium. The light areas indicate a high photoyield produced by the presence of sodium on the interface.

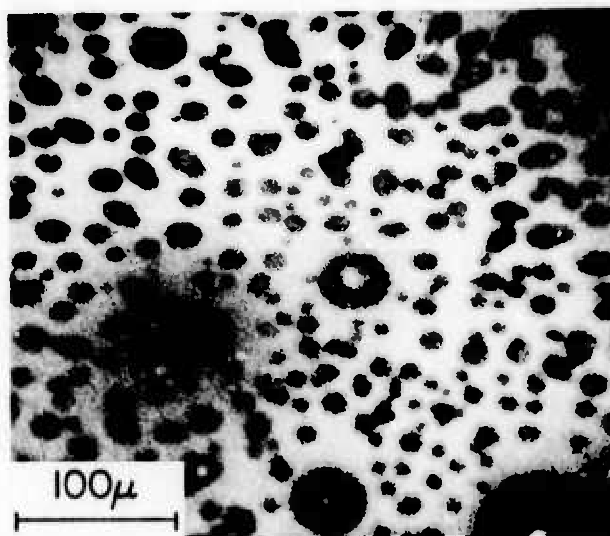

Figure 5: Scanning Interface Photoemission map of an Si-SiO_2 interface covered with $4 \times 10^{12}/cm^2$ sodium. The light areas indicate a high photoyield produced by the presence of sodium on the interface.

Figure 6: Scanning Internal Photoemission map of an Si-SiO_2 interface covered with $4 \times 10^{12}/cm^2$ sodium. The light areas indicate a high photoyield produced by the presence of sodium on the interface.

diameter. The microscratches, which are "stained" by an excess of sodium, are nearly straight lines several hundred microns long. These lines appear to be resolution limited, with a width of 1μ or less. There appears to be no relationship between the line direction and the crystallographic axes of the silicon, which has a (100) surface oriented so that the [110] is horizontal. It is interesting that interface microscratches on such a fine scale can lead to local sodium accumulation along the scratch and a degradation of the dielectric. Another feature seen in the SIP maps is the presence of small light spots that are approximately the dimension of the resolution limit. The explanation for these sodium spots is an open question at present. One might postulate that the spots are sodium which has naturally segregated into clusters due to a mechanism proposed by Williams and Wood.[8] However, the large and irregular spacing between the spots and the presence of uniform areas without spots suggests that the spots are associated with a defect or impurity in the sample itself. The SIP technique promises to be fruitful in finding the explanation of this clustering. A third and somewhat puzzling feature, the dark circles about 10μ in diameter appearing in SIP maps 4-6, was also found in other Si-SiO_2 interfaces which were formed on heavily phosphorus doped silicon. These are two possible explanations for these dark circular regions which form a "Swiss cheese" pattern. Either sodium does not cover the interface in these areas or the sodium which does reach the interface is rendered ineffective, perhaps by chemical combination with an impurity such as phosphorus on the interface. The questions raised about the features

in the SIP maps are timely in that the answers will provide information about the physical structure of the extremely important Si-SiO_2 interface.

High contrast measurements are very effective in bringing out details in SIP maps. As an example, the map in Fig. 7, of an Si-SiO_2 interface coated $4 \times 10^{12}/cm^2$ sodium, includes a dark spot with a surrounding halo. The same area is shown on the high contrast map in which the photocurrent signal is amplified and biased to remove the background so that only the halo stands out above the uniform background In a similar way, the background photoemission is removed from the map in Fig. 9, leaving excess photoemission from a broad line, about 15μ in length along the [110] direction with respect to the silicon substrate. This line is tentatively identified as a microsplit of the silicon surface.[9] Although the microsplits are far too narrow to be resolved optically, they show up clearly as excess photocurrent in the SIP maps.

The SIP technique was also used to study the Nb_2O_5-Bi interface, which is of interest because of the fast switching found in Nb_2O_5 capacitors. In this case, photocurrent was emitted from a 200 Å thick bismuth electrode into the Nb_2O_5.[10] A He-Ne laser at 6328 Å was used to excite photocurrent from the bismuth. A representative SIP map, shown in Fig. 10, displays about 250μ x 250μ of the interface. Spotty dark regions in the map apparently result from a contact barrier which is higher than average. The vertical striations are produced by slow variations of the leakage current through the sample. For comparison, a high contrast reflectivity map of the same area of the sample is shown in Fig. 11. The dark areas in the reflectivity

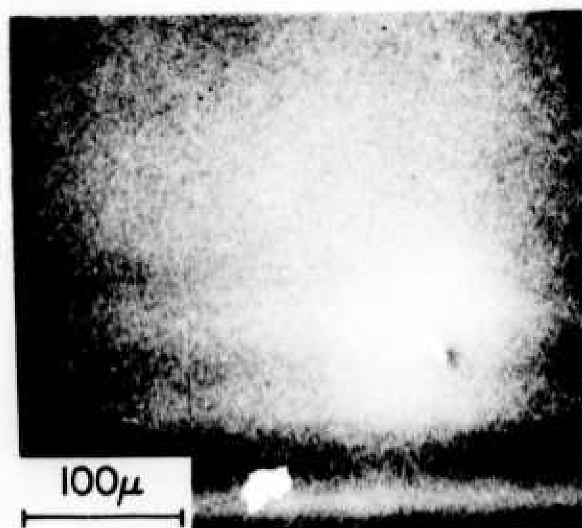

Figure 7: Scanning Internal Photoemission map of an $Si-SiO_2$ interface covered with $4 \times 10^{12}/cm^2$ sodium.

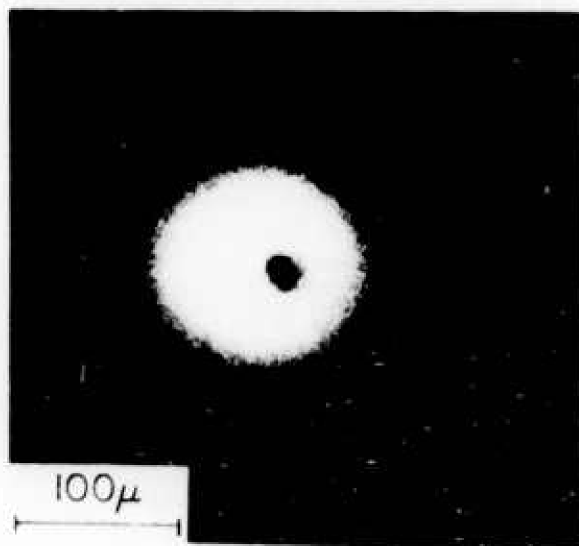

Figure 8: High contrast Scanning Internal Photoemission map of the same area that is shown in Fig. 7.

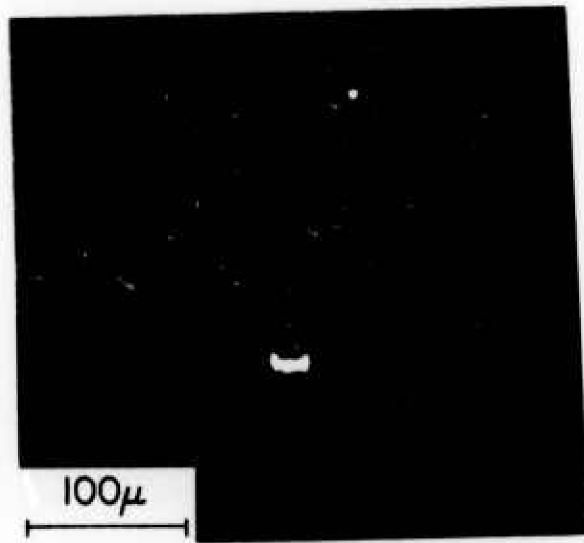

Figure 9: High contrast Scanning Internal Photoemission map of an Si-SiO_2 interface covered with $4 \times 10^{12}/cm^2$ sodium. The X and Y axes correspond to [110] and [$\bar{1}$10] on the silicon surface.

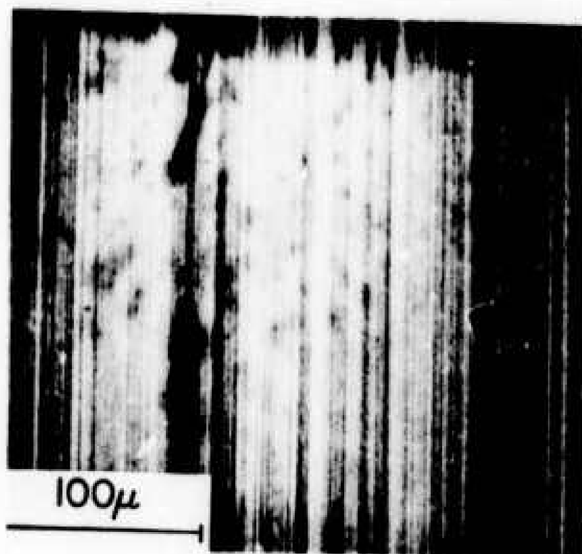

Figure 10: Scanning Internal Photoemission map of an Nb_2O_5-Bi interface, measured with light at 6328 Å.

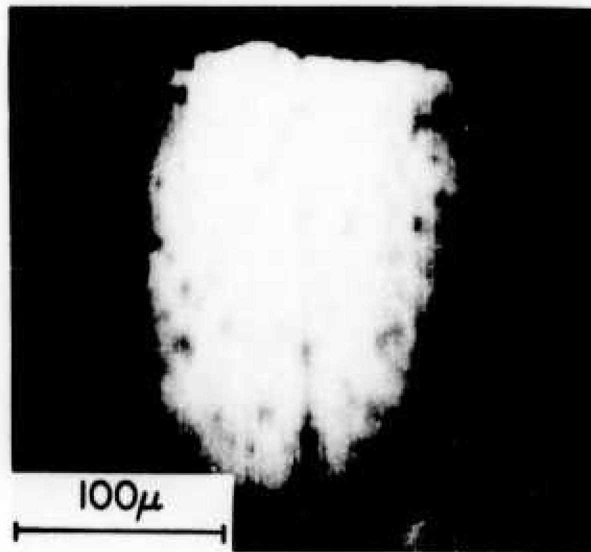

Figure 11: High resolution reflectivity map of the sample shown in the SIP map of Fig. 10.

coincide with the areas of high contact barrier. This sort of reflectivity variation is typical of a metal-dielectric system in which an interface reaction has taken place. The patchy barrier, which is characteristic of the Nb_2O_5-Bi system, is the subject of a more general study.[11]

The value of the SIP technique is apparent from our investigations of the simple systems reported here. It is anticipated that SIP will be useful in studies of interface reactions, of impurity segregation and diffusion on interfaces, and of structural defects on semiconductor interfaces with other materials. In particular, defect studies on an Si-SiO_2 interface stained with mobile alkali ions will continue to be fruitful.

The authors wish to acknowledge discussions with E. Bassous, R. B. Laibowitz, and J. E. Lewis, all of IBM Research, Yorktown Heights.

References

1. T. H. DiStefano, Appl. Phys. Lett. 19, 280 (1971).
2. T. H. DiStefano, J. Appl. Phys. 44, 527 (1973).
3. R. Williams and M. H. Woods, J. Appl. Phys. 43, 4142 (1972).
4. H. C. Andrews, Computer Techniques in Image Processing, (Academic New York, 1970).
5. R. Williams, "Injection by Internal Photoemission," in Semiconductors and Semimetals, Vol. 6, edited by R. K. Willardson (Academic, New York, 1970).
6. T. H. DiStefano and J. E. Lewis, presented at the Thirty-Second Annual Conference on Physical Electronics, Albuquerque, N.M., 1972 (unpublished).
7. T. H. DiStefano and J. E. Lewis, to be published.
8. R. Williams and M. H. Woods, Appl. Phys. Lett. 22, 458 (1973).
9. G. H. Schwuttke, Technical Report No. 1, ARPA Contract No. DAHC 15-72-C-0274 (1973).
10. For the case of the Nb_2O_5-Bi interface, some component of the measured photocurrent may be due to excitation from traps near the interface rather than from the bismuth electrode itself.
11. T. H. DiStefano and R. B. Laibowitz, Bull. Am. Phys. Soc. 18, 133 (1973).

B. THE INFLUENCE OF SODIUM ON THE Si-SiO_2 INTERFACE

T. H. DiStefano
and
J. E. Lewis

IBM Thomas J. Watson Research Center
Yorktown Heights, New York 10598

I. INTRODUCTION

The interface between silicon and SiO_2 is the most intensively studied and perhaps the best understood of all insulator interfaces. The energy barrier which forms between the two materials is surprisingly independent of the various preparation conditions and measurement techniques used by many investigators. As determined by internal photoemission measurements,[1] the barrier is between[1-5] 4.15 eV and 4.35 eV, with no electric field in the insulator. This barrier can be somewhat reduced[2] due to the Schottky effect by a field in the insulator. However, in Si-SiO_2 systems containing small amounts of sodium, several investigators have observed a rather puzzling photocurrent at photon energies well below the threshold energy for pure interfaces.

In each case, the mobile sodium was moved to the interface by an electric field in a configuration analogous to electrolytic deposition. Although the role of the sodium is not fully understood, several models have been proposed to explain the excess photocurrent: photoemission of electrons from the silicon conduction band,[6,7] a polarization of the SiO_2,[7] or a reduction of the interface barrier by a sodium induced dipole layer.[7-9] The work presented here provides clear evidence for an actual reduction of the Si-SiO_2 energy barrier produced by sodium.

A photoemission study of sodium coated $Si-SiO_2$ system is complicated by several factors. Firstly, in order that the measurements be meaningful, the sodium must be distributed uniformly along the interface. Recent Scanning Internal Photoemission measurements[8,9] indicate that uniformity is not a trivial problem, but the inhomogeneities can be minimized by careful sample preparation. A second problem is that of the rapidly falling optical absorption below a photon energy of about 3.2 eV.[10] The rapid change of absorption in the region of interest obscures the threshold of the photocurrent, and makes interpretation difficult. However, a simple model of the photoemission process permits accounting for the optical absorpton and a determination of threshold energies. The photoemission determined barrier was found to decrease with increasing sodium concentration down to a saturation level of 2.6 ± 0.1 eV at 1.3×10^{15} Na/cm^2.

Thermionic emission measurements confirm the observed reduction of the contact barrier of $Si-SiO_2$ by sodium. The contact barrier, determined by fitting the thermionic emission results to the Richardson equation, is in good agreement with the photoemission results. Recent photovoltage measurements by Williams and Woods[9] are in qualitative agreement with the barrier reduction model. But, because of the lateral non-uniformity of the sodium in the photovoltage measurements, it is difficult to compare quantitatively these results with our photoemission and thermionic emission results.

II. THE PHYSICAL SYSTEM

The system considered here is an $Si-SiO_2$ interface which has been

electrolytically coated with sodium. The interface was formed by first oxidizing the (100) surface of n-doped silicon to an oxide thickness of 1000 Å. The initial doping level of the silicon was $\sim 10^{20}$ P/cm^3. Sodium was then distributed uniformly on the sample by vacuum evaporation of radiotagged NaCl onto the SiO_2 surface. Finally, semitransparent aluminum electrodes were evaporated onto the sample surface to complete an electrolytic cell in the form of the capacitor structure shown in Fig. 1. Approximately 95% of the sodium at the aluminum interface was drifted to the silicon by a nominal electric field of 10^6 V/cm at 150°C for 1 hour. This electrolytic deposition from NaCl has proven to be an effective way of uniformly introducing sodium into the Si-SiO_2 interface.[11]

The density and distribution of sodium on the interface were determined by radiotracer techniques. The NaCl was tagged with a small percentage of $Na^{22}Cl$ before evaporation onto the sample. To perform the evaporation, a drop of the tagged NaCl in aqueous solution was dried in a tungsten boat. The NaCl residue was then vacuum evaporated at less than 2×10^{-6} Torr. Before electrolytically drifting the sodium to the silicon interface, the uniformity of the $Na^{22}Cl$ layer was established by autoradiographic exposure on x-ray film. On a scale of 10μ, the initial Na^{22} distribution was found to be quite uniform. After the sodium was drifted to the silicon interface and measurements of the energy barrier were performed, the lateral distribution of Na^{22} at the interface was determined again by autoradiographic techniques. Before this final autoradiographic measurement, the aluminum electrode

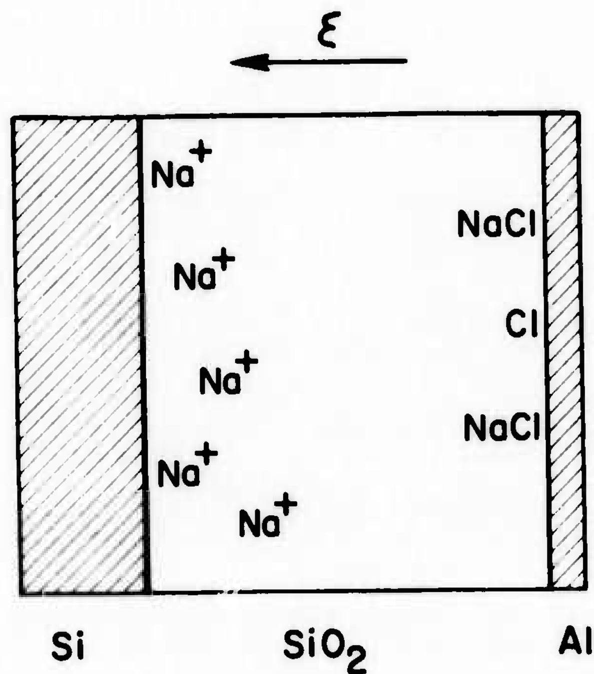

Figure 1: Sample arrangement showing an $Si-SiO_2$ interface which has been coated with sodium by electrolytic deposition. The tracer Na^{22} was used to allow a determination of the local sodium concentration on the interface.

and the extraneous NaCl remaining at that interface were removed by an H_3PO_4-HNO_3 etch. Samples displaying an inhomogeneous final distribution of sodium at the Si-SiO_2 interface were disregarded in the energy barrier determinations.

The areal density of sodium at the Si-SiO_2 interface was determined on the samples used for the thermionic emission and photoemission measurements. The Na^{22} distribution in the SiO_2 was profiled by incrementally sectioning the SiO_2 in "P-etch". The thickness of the removed sections was monitored by ellipsometric measurements, and the Na^{22} concentration associated with each section was ascertained from differential counting measurements on the sample. The sodium profiles exhibit a characteristic "U" shaped distribution, in which all but a small trace of the sodium is found at one or the other interface.[12] Figure 2 shows the distribution of sodium near the Si-SiO_2 interface for the sample containing 1.3×10^{15} Na/cm^2. In each case, the sodium density associated with the respective sample is the total density within 500 Å of the Si-SiO_2 interface. No appreciable sodium was found to penetrate into the silicon.

III. INTERNAL PHOTOEMISSION

Internal Photoemission, as developed by Williams,[1,13] has become a quite reliable technique for the determination of interface energy barriers. The minimum energy of the photon necessary to excite an electron over the contact barrier is determined by examining the dependence of photocurrent on photon energy near threshold. The form of the photoyield, Y above threshold Φ was determined[14] theoretically to be,

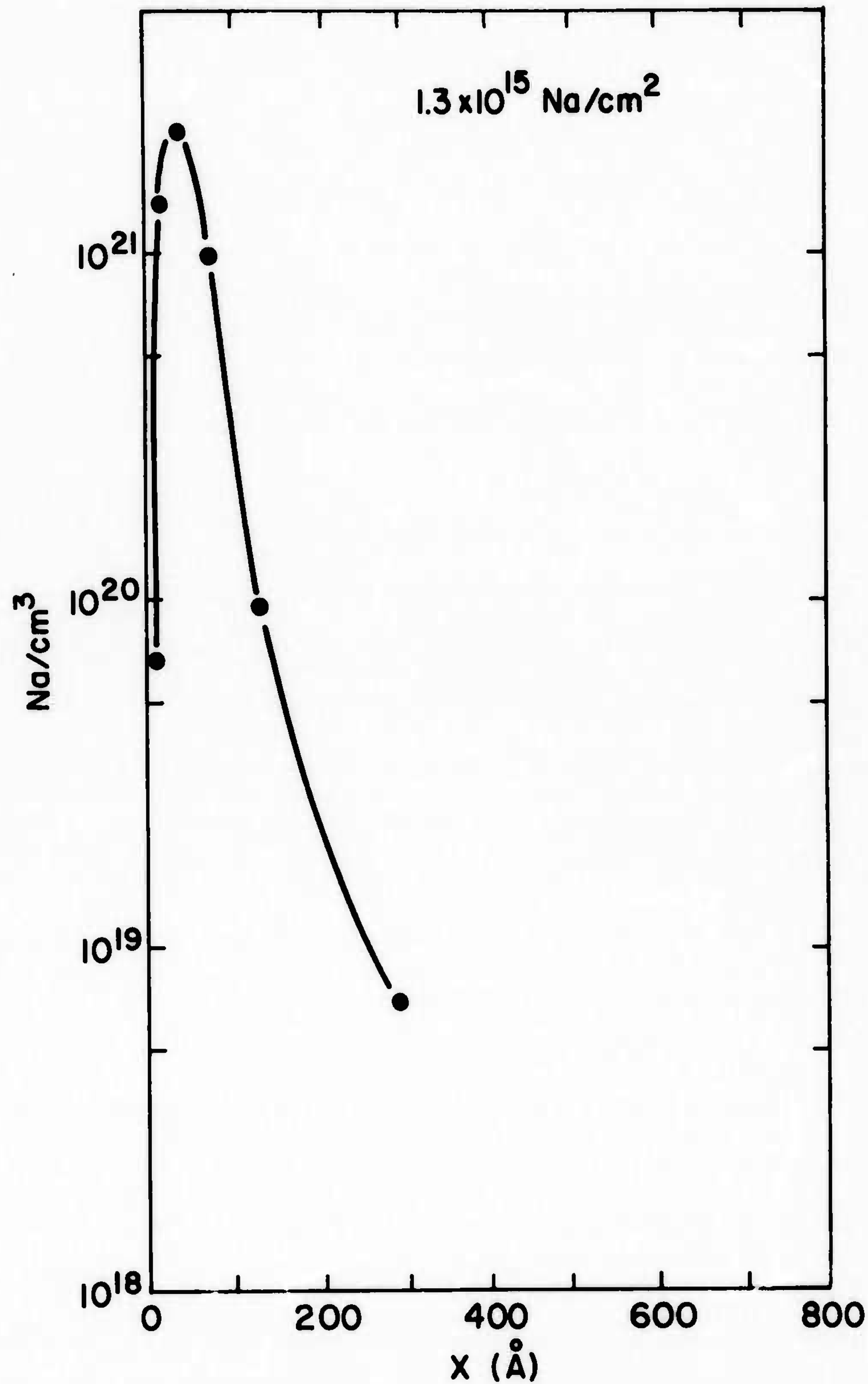

Figure 2: Sodium distribution near the Si-SiO_2 interface at X = 0. This interface is covered with 1.3 x 10^{15} Na/cm^2, most of which is within 100 Å of the interface.

$$Y = K\,(\hbar\omega - \Phi)^{n/2} \quad ,$$

where n is an integer between 2 and 5. Typically, the threshold is determined by fitting the yield to a power law[4,13,15] using n = 4 or 6. However, the analysis for Si-SiO_2 is complicated by a rapid variation of the optical constants of silicon in the range of interest. The rapid drop in optical absorption below the direct gap at $\hbar\omega \cong 3.2$ eV produces a corresponding drop in photoyield which obscures the threshold behavior.

A simple method is used to correct for the rapid variation of the silicon optical absorption coefficient α which allows a relatively accurate determination of the threshold energy. As in the case of vacuum photoemission, the photoelectric yield Y can be written[16] as,

$$Y\,(\hbar\omega) = \int_{\Phi}^{\infty} \frac{L(E)\,\alpha(\hbar\omega)}{1 + L(E)\,\alpha(\hbar\omega)}\; T(E)N(E,\hbar\omega)dE$$

where, L = electron scattering length

α = optical attenuation

T = barrier transmission probability

N = Electron energy distribution at the silicon surface

E = Electron energy.

A simplification can be made for the case,[17,18]

$$L(E)\,\alpha(\hbar\omega) << 1$$

then

$$Y(\hbar\omega) \cong \alpha(\hbar\omega) \int_{\Phi}^{\infty} \frac{T(E)N(E,\hbar\omega)}{L(E)} \, dE.$$

From Kane,[14] we have near threshold,

$$\int_{\Phi}^{\infty} \frac{T(E)N(E,\hbar\omega)}{L(E)} = K\,(\hbar\omega - \Phi)^{n/2}.$$

Finally, we can define a corrected photoyield, $Y(\hbar\omega)/\alpha(\hbar\omega)$ which allows a determination of the threshold energy by a fit to a power law relationship,

$$Y(\hbar\omega)/\alpha(\hbar\omega) \cong \beta\,(\hbar\omega - \Phi)^{n/2}$$

For silicon, this relationship is valid for $\hbar\omega \lesssim 3.5$ eV. Using a corrected yield, equal to $Y(\hbar\omega)/\alpha(\hbar\omega)$, we have been able to determine the photoelectric threshold Φ.

The spectral response of photocurrent was measured from samples which were uniformly covered with sodium at three different densities. After correcting for reflectivity, the absolute photoyield Y was obtained as a function of photon energy, as shown in Fig. 3. The nominal electric field used to sweep the electrons through the SiO_2 was 1×10^6V/cm in each case. Notice that the absolute photoyield is increased at all photon energies by an increase in the sodium density, particularly at photon energies below 4.0 eV. The photoyield drops

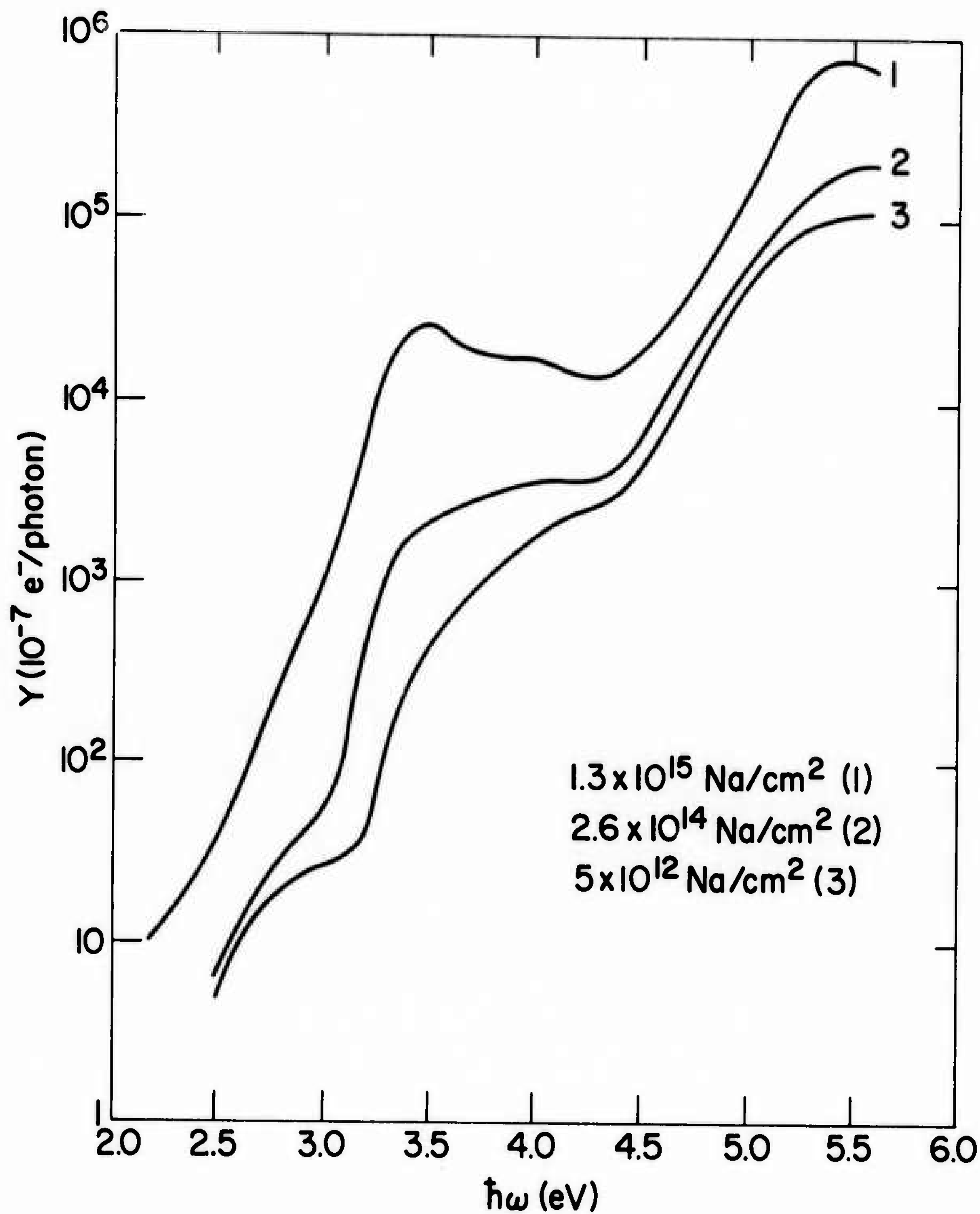

Figure 3: Absolute photoemission yield from Si-SiO_2 interfaces, which were coated with sodium at three widely different concentrations. The measurements were obtained with a nominal electric field $\varepsilon = 10^6$ V/cm in the SiO_2.

rapidly below 3.2 eV due to the decreasing optical absorption as well as the energy threshold. Dips seen in the photoyield at 3.6 eV and 4.4 eV are due to strong optical transitions[19] at $\Delta_3 - \Delta_1$ and $X_4 - X_1$ in the zone, each of which produces only low energy electrons with insufficient energy to surmount the barrier. Similar structure is seen in vacuum photoemission from a cesiated silicon surface. The physical situation in the internal photoemission is analogous to that for vacuum cesiated silicon, except that the alkali ion is applied internally. The absolute magnitude of the internal photoyield was somewhat influenced by conditions during drift of the sodium to the silicon interface.

An increase of the electric field in the SiO_2 increases the photoyield but does not greatly influence the major features of the distribution. The representative family of curves in Fig. 4 was measured at nominal fields of 1, 2, and 3 x 10^6 V/cm for a sample containing 1.3 x 10^{15} Na/cm^2; a similar field dependence was found at 5 x 10^{12} and 2.6 x 10^{14} Na/cm^2. We find that the dependence of photoyield upon the electric field does not follow the relationship which has been used for photoemission from a pure Si-SiO_2 interface.[20] This is hardly surprising since the sodium at the interface is redistributed by any change in the applied electric field. Also, the gross distortion of the electric field by sodium near the interface as well as the large number of sodium related scattering centers cause the sodium coated interface to deviate far from the ideal Si-SiO_2 interface.

The photoelectric thresholds are determined by examining the corrected photoyield (Y/α) near the threshold energy. For a sodium

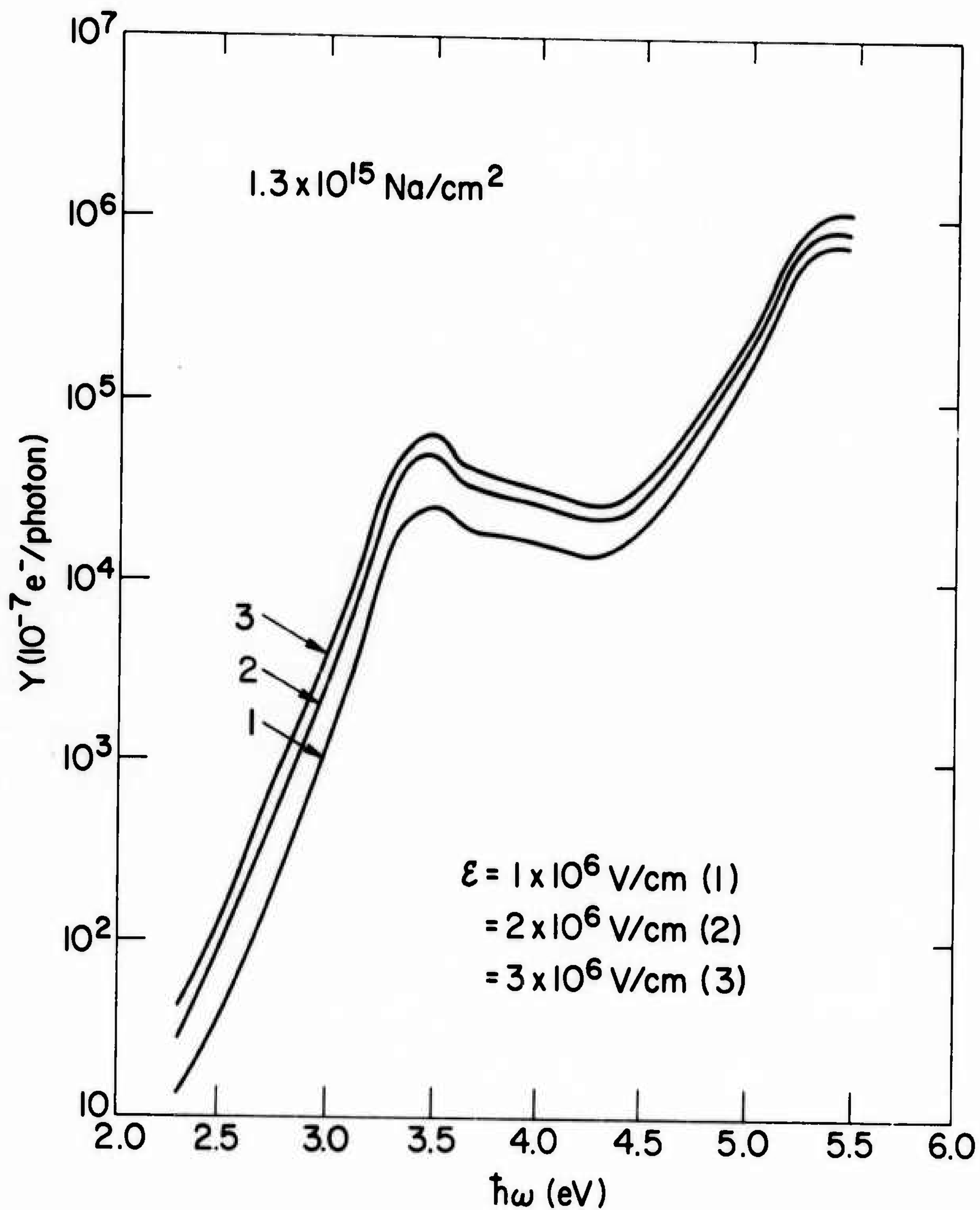

Figure 4: Absolute photoemission yield from an Si-SiO_2 interface which was coated with 1.3×10^{15} Na/cm^2 Photocurrent was measured for nominal electric fields of $\varepsilon = 1,2,$ 3×10^6 V/cm in the SiO_2.

density of 1.3 x 10^{15} Na/cm^2, the one-half power of (Y/α) is displayed against photon energy in Fig. 5. A best fit of the data to the theoretical model was obtained by n = 4, which gives a linear relationship between $\sqrt{Y/\alpha}$ and photon energy. The extrapolated photoelectric thresholds are 2.46, 2.38, and 2.34 eV for nominal electric fields of 1, 2, and 3 x 10^6 V/cm respectively. The field dependence of the threshold is considerably less than that predicted by the Schottky effect for a simple clean interface. Of course, there is no _a priori_ reason to expect that the Schottky effect should be applicable because the sodium near the interface is redistributed by a changing electric field and the field near the interface is distorted by the presence of ionized sodium. An extrapolation of the photothreshold energy to zero electric field indicates an interface barrier of 2.6 $\pm$ 0.1 eV for 1.3 x 10^{15} Na/cm^2, assuming a parabolic dependence of threshold upon field.

Similarly, the photoelectric threshold is determined for 2.6 x 10^{14} Na/cm^2 from the data in Fig. 6. Here, the photoyield near threshold is somewhat distorted by a shoulder which appears at 2.8 eV. This shoulder, which appears more prominently in the photoyield at 5 x 10^{12} Na/cm^2, will be discussed below. The thresholds determined by extraplation are 2.69 and 2.73 eV for fields of 3 and 2 x 10^6 V/cm. An extrapolation of threshold to zero electric field yields a barrier of 2.9 $\pm$ 0.1 eV.

The corrected photoyield near threshold for 5 x 10^{12} Na/cm^2 is complicated by a peak at 2.8 eV. This peak, also seen at 2.6 x 10^{14}Na/cm^2, appears to have a magnitude which is nearly independent of sodium

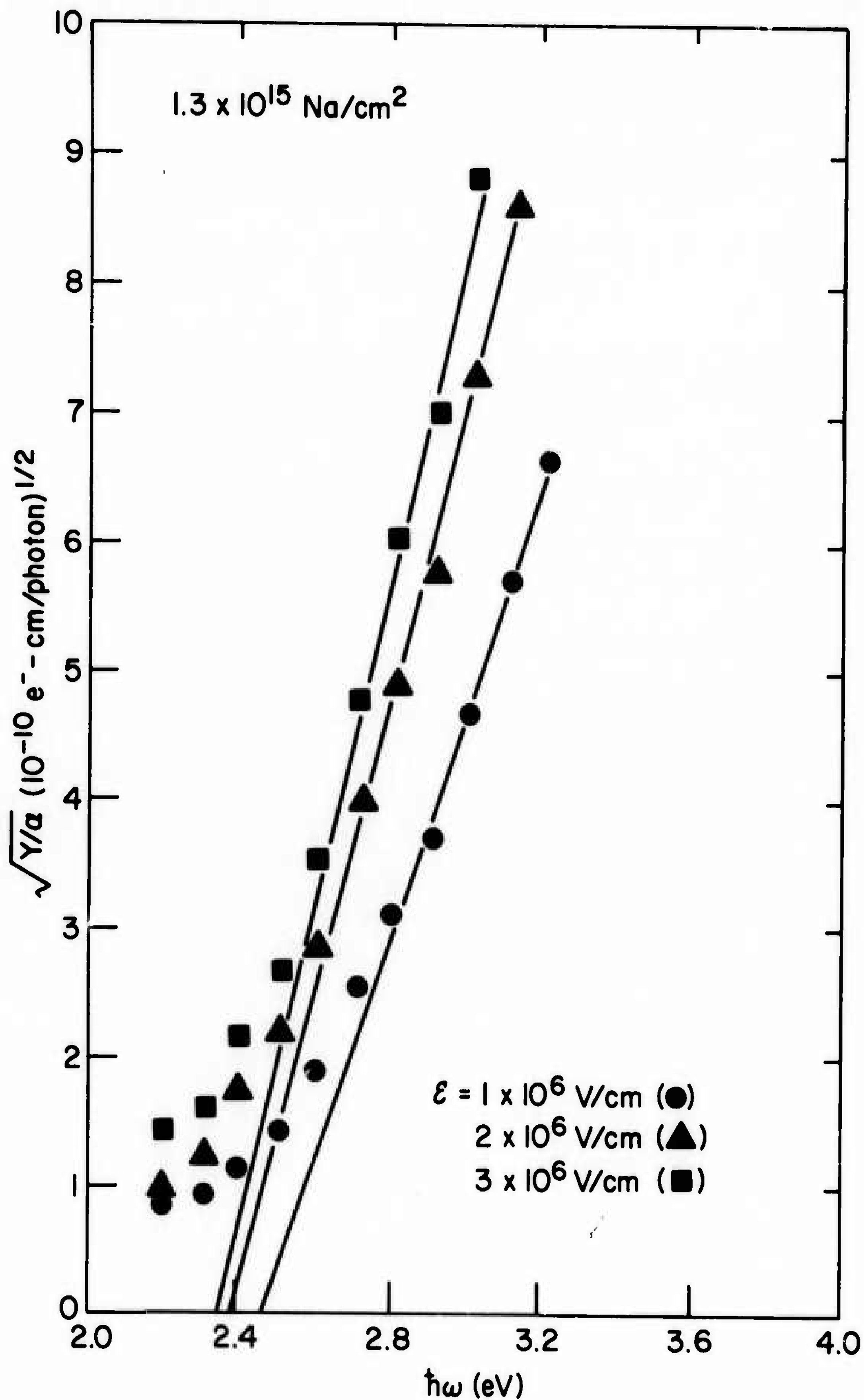

Figure 5: Half power of the photoyield, corrected for the optical attenuation α length of silicon, as a function of photon energy. The extrapolated thresholds for photoemission are 2.46, 2.38, and 2.34 eV for nominal electric fields of ε = 1, 2, and 3 x 10^6 V.cm respectively.

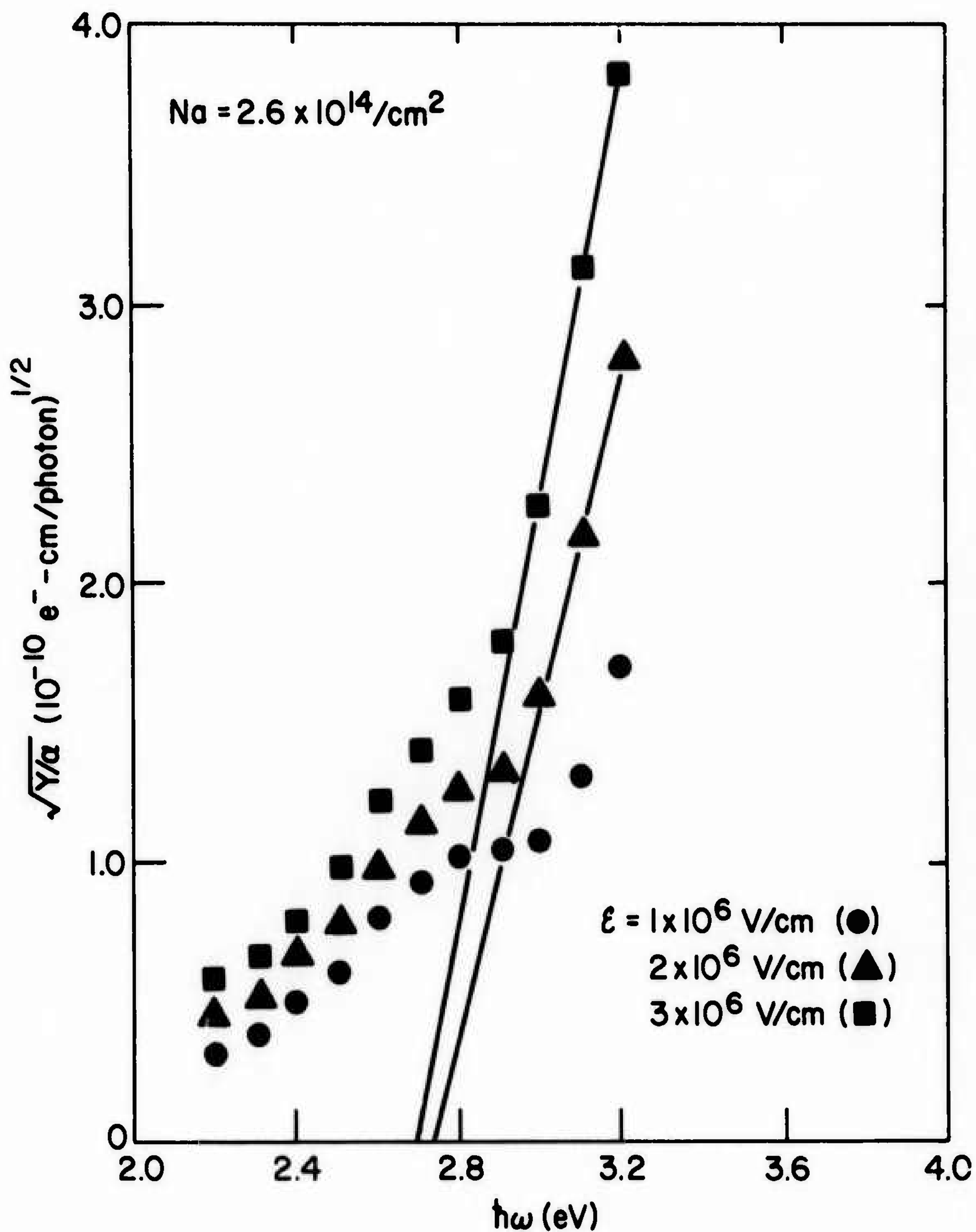

Figure 6: Half power of the photoyield, corrected for the optical attenuation α of silicon, as a function of the photon energy. The extrapolated thresholds for photoemission are 2.69 and 2.73 eV for nominal electric fields of $\varepsilon = 2$ and 3×10^6 V.cm respectively. The threshold for $\varepsilon = 1 \times 10^6$ V.cm is observed by the presence of a shoulder in the curve at $\hbar\omega = 2.8$ eV.

concentration. Also, the absolute photoyield Y is of the same order of magnitude as that found by Goodman for emission from the conduction band of degenerately doped Si. It seems reasonable that this extra peak is due to the photoemission of electrons from the conduction band of the degenerately doped silicon substrate. The photothresholds can be estimated in this case to be about 3.0 ± 0.1, 3.1 ± 0.1, and 3.2 ± 0.1 eV for electric fields of 3, 2, and 1 x 10^6 V/cm. Very approximately, the energy barrier at zero field is 3.4 ± 0.1 eV.

IV. THERMIONIC EMISSION

Thermionic emission of electrons from silicon into SiO_2 was measured in order to provide an independent check of the interface energy barrier. To facilitate a comparison with the photoemission results, thermionic emission and photoemission measurements were performed on the same sample, with 1.3 x 10^{15} Na/cm^2. The measurements were performed in an ambient atmosphere of N_2 gas which was dried at the temperature of liquid nitrogen. The nominal electric field in the SiO_2 was 1 x 10^6 V/cm. In the sequence of measurements, the sample was allowed to stabalize at 600°C for 2 hours, and then the current was determined at each temperature after the sample had been at equilibrium for 20 minutes. The results are shown in Fig. 8 as the points (J/T^2) vs $(1/T)$, to which a best fit was made to the Richardson equation. The solid line in Fig. 8 is the relation,

$$J = A^* T^2 e^{-\Phi_o/kT} ,$$

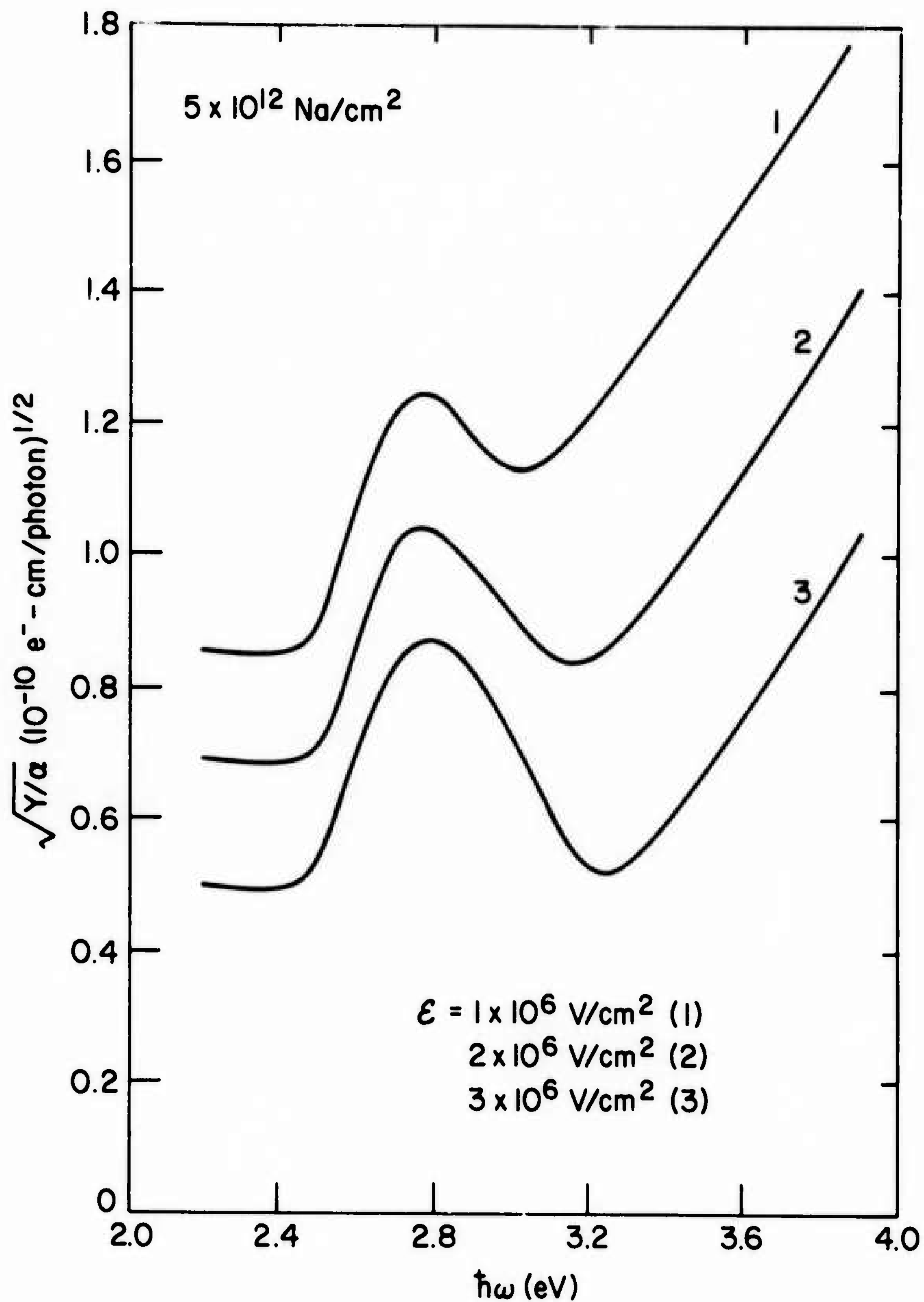

Figure 7: Half power of the photoyield, corrected for the optical attenuation α in silicon, as a function of the photon energy. The extrapolated threshold for photoemission is obscured by a peak which appears at 2.8 eV in each curve. The threshold for photoemission from the silicon valence band is estimated to be 3.1 ± 0.1 eV.

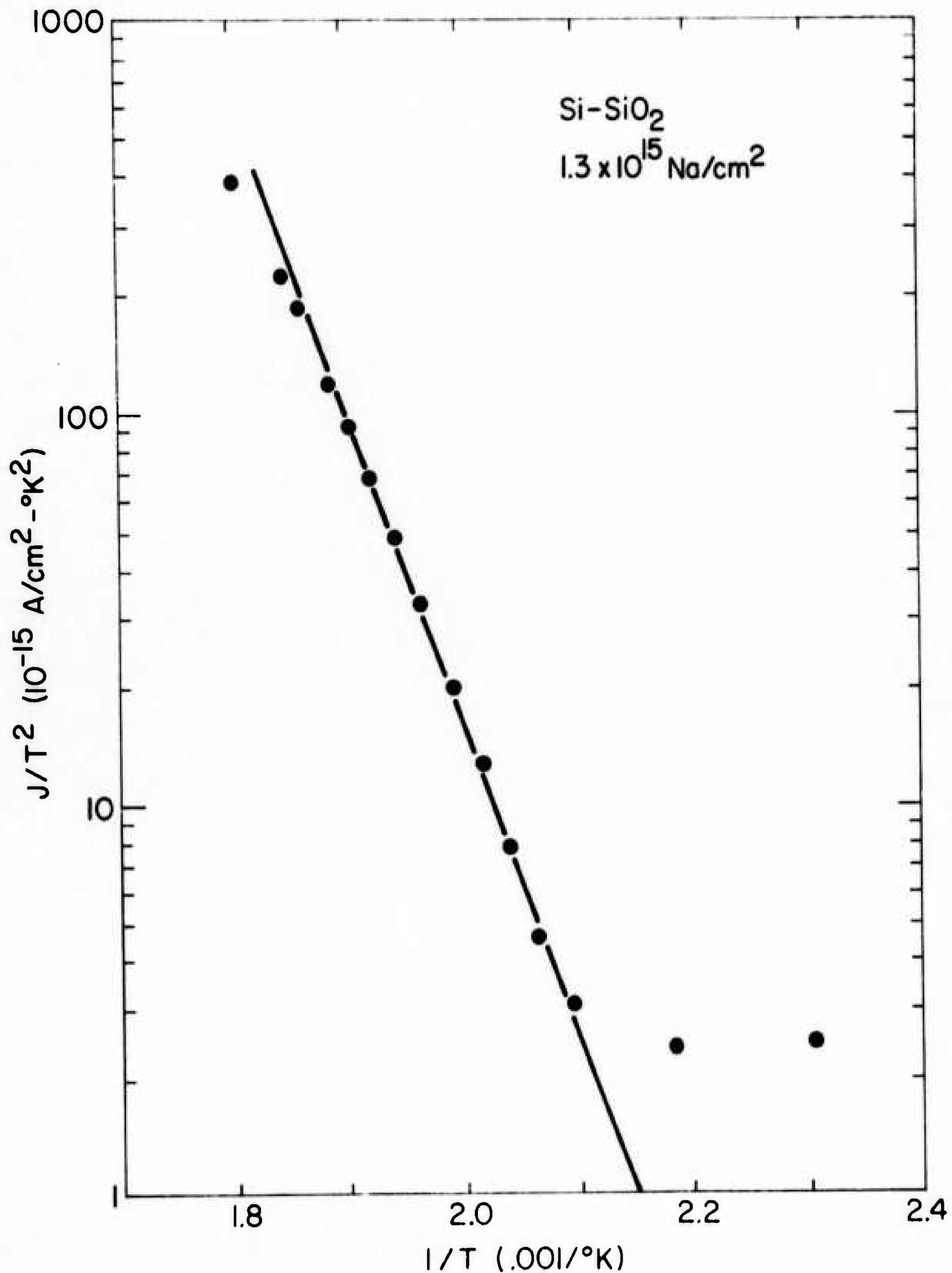

Figure 8: Thermionic emission from a Si-SiO_2 interface covered with 1.3×10^{15} Na/cm^2. A fit of the Richardson equation to the temperature dependence indicates a barrier of $\Phi = 1.60 \pm .01$ eV. The nominal electric field ε is 1×10^6 V/cm.

with Φ_o = 1.60 eV and A* = 215 $A.cm^2$-°K. The fit is relatively insensitive to A, but the work function Φ_o is determined to within $\pm$ 0.02 eV. The deviation from the Richardson equation at the higher temperatures is thought to be due to a small shift of the Fermi level toward the center of the gap in the heavily doped silicon. At the low temperature end, the current saturates at 4.5×10^{-10} A/cm^2, independent of temperature; this appears to be a direct tunneling current.

The work function Φ_o determined by thermionic emission can be related directly to the threshold, Φ, for photoemission from the valence band in this case because the Fermi level in the heavily doped silicon is within 0.1 eV of the conduction band over the range of temperatures used to determine Φ_o. From thermionic emission, one would predict a photoemission threshold of 2.7 $\pm$ 0.1 eV for an $Si-SiO_2$ interface with 1.3×10^{15} Na/cm^2 and an electric field of 1×10^6 V/cm. This compares favorably with the measured threshold of 2.5 $\pm$ 0.1 eV.

Both thermionic and photoemission results indicate that sodium at an $Si-SiO_2$ interface will appreciably reduce the contact energy barrier. A simple model for this reduction is outlined in Fig. 9. For the pure $Si-SiO_2$ interface, the electric field in the SiO_2 and the image potential of an electron near the interface combine to produce an effective potential shown as the dashed line in Fig. 9(a). The barrier Φ for injection of electrons into the SiO_2 is reduced by the Schottky effect. When a layer of positive sodium ions is placed near the silicon surface, the SiO_2 conduction band is distorted, as

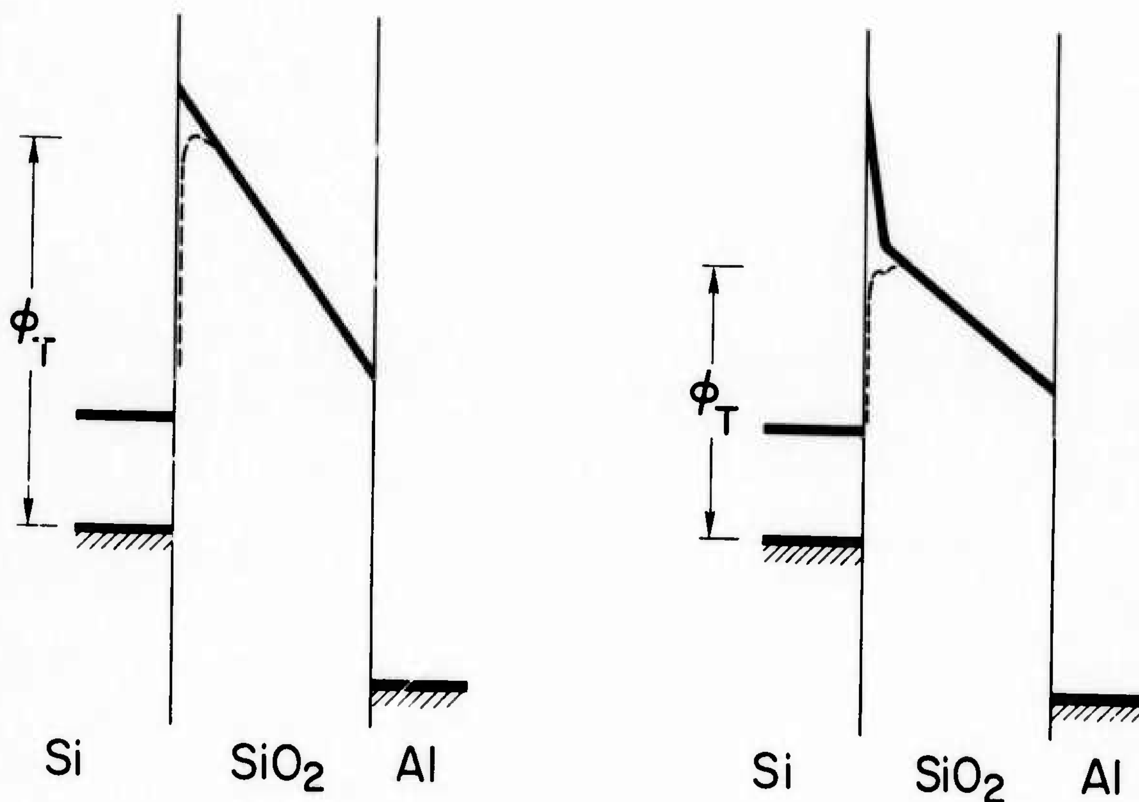

Figure 9: Energy diagrams for the Si-SiO_2-Al system. (a) The barrier Φ at a pure Si-SiO_2 interface is reduced by the Schottky effect due to the electric field. The dashed line shows the effective potential seen by an electron. (b) The barrier Φ at an Si-SiO_2 interface is reduced by a layer of positive ions near the interface. The effective potential seen by an electron shown as the dashed line, deviates considerably from the conduction SiO_2 band bottom.

represented in Fig. 9(b). As in 9(a), the image potential is added to the SiO_2 conduction band bottom to produce an effective potential. In this case, the barrier Φ is considerably reduced by the dipole layer at the silicon surface. One should note that the reduction of the barrier for electron injection may or may not be equal to the potential drop across the interface dipole.

V. CONCLUSIONS

A reduction of the energy barrier between silicon and SiO_2 by the presence of sodium has been confirmed by careful photoemission and thermionic emission measurements of uniformly coated interfaces. A good agreement is found between the barrier determined by the two different experiments on the same sample. The barrier reduction is attributed to a dipole layer formed by sodium on the interface. The barrier can be further reduced by an electric field in the SiO_2, but this reduction is considerably less than that expected for the Schottky effect on a clean interface.

The electronic barrier is reduced from 4.2 eV to 2.5 eV by 1.3×10^{15} Na/cm^2, or approximately one monolayer at the Si-SiO_2 interface. For this lowest barrier, a maximum absolute photoyield of 10% was found. A significant barrier reduction was observed for considerably smaller sodium concentrations. This lowered barrier can lead to a greatly enhanced Fowler-Nordheim tunnel current at high electric fields.

VI. ACKNOWLEDGEMENTS

The authors wish to acknowledge helpful discussions with Drs. A. M.

Goodman and R. Williams of the RCA Sarnoff Lab. Prof. Murray Lampert of Princeton University and R. B. Laibowitz of the IBM Watson Lab.

REFERENCES

1. R. W illiams, Phys. Rev. 140, A569 (1965).

2. Alvin M. Goodman, Phys. Rev. 144, 588 (1966).

3. R. J. Powell, J. Appl. Phys. 40, 5093 (1969).

4. B. E. Deal, E. H. Snow, C. A. Mead, J. Phys. Chem. Solids 27, 1873 (1966).

5. V. F. Korzo, P. S. Kireev, and G. A. Lyaschenko, Soviet Physics-Semiconductors 2, 1545 (1969).

6. R. Williams, J. Appl. Phys. 37, 1491 (1966).

7. C. R. Viswanathan and S. Ogura, Appl. Phys. Lett. 12, 220 (1968); Proc. IEEE 57, 1552 (1969).

8. T. H. Di Stefano, Appl. Phys. Lett. 19, 280 (1971).

9. R. Williams and M. H. Woods, J. Appl. Phys. 43, 4142 (1972).

10. H. R. Philipp and H. Ehrenveich, Phys. Rev. 129, 1550 (1963).

11. This was suggested by D. Kerr, IBM E. Fishkill.

12. E. H. Snow, A. S. Grove, B. E. Deal and C. T. Sah, J. Appl. Phys. 36, 1664 (1965); E. Yon, W. H. Ko and D. A. Kuper, IEEE Trans. Electron Devices 13, 276 (1966); Steven R. Hofstein, IEEE Trans. Electron Devices 13, 222 (1966); IEEE Trans. Electron Devices 14, 749 (1967).

13. R. Williams, in Semiconductors and Semimetals, Vol. 6 edited by R. K. Wilardson (Academic Press, New York, 1970).

14. E. O. Kane, Phys. Rev. 127, 131 (1962).

15. A. M. Goodman, "Internal Photoemission as a Tool for the Study of Insulators", in Optical Properties of Dielectric Films (ECS Symposium, Boston, 1968) p.99.

16. C. N. Berglund and W. E. Spicer, Phys. Rev. 136 A1030 (1964).

17. E. O. Kane, J. Phys. Soc. Japan Supplement 21, 37 (1966).

18. The electron scattering attenuation length L(E) was assumed to be less than 100 Å over the range of interest here.

19. F. Herman et al., "New Studies of the Band Structure of Silicon, Germanium, and Grey Tin", in _Quantum Theory of Atoms, Molecules, and the Solid State_, (Academic Press, New York 1966) p.381.

20. R. J. Powell, J. Appl. Phys. **41**, 2427 (1970).

21. N. Ainsley, Private Communication , 1972.

II. BAND STRUCTURE AND SWITCHING IN TRANSITION METAL OXIDES

Amorphous thin films of the transition-metal oxides Nb_2O_5 or Ta_2O_5 are interesting because of the relatively fast bistable switching found in these materials. A capacitor of Nb_2O_5 with opposite electrodes of Nb and Bi can be made to switch between two different resistance states by the application of voltage pulses of the proper sign and magnitude. The actual switching takes place in a filament formed by a controlled breakdown of the amorphous Nb_2O_5. The conditions which determine the filament formation as well as the mechanism of switching in the filament were not previously understood. From the work presented here, we have gained some understanding of the filament formation process and of the mechanism of conduction in the filament. A good understanding of the switching is essential if this type of switchable device is to be considered seriously for large scale computer applications. Our results indicate that filament formation and switching are structural rather than electronic, and as such are not attractive for device application in any situation where reliability is required (i.e., computers).

The following sections are concerned with the mechanism of filament formation and switching in the niobium oxide system. These studies were facilitated by using two different sample configurations. In the first section, a planar geometry with laterally spaced electrodes allows us to measure simultaneously the electrical resistance of the Nb_2O_5 while viewing the sample with a transmission electron microscope. With this technique, we have found that a high voltage on the Nb_2O_5 leads to an amorphous to crystalline transformation. The crystallized

region has a much lower resistance than the surrounding amorphous matrix. Such studies also show that the filament generally starts at irregularities or asperities on the metal electrodes at which the local electric field is enhanced. Thus, the formation of a conducting filament is determined by gross physical structure rather than by an electronic process. Subsequent switching of the filament takes place in the polycrystalline material, with the conductivity taking place in the grain boundaries.

The second article gives the results of our Scanning Internal Photoemission (SIP) study of Nb_2O_5 in a typical sandwich geometry. SIP studies can be used to detect points at which the potential barrier at a metal-insulator interface is a minimum. This would be a preferred location for the filament formation and switching process if the forming process is barrier controlled. However, our results show that, to a resolution of about 1μ, the local contact barrier does not correlate with the switching process. On the contrary, local inhomogenieties or asperities seem to determine the preferred sites for filament formation. In addition, the photoemission results also show that electronic processes such as trap filling and emptying have no significant influence on the filament formation or switching. Thus, the combination of electrical and optical measurements along with electron microscopy indicates that the forming process is controlled by metallurgical defects on the electrodes. A local field enhancement leads to current injection and thermal runaway producing a crystalline, low resistance, filamentary path. The lowest resistance state appears to be dominated by the agglomoration of metallic impurities in the crystalline region,

presumably at grain boundaries. Work is underway to test this agglomeration by experiments on intentionally doped materials, such as Nb_2O_5 : Bi.

A. DIRECT OBSERVATION OF FIELD-INDUCED CRYSTALLIZATION IN NIOBIUM OXIDE FILMS

R. B. Laibowitz
S. Mader

A wide variety of amorphous materials exist which form the active element in bistable devices. These materials are usually fabricated by simple vacuum deposition techniques. A prominent example of such materials are the chalcogenide glasses,[1] although transition metal oxides[2,3] such as Nb_2O_5 can also be used as the active element. The devices so constructed are characterized by two resistance states and have the ability to switch between these states. The mechanism of switching is not well understood although in the case of the chalcogenides, the switching is usually associated with the formation of a conductive crystalline filament in the amorphous matrix. Such a filament was observed for the first time in our previous work on GeTe[4] in which a new technique allowed us to view directly the structural changes that take place in an amorphous material by transmission electron microscopy, while the sample is switched by an applied electric field. In this paper, we extend the use of this technique to the study of structural transformations and conduction in Nb_2O_5.

An oxidized Si wafer is generally used as the substrate for preparing samples. These wafers are readily available, flat and relatively smooth. On the surface, a pair of closely spaced metal electrodes is formed by electron beam techniques.[4] The space or gap between these electrodes is controllable and generally in the range of 2000-5000 Å. Into this gap, the active material is deposited to thicknesses of 600-800 Å - for Nb_2O_5 rf sputtering is used. The back part of the wafer is

then jet-etched in a HNo_3-HF solution producing the sample as shown in Fig. 1. As a result of the thinning procedure the active element region of the sample is now transparent to the 100 KeV electrons used in the microscope. The biasing circuit usually consists of a transistor curve tracer oscilloscope and a variable current limiting series resistor. For more elegant switching studies pulse equipment can also be used.

Our initial experiments used Nb electrodes spaced apart about 2000 Å, a section of a typical sample as viewed in the electron microscope is shown in Fig. 2a. The Nb electrodes which are opaque to the electrons appear black in the micrograph while the amorphous Nb_2O_5 appears much lighter. In situ electron diffraction on the amorphous material which is both between the electrodes and around them shows the typical amorphous patterns. Under electrical bias, the samples initially exhibit a high resistance ($>$ 10 MΩ) up to about 30 V. At this field, crystallization of the amorphous Nb_2O_5 results. The shape of the crystallized region is filament-like and generally begins at an asperity on the electrode. Often, such crystallized regions will form at the edges of the electrodes and an example of such a formation is shown in Fig. 2b. Such edge filaments occur more regularly with narrow gaps in which poor contact between the Nb_2O_5 within the gap and the electrode is found. However, it is through these crystallized regions that the current flows.

Before discussing the conductivity of the crystallized regions, it is interesting to review the results of the in situ electron diffraction measurements. An electron diffraction example taken from

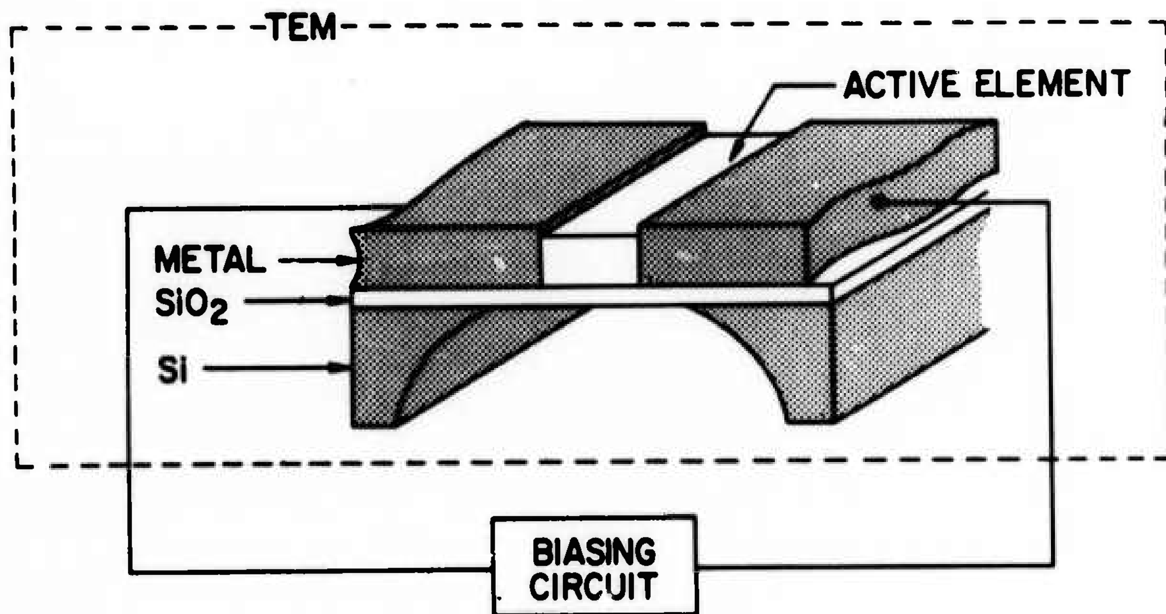

Figure 1: Schematic diagram of a sample prepared for simultaneous transmission electron microscopy (TEM) and electrical biasing measurement.

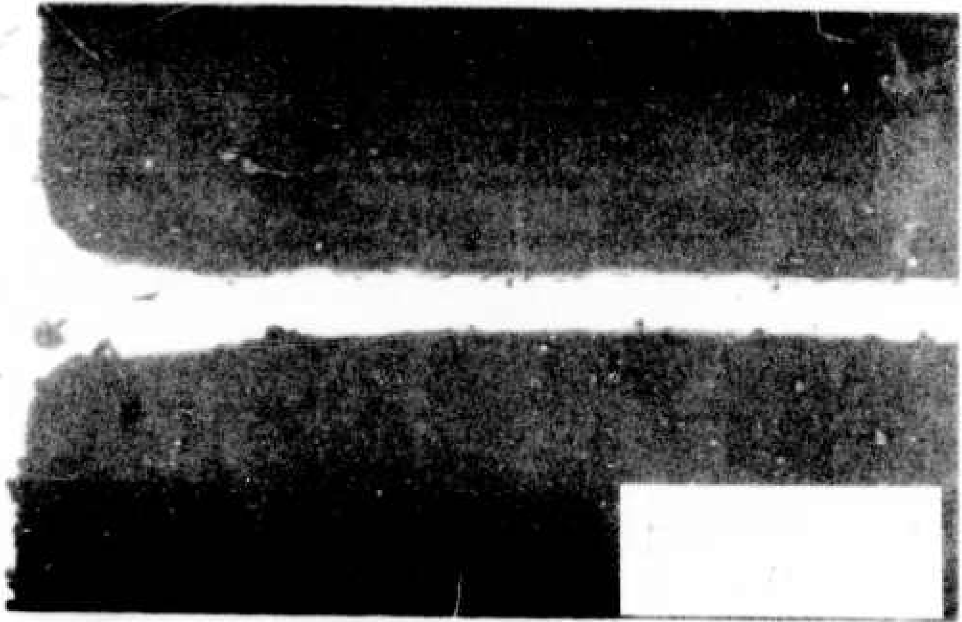

Figure 2: (a) Electron micrograph of the gap between two Nb electrodes. Amorphous Nb_2O_5 is between and around these electrodes.

(b) Typical edge - formed, crystalline filament after application of 30 volts across the gap.

the crystalline filament is shown in Fig. 3. Analysis of such data shows that the crystallities have the d-spacing corresponding to a high temperature, monoclinic phase of Nb_2O_5. The particular monoclinic form observed is very close to a tetragonal variation and thus in general the crystals have lattice constants of about 3.9 Å and 13.0 Å. Often the long axis is in the direction of current flow and follows a curvature defined by the expected field pattern. Upon further application of high currents, the crystallized regions grow in particular directions. Knowledge of the particular phase that forms (from electron diffraction) the shape (from electron microscopy) and the I-V curves should lead to determination of possible mechanisms for crystallization and filament formation in such amorphous materials.

An example of an I-V curve before (a) and after (b) forming is shown in Fig. 4. The nonlinear curve is the result of forming and at higher current levels, instabilities typical of heating appear. However, at more reasonable biases (below 1 volt) a resistance of about 1.5 M Ω is found. Such a resistance is somewhat greater than generally encountered in the high resistance state found in bistable resistors of $Nb/Nb_2O_5/Bi$. In addition, switching is not observed in our samples of $Nb/Nb_2O_5/Nb$ and none was expected in this symmetrical system as past work has shown that a Bi electrode is necessary for good switching. Efforts are underway to make electron-beam fabricated planar structures with different electrodes, e.g. Nb and Bi. Such a problem is nontrivial and has broad applications for electron beam fabrication in general. Doped oxides and all Bi electrodes will also be used to study both the crystallization and conduction mechanisms

Figure 3: In situ electron diffraction pattern taken from the filaments formed from the amorphous Nb_2O_5.

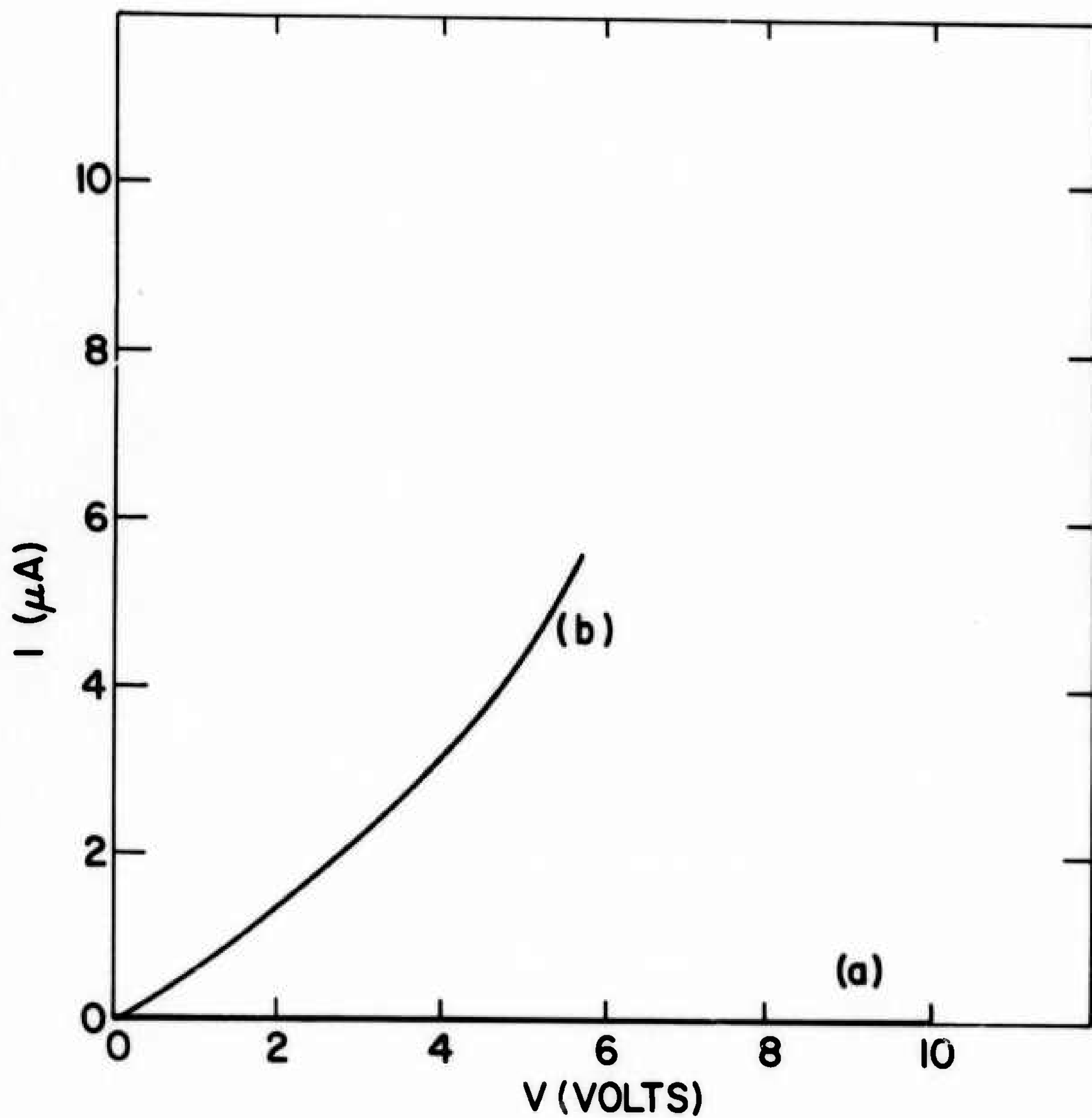

Figure 4: I-V curves before (a) and after (b) filament formation.

in these amorphous materials. From our past work[3] we expect the conductivity of the doped filaments to be much higher and with a Bi electrode switching should occur.

REFERENCES

1. S. R. Ovshinsky, Phys. Rev. Let., 21, 1450 (1968).
2. T. W. Hickmott, and W. R. Hiatt, Sol. State Electron., 13, 1033 (1970).
3. R. B. Laibowitz, and A. A. Levi, Conduction in Low Mobility Materials, Taylor and Francis, London, 1971, p. 63.
4. P. Chaudhari and R. B. Laibowitz, Thin Solid Films, 12, 239 (1972).

B. PHOTOEMISSION STUDY OF FILAMENT FORMATION IN Nb_2O_5

T. H. DiStefano
R. B. Laibowitz

A conductive channel, formed in a thin amorphous film of Nb_2O_5 by a controlled breakdown, shows bistable resistive switching. The mechanism of filament formation and switching are not understood at present, but several plausible models have been proposed. One possibility[1,2] is that the change in conductivity is the result of a contact barrier which is reversibly altered by the application of an electric field of the proper polarity. The concept of this barrier modification is outlined in Fig. 1. The Nb-Nb_2O_5 interface is an injecting contact, while that at Nb_2O_5-Bi is blocking.[3] Therefore, current flow through this system is limited by the barrier ϕ at the Nb_2O_5-Bi interface. We investigated the possibility that an applied electric field, along with some local heating, may induce a change in the barrier ϕ by the formation of a polarization layer at the interface. A small, stable change of the interface barrier from ϕ_a to ϕ_b will cause a large increase of the injection current.

Scanning Internal Photoemission (SIP) was used to study the Nb_2O_5-Bi interface barrier. In particular, we attempted to find a field induced or a temperature induced local barrier change on the Nb_2O_5-Bi interface. Also, from an SIP map of the interface, we looked for a correlation between the local photoemission yield and the point at which a conductivity filament was formed. From the model based on a changing contact barrier, one might expect filament formation to occur at a point where the initial barrier is lowest. The photoemission map was used to find the point of lowest initial barrier, or correspondingly, highest photocurrent.

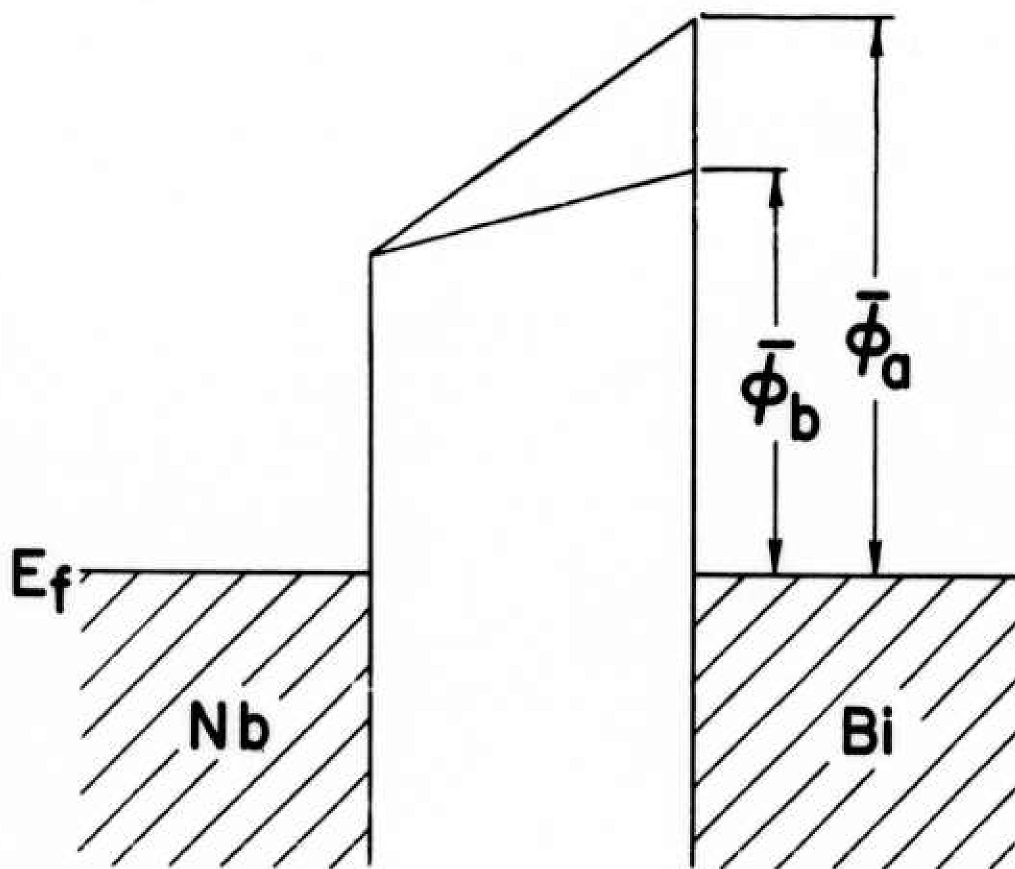

Figure 1: Energy diagram showing an Nb_2O_5-Bi interface with a variable contact barrier. One possible model for switching in the Nb-Nb_2O_5-Bi system involves a field induced change in the contact barrier ϕ.

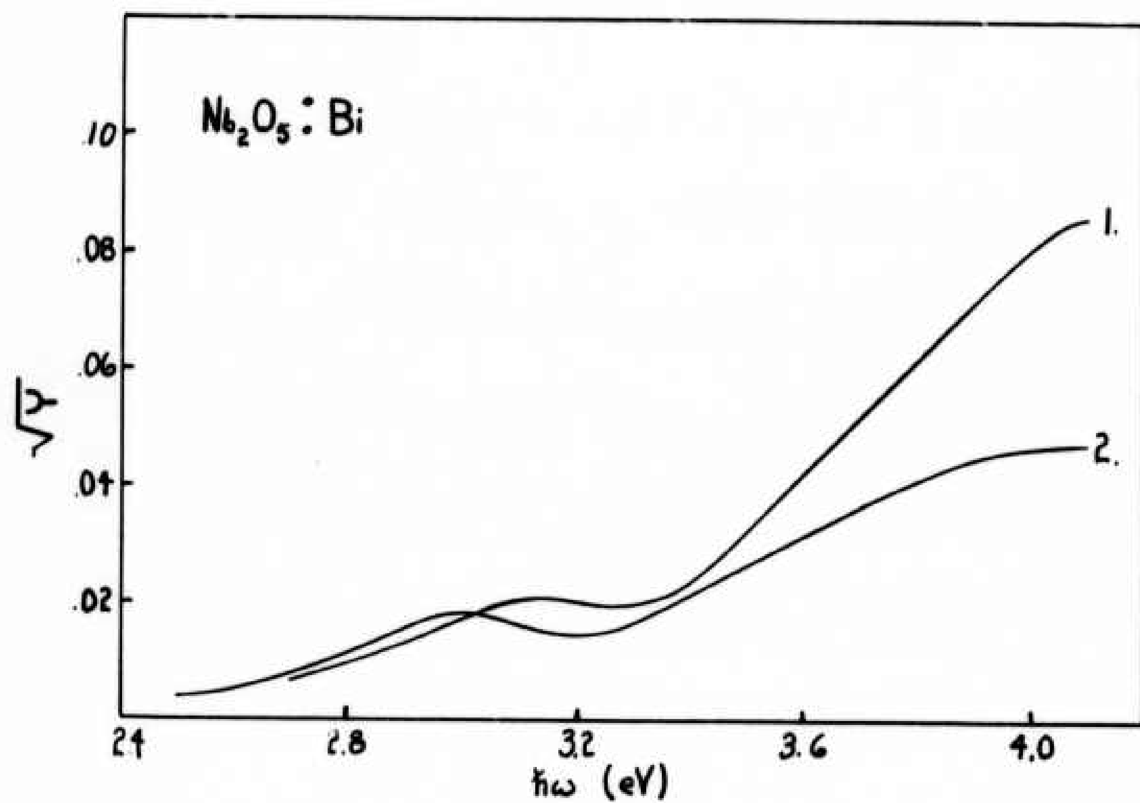

Figure 2: Absolute photoconductivity of (1) Nb_2O_5 and of (2) $(Nb_2)_{88}(Bi_2)_{12}O_5$ near the photoconductivity edge.

All of the photoemission experiments were performed on Nb_2O_5 thin films on a niobium substrate. Both sputtered and anodized films were examined, with similar results. The Nb_2O_5-Bi contact was formed by vacuum evaporation if a of a 200Å of bismuth onto the Nb_2O_5 film at room temperature. Then, photoemission of electrons from the bismuth into the Nb_2O_5 was measured from local areas about 1μ in diameter. The local photocurrent, displayed as a function of x and y on the sample, mirrors the Nb_2O_5-Bi contact barrier. A 6328Å laser was used as the light source for the photoemission measurements. A high photocurrent corresponds to a low contact barrier.

Along with photoemission from the bismuth itself, our measurements may include emission from traps near the Nb_2O_5-Bi interface as well as emission from a mixed Nb-Bi oxide which could form near the interface. We found no effective way to distinguish between the emission from traps near the interface and that from the bismuth itself. However, we did find that a mixed Nb-Bi oxide near the interface will not contribute to the photocurrent, since the mixed oxide is a good insulator with a well defined bandgap well above the 1.96 eV photon energy. The photoconductivity measured from a mixed oxide $(Nb_{.85}Bi_{.15})_2O_5$ is shown in Fig. 2, along with the photoconductivity from pure Nb_2O_5. The bandgap of the mixed oxide is 3.2 eV, somewhat less than the 3.5 eV of the Nb_2O_5. The photoconductivity measured below 3.2 eV is due to photoemission from the contacts. Clearly, we should not see photoemission from the valence band of any mixed Nb-Bi oxide which may form near the interface.

An SIP map of a typical Nb_2O_5-Bi interface is shown in Fig. 3(a).

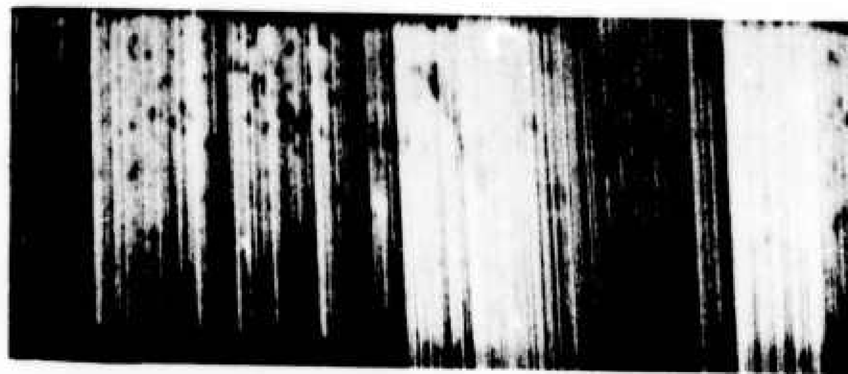

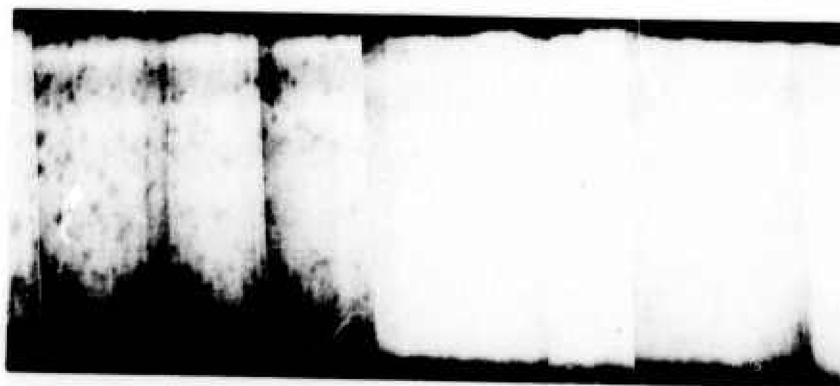

Figure 3: (a) Scanning Internal Photoemission map of the Nb_2O_5-Bi interface. The bright areas correspond to a relatively large photoelectric yield. (b) High contrast scanning reflectivity measurement of the same area as that shown in the photoemission measurement in (a).

Here, light areas correspond to areas where the photocurrent is relatively high. Both sputtered and anodized Nb_2O_5 films displayed the spotty character shown here; the dark spots about 10μ in diameter are regions where the photoyield is relatively low. On this and other samples, the photoemission map was not changed after the sample had been exposed to temperatures up to 200°C, at which point, the sample became so conductive that the photoemission measurements could not be obtained. Apparently, the increased conductivity was not due to a reduction of the Nb_2O_5-Bi barrier. For reference, Fig. 3(b) shows reflectivity measured from the same sample.

The sample in Fig. 3 was "formed" twice by the application of a 40 volt pulse to the bismuth. Surprisingly, both filaments formed at points where the photoyield was relatively low. A filament did not form at the bright spot seen in the middle of Fig. 3(a), as might be expected. In no case did we find a correlation between filament formation and a low contact barrier.

In conclusion, there appears to be no connection between conductivity of an unformed Nb_2O_5 sample and photoemission at the Nb_2O_5-Bi contact. The location of filament formation is thus not determined by contact barrier lowering, at least to a resolution of 1μ.

References

1. R. B. Laibowitz, L. Esaki and P. J. Stiles, Phys. Let. 36A, 429 (1971).

2. T. H. DiStefano and R. B. Laibowitz, Bull. Am. Phys. Soc. 18, 133 (1973).

3. T. W. Hickmott and W. R. Hiatt, Sol. St. Electr. 13, 1022 (1970).

C. QUASIELASTIC ELECTRON SCATTERING IN EuO; A POSSIBLE EXPLANATION FOR OBSERVED "PARAMAGNETIC" SPIN-POLARIZED PHOTOEMISSION

D. E. Eastman

ABSTRACT: Photoemission energy distributions and yield measurements for (100)EuO show that "quasielastic" rather than inelastic electron scattering dominates the photoemission escape process for electrons excited $\lesssim$ 3.5 eV above threshold. In this "quasielastic" scattering regime (with a large effective escape depth ∿ 50-100 Å), it is suggested that the spin-polarization need not be conserved in the photoemission escape process, and that reported "paramagnetic" spin-polarized photoemission at 10°K is possibly due to quasi-elastic spin-flip scattering.

EuO is known as an ideal model Heisenberg ferromagnet and has been intensively studied due to its interesting magnetic, electrical, optical and photoemission properties[1-3]. EuO is unusual among the Eu-chalcogenides and other rare-earth chalcogenides in that it has a very low electron affinity ($\phi_A \simeq 0.6$ eV for (100)EuO[3]) together with a large band gap ($E_g \sim 4$ eV) between the valence p-bands and the bottom of the conduction band. This has the interesting consequence that quasi-elastic electron scattering, rather than the more usual inelastic pair-production electron scattering, dominates the photoemission escape process for emitted electron energies within $E_g - \phi_A \simeq 3.4$ eV of threshold. In this note we present photoemission energy distribution and quantum yield measurements for single crystal (100)EuO which show these scattering effects for excitations of both localized 4f-electrons and valence p-electrons.

Recently, interesting spin-polarized photoemission measurements[2] have been reported for single crystal (100)EuO and a surprizing result was obtained. Namely, the spin-polarization of photoemitted 4f electrons exhibited a "paramagnetic" behavior at ~ 10°K and did not saturate in a magnetic field up to ~ 25kOe, well above the bulk saturation field of ~ 8kOe. This behavior was attributed to a "paramagnetic surface sheet". The observed field-dependent spin polarization was attributed mainly to photoemission from this paramagnetic sheet (with conservation of spin-polarization), together with possible spin-disorder scattering of "bulk" photoelectrons by this sheet.

Based on our observation of predominant quasielastic electron scattering for energies involved in the spin-polarized photoemission experiments, an alternative explanation of the observed "paramagnetic" behavior is that spin-polarization is not conserved in the photoemission process for (100)EuO with $h\nu \lesssim 5$ eV. Namely, in the quasielastic scattering regime with its large effective escape depth (~ 50-100 Å), electrons undergo multiple scattering

before being emitted and can undergo significant spin-flip scattering via magnons, impurities, the surface, etc., as well as via a possible paramagnetic surface layer.

An energy level diagram[3] for (100)EuO is shown in Fig. 1. As seen, EuO has a very low electron affinity $\phi_A \simeq 0.6$ eV; a wide energy gap $E^p_{gap} \simeq 4$ eV between the valence 2p band and the conduction band. Consequently, electrons excited within $E^p_{gap} \simeq 4$ eV of the bottom of the conduction band cannot scatter via inelastic pair-production scattering,[4] and quasi-elastic electron scattering (phonons, etc.) is expected to dominate and be observable in photoemission energy distributions and quantum yield measurements. Characteristic "crossover" energies for excitations of 4f electrons $\left(E^{4f}_{cr}\right)$ and 2p electrons $\left(E^{2p}_{cr}\right)$ are shown in Fig. 1, above which inelastic scattering becomes dominant.

Photoemission energy distributions (PED's) illustrating the effect of quasielastic scattering on 4f- and 2p- electron emission are shown in Fig. 2. Photon energies just below and above the "cross over" energies $E^{4f}_{cr} \simeq 5$ eV and $E^{2p}_{cr} \simeq 8$ eV for 4f- and 2p- electron emission are shown. Energy distributions were measured for a (100)EuO single crystal of area ~ 1 cm^2 cleaved in situ ($p \lesssim 1 \times 10^{-10}$ Torr) using a retarding sphere as an energy analyzer[5]. The quantum yield per absorbed photon shown in Fig. 3 was determined by comparing with a calibrated photodiode. Corrections for the transmission of a LiF window and the reflectivity[6] of EuO have been made.

In Fig. 2, the PED for $h\nu = 4.9$ eV shows a broad structureless triangular shape extending from the vacuum level $E^* = 0$ up to the top of the 4f level at $E^* \simeq 4$ eV. A similar behavior has been observed for $2.8 \leq h\nu \leq 4.9$ eV. Then, for photon energies $h\nu \gtrsim E^{4f}_{cr} \simeq 5$ eV, a sharper peak showing the ~ 1.2 eV level width of the 4f level in EuO is seen to emerge. This is seen in the PED for $h\nu =$ 5.6 eV in Fig. 2. As shown in Fig. 2, a similar behavior is seen for 2p-band

EuO - ENERGY LEVEL DIAGRAM

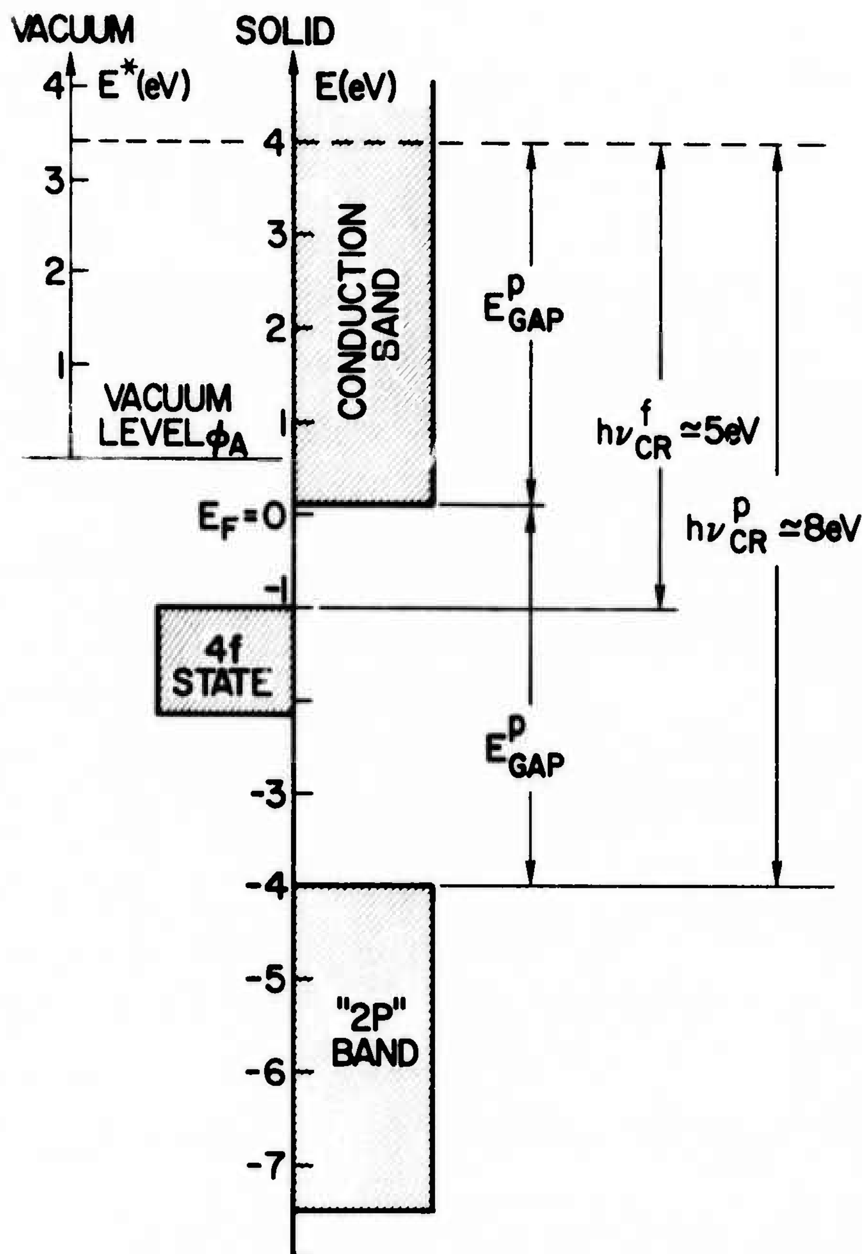

Fig. 1 Schematic energy level diagram for single crystal (100)EuO. The internal energy E is measured relative to the Fermi level near the conduction band minimum and the kinetic energy E^* is measured relative to the vacuum level. Localized 4f states (left side of ordinate) are distinguished from the valence- and conduction-band states.

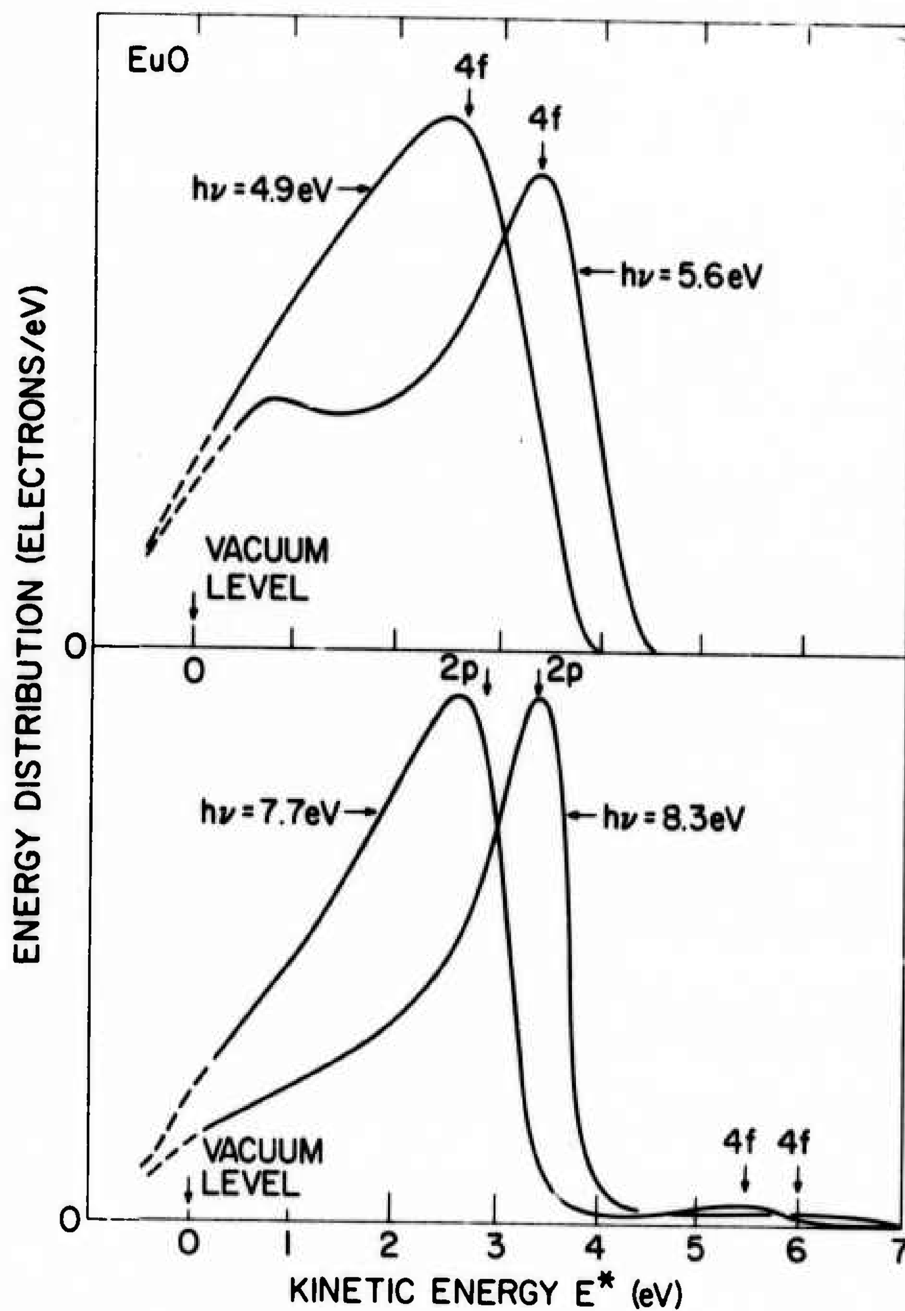

Fig. 2 Photoemission energy distributions (PED's) for (100)EuO. Kinetic energies E^* are measured relative to the vacuum level $E^* = 0$. Electron emission extends to energies below $E^* = 0$ due to edge effects of our EuO crystal, probably because of the low electron affinity $\phi_A \simeq .6$ eV.

emission. Namely, for $h\nu \lesssim E_{cr}^{2p} \sim 8$ eV (i.e. $h\nu = 7.7$ eV in Fig. 2), a broad structureless triangular shape extending from $E^* = 0$ to $E^* \simeq 3.5$ eV is seen. Then rather abruptly for $h\nu \gtrsim 8$ eV, a much sharper p-band emission peak develops (~ 0.8 eV wide for $h\nu = 8.3$ eV in Fig. 2). For both 4f- and 2p-electron emission, the sharp structures emerge when inelastic electron scattering becomes dominant. In this regime, electrons undergo large energy losses upon scattering and thus become separated from the primary emission of "unscattered" electrons which are related to band structure features. In contrast, when quasielastic electron scattering dominates ($E^* \lesssim 3$ eV in Fig. 2), scattered electrons only lose $\lesssim 0.1$ eV per collision and thus scattered electrons become indistinguishable from the "primary" electrons. The fact that no sharp structures are observed in the PED's for $E^* \lesssim 3$ eV indicates that these low energy emitted electrons have, on the average, undergone numerous "quasielastic" scattering events.

The quantum yield (Fig. 3) also illustrates the effect of quasielastic scattering. Namely, we expect a much shorter effective escape depth in the inelastic scattering regime (relative to the quasielastic regime) and thus a diminished quantum yield for $h\nu$ just above $E_{cr}^{4f} \simeq 5$ eV and $E_{cr}^{2p} \simeq 8$ eV. This behavior is seen in Fig. 3 as two pronounced dips in the yield at $h\nu \simeq 5.8$ eV and 8.5 eV, respectively.[7] Using the three-step model of photoemission[8], we can use the measured yield to make a rough estimate of the effective escape depth ℓ as follows. The yield is given as[8]

$$Y(\omega) \simeq \bar{T}_f(E^*) \cdot \frac{\alpha(\omega)\ell(E^*)}{1 + \alpha(\omega)\ell(E^*)} \cdot \Delta N(E^*)$$

where T_f is the free-electron escape probability, $\alpha(\omega)$ the absorption coefficient, $\ell(E^*)$ the effective escape depth, and $\Delta N(E^*)$ the appropriate fraction of electrons excited above the vacuum level. Using a reasonable

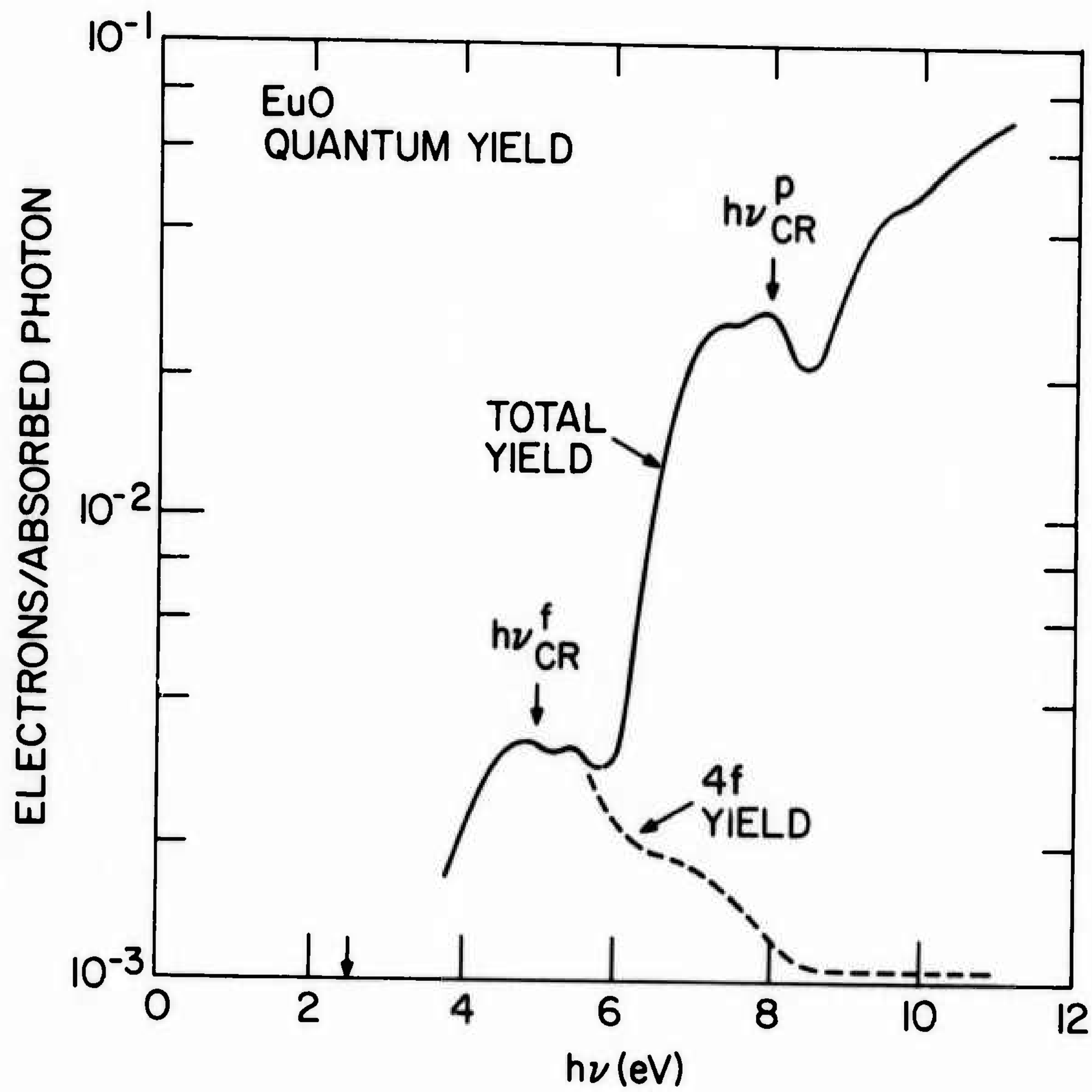

Fig. 3 Quantum yield for (100)EuO. The 4f-electron contribution to the total yield is shown by the dashed line.

inner potential of $V_i \underset{\sim}{\sim} 5$ eV, and the measured absorption coefficients[6] of $\alpha \sim 1 \times 10^5 cm^{-1}$ at 4 eV and $\alpha \sim 6\text{-}10 \times 10^6 cm^{-1}$ at $h\nu = 8$ eV, we estimate for both 4f-derived and 2p-derived electron emission an average effective escape depth $\bar{\ell}(E^*) \underset{\sim}{\sim} 50\text{-}100$ Å for electrons excited 1-3 eV above the vacuum level. This depth is much greater than is normally observed for metals (typically $5 \lesssim \ell \leq 20$ Å) such as Ni[9] and Ag[9].

Recently, interesting spin-polarized photoemission experiments have been reported[2] for (100)EuO which show an unexpected magnetic-field-dependent behavior above saturation ($H \underset{\sim}{\sim} 8$ kOe) at $\sim 10^o$K. These results have been interpreted as evidence of a paramagnetic surface sheet on EuO, possibly as thin as a few layers, which dominates the spin-polarized photoemission (with polarization conserved in the photoemission process). Our above-described measurements for EuO show that quasielastic scattering is predominant for photon energies used in the spin-polarized experiments[2] ($h\nu \lesssim 5$ eV) and that more than just the outer few layers (probably 50 Å-100 Å) contribute to the measured emission. Thus, while the cross-section for quasielastic non-spin-flip scattering is probably largest, quasielastic spin-flip scattering processes can likely occur (via magnons, bulk impurities, surface impurities, etc.) and the assumption of conservation of spin polarization is probably not valid. In this case, one need not postulate the existence of a paramagnetic surface sheet in order to explain observed field dependences above magnetic saturation. Namely, multiple spin-flip scattering in a magnetic field will yield a contribution to the spin-polarization P which varies roughly as $\Delta P \propto H/T$, and the cross-sections of various magnetic scatterers can be field-dependent. A paramagnetic surface layer might also be present, and in fact would be an effective spin-flip scattering mechanism. Quasielastic spin-flip scattering can also qualitatively explain the reported dependence of spin polarization on

photon energy (Fig. 1 in Ref. 2). Namely, quasielastic spin-flip scattering is expected to diminish (i. e. number of electron scattering events per emitted electron) with increasing energy. Thus the spin-polarization should be an increasing function of photon energy near threshold, as is observed. The large spin-polarization of La-doped EuO observed at low photon energies might be due in part to the impurity electrons (assumed ordered) having higher energy states than the 4f states and thus better preserving their spin-polarization upon escape.

In summary, we have presented data illustrating quasielastic and inelastic scattering processes exhibited by EuO. Reported spin-polarization photoemission experiments[2], together with our measurements, suggest that EuO exhibits interesting spin-flip electron scattering which warrants further study.

REFERENCES

1. S. Methfessel and D. C. Mattis, in Encyclopedia of Physics XVIII, Part 1, (Springer-Verlag, Berlin, 1968), pp 389-562.
2. K. Sattler and H. C. Siegmann, Phys. Rev. Letters 29, 1565 (1972).
3. D. E. Eastman, J. Appl. Phys. 42, 1396 (1971).
4. We disregard inelastic scattering via the 4f electrons (which have a gap $E^f_{gap} \simeq 1.1$ eV) since they are very localized and consequently have small inelastic-scattering cross sections.
5. D. E. Eastman, F. Holtzberg and S. Methfessel, Phys. Rev. Letters 23, 226 (1969).
6. G. Güntherodt and P. Wachter, Magnetism and Magnetic Materials-1972, AIP Conf. Proc. Vol. 10 (1973). G. Güntherodt, P. Wachter and D. M. Imboden, Phys. Kondens. Materie 12, 292 (1971).
7. Such a quasielastic scattering behavior is well known for wide band gap insulators such as the alkali halides.
8. D. E. Eastman, in Techniques of Metals Research VI, E. Passaglia, editor, Interscience (1972).
9. D. E. Eastman, unpublished.

III. INSTABILITIES ASSOCIATED WITH METAL-GLASS INTERACTIONS

In electronic device technology,there will be increasingly strong emphasis on utilization of multilayer glass-metal structures. The severe reliability problem in these structures are associated mainly with the instability of the glass layer; both electrical and mechanical failure modes have been encountered which lead to failure of the dielectric. In general, structural instabilities in the glass have been found to start with localized crystallization or phase separation initiated by a small amount of surface impurity such as Na and P ions, or by a direct interaction with a metal layer on the glass. We are particularly concerned with metal or impurity induced crystallization which occurs at temperatures below those used in semiconductor processing. In one study, we have found that the common dopant phosphorus, will induce crystallization even at temperatures down to 525°C. In this report, results of our investigation in two areas are presented: Crystallization of SiO_2 by P ions and a glass-vanadium interaction.

We found that when phosphorus is diffused into a clean film of SiO_2, it enhances crystallization of the oxide film. The enhanced crystallization has been found to occur at a temperature as low as 525°C. Using the autoradiographic method to map out P distribution after the diffusion, we have associated the high P concentration regions with crystallites in the SiO_2. Diffusion of P at 525°C leads to the formation of α-quartz crystals. These crystals transformed to α-cristobalite after a subsequent heat treatment at 1200°C for 25 hours. The low temperature crystallization of α-quartz could be induced by

the easy nucleation of compounds such as $P_2O_5 \cdot SiO_2$ and $P_2O_5 \cdot 2SiO_2$, which are typically used on the surface of quartz in semiconductor technology.

The enhanced crystallization cannot be understood without a detailed study of the P diffusion in SiO_2 films. We found that the P diffusion catalyzed a localized amorphous-to-crystalline transformation in the initially amorphous films thereby creating rapid diffusion paths at the interfaces between the crystalline islands and the surrounding amorphous matrix. The composite nature of the experimentally determined P^{32} penetration profiles confirmed that structural defects (i.e. crystallites) were contributing to the flux of P through SiO_2 film in addition to that anticipated from ordinary diffusion in the amorphous matrix. The reaction rate theory seems to explain readily the temperature activated behavior for diffusion in glass, and the free volume the extremely small preexponential factor. It seems that P might migrate with a surrounding tetrahedra of xoygen atoms as a complex of $(PO_4)^+$. The complex moves through the network by successively breaking and remaking Si-O bonds. The strength of a saturated Si-O bond (∿2 eV) is close to the activation energy of 1.8 eV that we measured experimentally. Diffusion down the crystalline-amorphous interface is characterized by an activation energy (1.0 eV) which is very close to the 1.8 eV found for the amorphous network. This suggests that migration along the interface may be due to a similar bond breaking process as in the network except that the average free volume in the interface is much larger than in the amorphous network. This explains

why the grain surface diffusion of phosphorus is much faster than bulk diffusion.

Glass-vanadium interation. Most conducting metals interact rather weakly with glass as shown by their poor adhesion to the glass surface. The adhesion can be greatly improved by first depositing a very thin underlayer of Cr, Ti or V on the glass surface. The interaction between these metals and glass develops the strong bonding needed for adhesion, but at the same time it endangers the stability of the glass by decomposition or recrystallization. We found that the metal vanadium and oxidized SiO_2 film reacts at temperatures above 800°C. The reaction decomposes SiO_2 and results in the formation of vanadium-rich silicides: V_3Si and V_5Si_3. The V_3Si forms as a continuous layer, has a β-tungsten structure and becomes superconducting at about 15°K. We note that silicide formation are commonly observed in contact reaction between metals and silicon, however, the silicides formed by contact reaction are generally silicon-rich rather than metal-rich. Thus the glass-metal reaction has introduced new information about the formation of compounds.

A. CATALYZED CRYSTALLIZATION AND TRANSFORMATION IN SiO_2 THIN FILMS

E. I. Alessandrini and D. R. Campbell

Although it is known that silica films grown under contaminating circumstances contain crystallites,[1] it wasn't until recent diffusion studies[2] that evidence was obtained which indicated a catalytic influence on the amorphous-to-crystalline transformation. The rapid diffusion mode of P^{32} in SiO_2 films was correlated with the existence of islands of crystalline SiO_2 in the amorphous film matrix. In this study, using electron microscope and diffraction techniques, the effect of phosphorus diffusion on the crystalline transformation was investigated. Diffusion heat treatments using P^{32} were carried out as a function of varying times and temperatures and the results were compared with similar treatments in undiffused SiO_2 films. It was found that devitrification, in the case of P^{32} diffused films, occurred at temperatures as low as 525°C. The undiffused films did not show any phase change up to temperatures as high as 1200°C for 25 hours. The crystallization was dependent on the presence of the impurity and three distinct phases were observed and identified in the P^{32} diffused films. By selected area electron diffraction the crystal phase which appeared after 100 hrs @ 525°C was identified as $2SiO_2 \cdot P_2O_5$. With an additional heat treatment at 1200°C for 25 hours, the low temperature α quartz phase and the high temperature α cristobalite phase were observed. The experimental evidence suggests that the P rich phases may be the nuclei which catalyzed the crystalline behavior and growth of SiO_2.

Introduction

Considerable interest has been shown in thermally grown silicon oxide films from the standpoint of studying device oriented properties as well as structural properties. Since it is a common material for surface passivation and insulation, defects in oxide films have been reported[3-6] and are generally believed to be small crystallites formed at localized nucleation centers, such as impurities, during the early stages of growth. However, the type of impurities and the conditions which induce crystallization in the amorphous films are not clearly understood.

This paper describes the structural aspects of phase transformations in SiO_2 films when P^{32} is diffused in the amorphous oxide. The purpose of this investigation was to determine the effect of the impurity as a function of time and temperature and compare the results with similarly treated undiffused films. It will be shown that the transformation from the amorphous to a crystalline phase was dependent on the catalytic behavior of the phosphorus.

Experimental Procedure

Thin films of amorphous SiO_2 were prepared by thermal oxidation and grown to 1000Å in thickness on silicon wafers (Czocharlski, p-type, boron doped, 2 ohm-cm) one inch in diameter and a (100) orientation. Two series of experiments were carried out: (1) Phosphorous was diffused into the amorphous films using P^{32} isotope at two different times and temperatures (525°C for 100 hrs. under a low P pressure followed by 25 hrs. @ 1200°C anneal in vacuum) and (2) undiffused films given the same heat treatments. The source of the radioisotope was neutron activated, red phosphorous

powder which was encapsulated together with the SiO_2/Si samples in evacuated silica ampoules. At the temperatures of treatment the phosphorous source was completely vaporized.

Upon completion of the heating cycles, autoradiographs were made of the P^{32} diffused samples (Fig. 1), and structural defects were suggested by the appearance of numerous, small areas of high P^{32} concentration. Some of these wafers were diced and portions which showed high P^{32} concentrations as well as portions showing the least structural defects were prepared for examination in an electron microscope. In addition, undiffused wafers were also diced and back jet-etched, using a $9:1HNO_3:HF$ etchant, for structure observation using electron diffraction and microscopy techniques.

Experimental Results and Discussion

Prior to heat treating the SiO_2/Si transmission and reflection electron diffraction patterns were obtained. The results indicated that the 1000Å SiO_2 film was amorphous, and the electron micrographs confirmed this. After P^{32} was diffused at 525°C for 100 hrs. samples were taken, using the autoradiographs, from heavily concentrated P^{32} areas as well as from areas of the lowest concentration in the amorphous films. Electron micrographs and selected area diffraction patterns from these areas showed the onset of crystallization (Fig. 2), and the areas of heavy concentration of the radio active isotope were completely crystalline while the least concentrated areas showed crystallites in an amorphous matrix. The particles, shaped as spherulites, can be seen in dark field (Fig. 3) when a reflection of the diffraction pattern is used for image formation.

The electron diffraction patterns showed random orientation of the

P^{32}-DIFFUSED SiO_2 WAFER

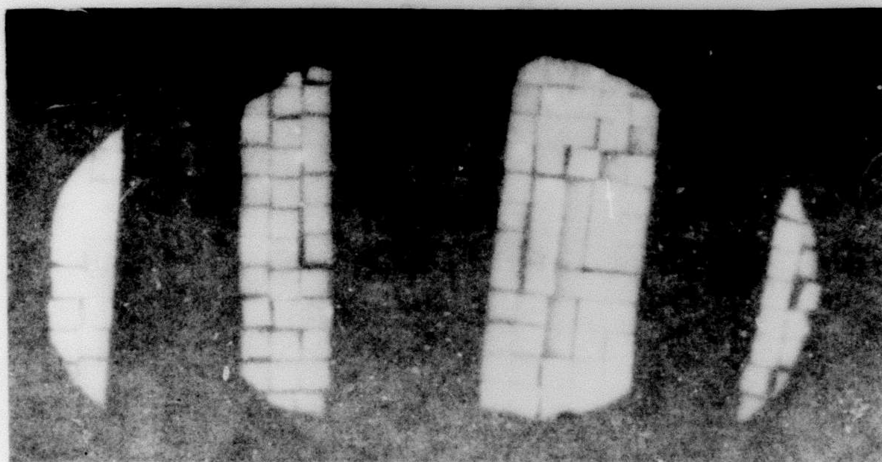

WAFER DICED

Fig. 1. Autoradiographs of P^{32} diffuse SiO_2/Si wafer heat treatment 100 hrs. @ 525°C.

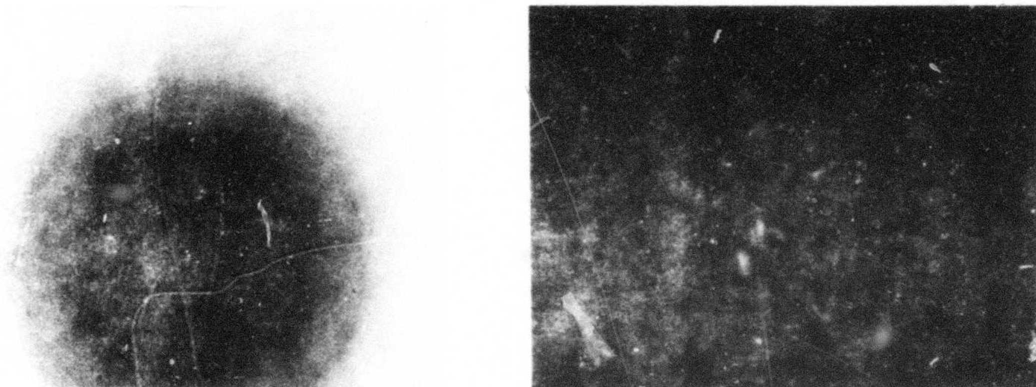

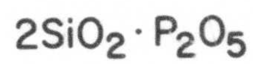

Fig. 2. P^{32} diffused SiO_2 film on (100) Si wafer. 525°C 100 hrs. $2SiO_2 \cdot P_2O_5$

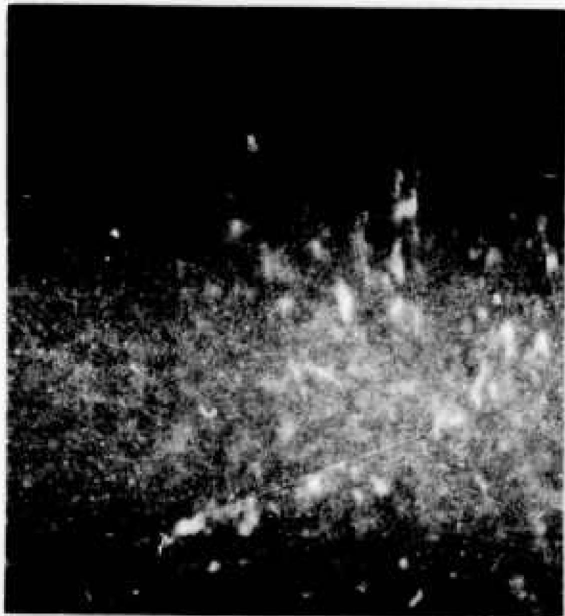

BRIGHT FIELD

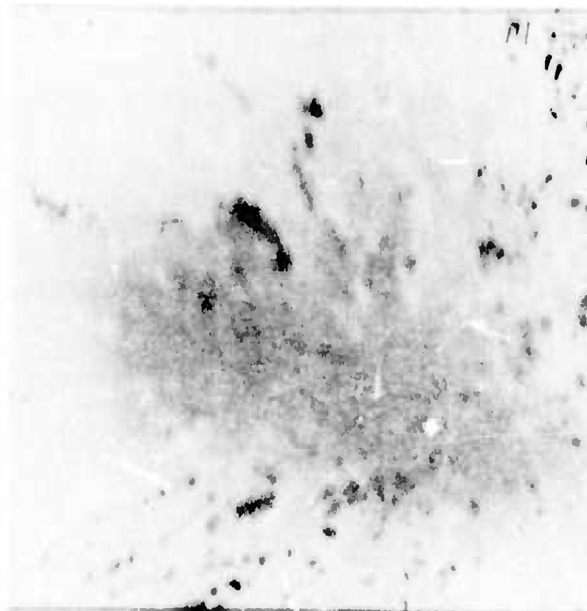

DARK FIELD

Fig. 3. P^{32} diffused SiO_2 film on (100) Si wafer. 525°C 100 hrs. Bright field Dark field.

crystallites. The data was analyzed, and the structure was identified as that of $2SiO_2 \cdot P_2O_5$. According to the phase diagram (Fig. 4) the appearance of this structure seemed reasonable.

In the second portion of this investigation, these films were given an annealing treatment at 1200°C in evacuated silica ampoules for 25 hours. A transformation was apparent from both the electron diffraction patterns and micrographs (Fig. 5). The analysis of the diffraction data proved that two polymorphic SiO_2 structures were now present. They were the low temperature form α quartz as well as the high temperature form α cristobalite (Fig. 6).

The undiffused films were given heat treatments of similar times and temperatures. Results were obtained using the identical techniques for sample preparation and examination as in the case of the diffused films. They showed that no crystalline phase developed (Fig. 7).

In this portion of the study, the primary concern was the correlation between impurity and its effect on the formation of crystallites of SiO_2 in the amorphous film matrix. No attempt was made to analyze the steps that constitute the chemical reaction which led to crystalline compound formation. Rather, we simply note that the phase segregation after the heat treatment @ 525°C for 100 hrs. as shown by varying P^{32} concentrations in the autoradiographs and determined by electron diffraction suggests evidence of a first stage catalyzed crystallization. This stage is characterized by the appearance of phosphosilicate compounds which in turn become the nuclei for the subsequent growth of crystalline phases of SiO_2.

Heating these films in vacuum an additional 25 hrs. @ 1200°C resulted

TABLE I

PHASE IDENTIFICATION OF CRYSTALLITES FORMED AFTER P^{32} WAS DIFFUSED @ 525°C FOR 100 HRS

Observed d(Å)	Observed I	$2SiO_2 \cdot P_2O_5$ (Ref. 7-8) d(Å)	hkil	I/I
		8.06	0003	
		6.55	$10\bar{1}1$	34
5.905	S	5.93	$10\bar{1}2$	19
4.018	S	4.024	0006	44
3.948	VS	3.941	$10\bar{1}5$	52
		3.932	$11\bar{2}0$	
3.550	VS	3.533	$11\bar{2}3$	100
3.401	M	3.364	$20\bar{2}1$	17
		3.277	$20\bar{2}2$	6
		3.078	$10\bar{1}7$	7
2.823	M	2.812	$11\bar{2}6$	36
		2.783	$20\bar{2}5$	52
2.669	VW	2.684	0009	6
2.549	W	2.559	$21\bar{3}1$	17
		2.517	$21\bar{3}2$	9
2.430	W	2.423	$20\bar{2}7$	3
		2.367	$21\bar{3}4$	18
2.281	S	2.272	$21\bar{3}5$	14
		2.270	$30\bar{3}0$	
		2.259	$20\bar{2}8$	
		2.216	$11\bar{2}9$	17
2.188	W	2.185	$30\bar{3}3$	8
		2.090	$10\bar{1},11$	5
2.057	W	2.063	$21\bar{3}7$	11
1.972	WM	1.977	$30\bar{3}6$	25
1.913	VVW	1.910	$22\bar{4}3$	4
		1.883	$31\bar{4}1$	3
		1.845	$20\bar{2},11$	3
1.800	W	1.792	$10\bar{1},13$	5
		1.792	$11\bar{2},12$	
1.756	W	1.766	$22\bar{4}6$	12
		1.761	$21\bar{3},10$	
		1.759	$31\bar{4}5$	
1.700	VW	1.685	$40\bar{4}2$	4
1.657	W	1.670	$21\bar{3},11$	10

Intensities-Relative

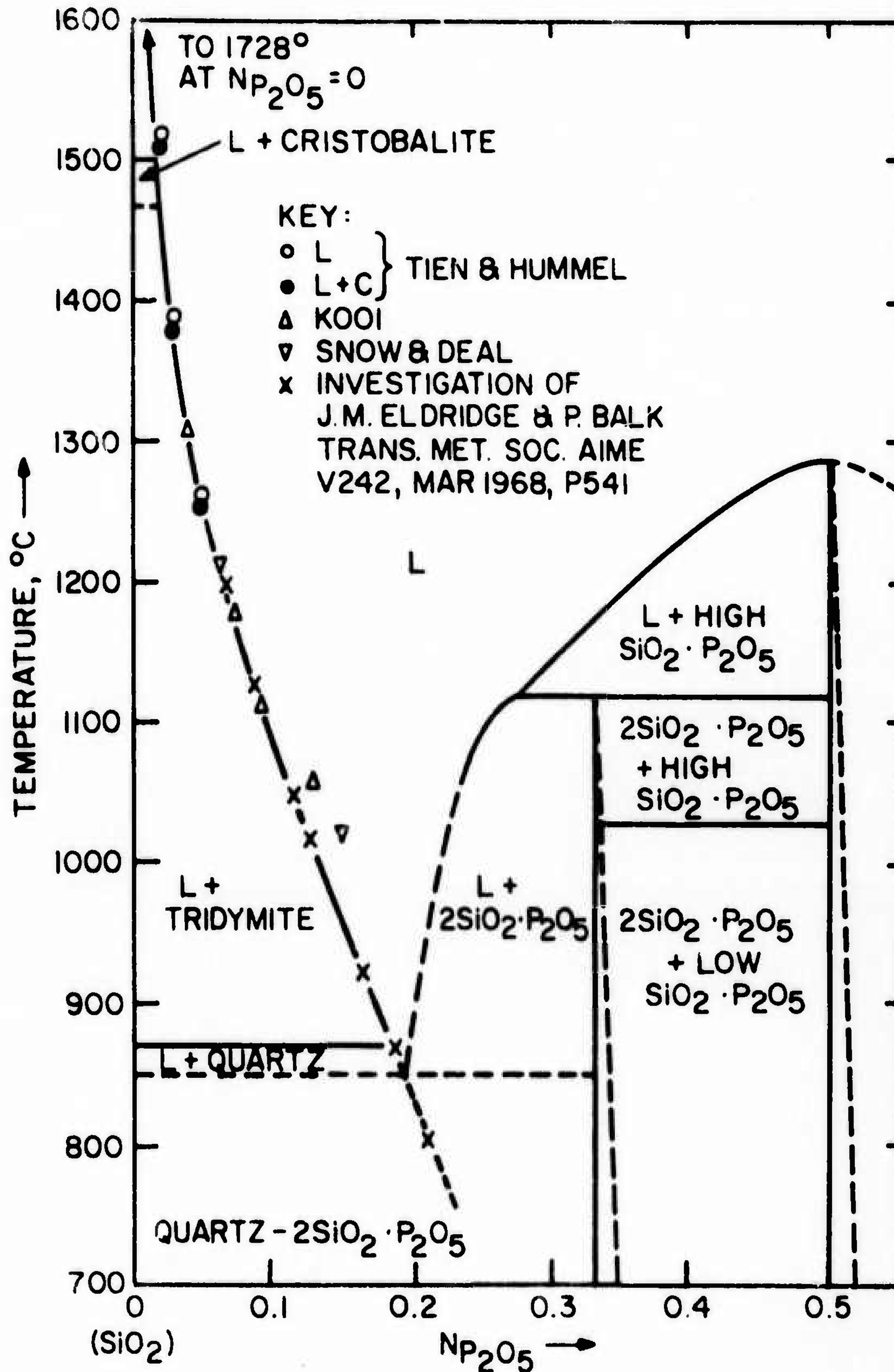

Fig. 4. Correspondence of PSG composition with the maximum solubility of crystalline SiO_2 in phosphosilicate liquid solution. Phase diagram from R. Y. Tien and F. A. Hummel, J. of Amer. Ceram. Soc., 1962, Vol. 45 422-424.

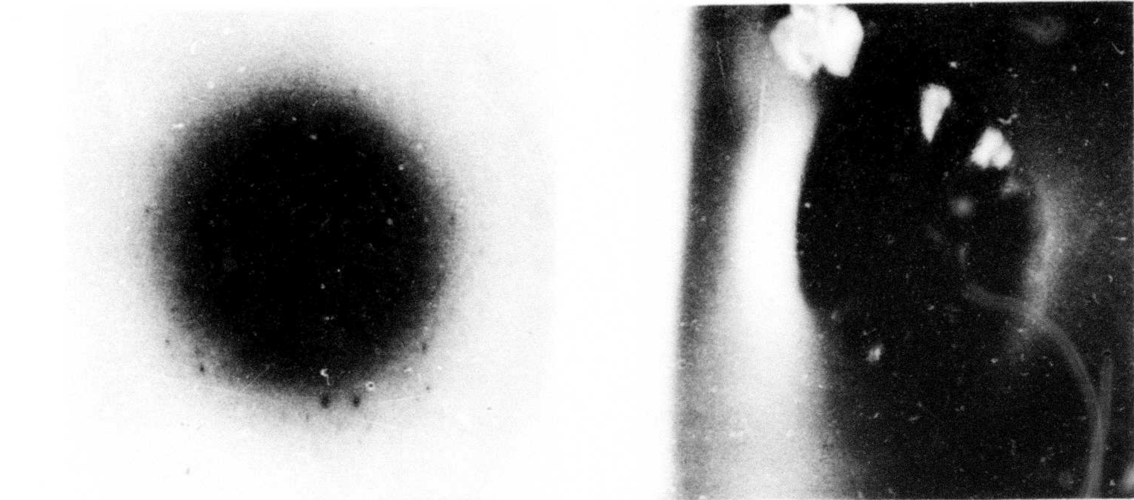

α QUARTZ
α CRISTOBALITE

Fig. 5. P^{32} diffused SiO_2 film on (100) Si wafer. 525°C 100 hrs. 1200°C 25 hrs.

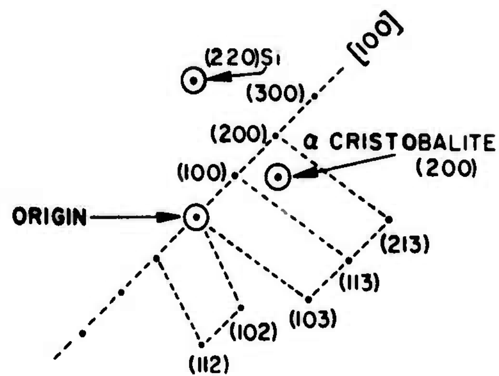

Fig. 6. Transmission electron diffraction.

Pattern showing crystals of α quartz and α crystobalite.

Schematic diagram.
Indexed α quartz reflections represented by dots.

Type $11\bar{2}1$ Planes ⊥ to beam
$11\bar{2}5$ Planes ‖ and horizontal to beam
$10\bar{1}0$ Planes ‖ and vertical to beam

a and c axis tilted 24° to each other.

AMORPHOUS SiO_2

Fig. 7. Undiffused SiO_2 film on (100) Si wafer
Heat treated 525°C 100 hrs.
1200°C 25 hrs.

in the formation of crystallites of SiO_2. Both the low temperature form α quartz (stable under 573°C), and the high temperature form α cristobalite (Fig. 8) were present. The major constituent was α quartz. Since it is known that the polymorphic phase transformation of SiO_2 is very sluggish, it seems likely that continued annealing for long periods of time @ 1200°C would result in the complete phase change to α cristobalite.

In summary, our work shows that catalyzed crystallization does occur when P rich crystallites form, and their formation is directly dependent on the sufficient transport, by diffusion, of P into localized areas of the amorphous SiO_2 films. In this study, the presence of a gas phase provided for the rapid transport of P^{32} at the film surface. The formation of $2SiO_2 \cdot P_2O_5$ in turn catalyzed the SiO_2 phases. That crystallization did not occur in the uniformly P-doped samples of Sugano et al[5] does not seem surprising since diffusion in the solid amorphous phase is probably too low to allow for the formation of suitable nuclei.[7]

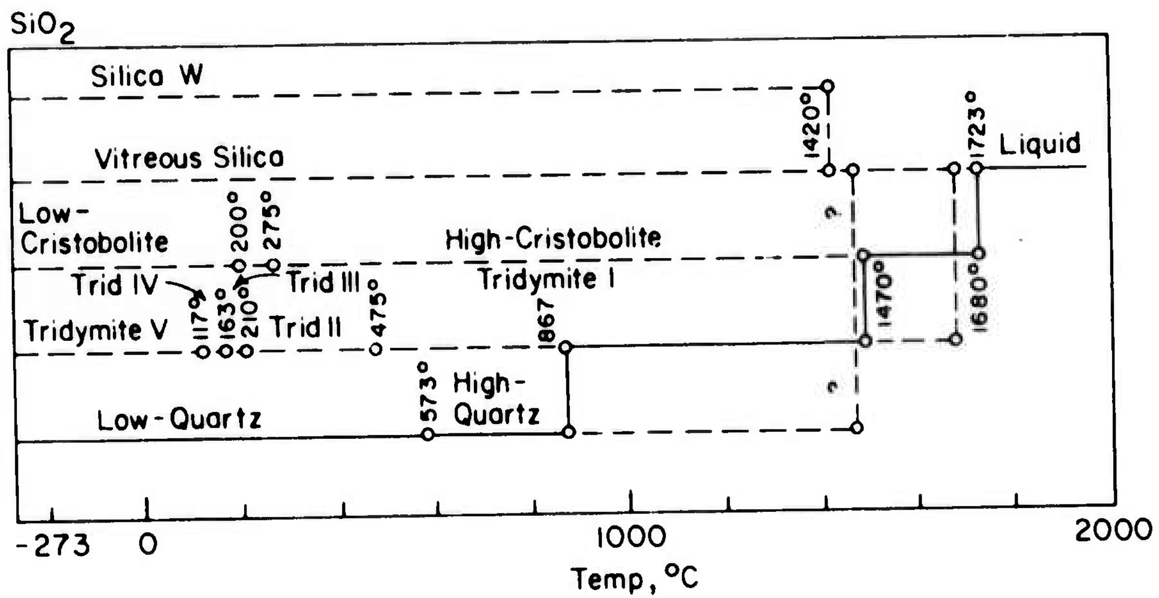

Fig. 8. SiO_2; stability relations at atmospheric pressure ordinate is undefined measure of stability. Solid lines represent stable stabe; dashed lines represent metastable state. Ref. R. B. Sosman, Trans. Brit. Cerm. Soc., 54, 663 (1955).

References

1. N. Nagasima and H. Enari, Japanese J. of App. Phys., 10, 441 (1970).

2. D. R. Campbell, E. I. Alessandrini, K. N. Tu, and J. E. Lewis, "Phosphorus Diffusion and Catalyzed Crystallization in Amorphous Films of SiO_2," presented Electrochem Soc. Meeting, Florida, October 8-13, 1972, Extended Abstract No. 252.

3. N. Nagasima, Japanese J. Appl. Phys., 9, 879 (1970).

4. A. N. Knopp and R. Stickler, Electrochem. Tech., 2, 298 (1964).

5. T. Sugano and K. Hou, K. Kudo and N. Hishinuma, Japanese J. of App. Physics, 7, 715 (1968).

6. A. N. Knopp, Electrochem. Tech., 5, 37 (1967).

7. D. R. Campbell, E. I. Alessandrini, K. N. Tu, and J. E. Lewis, "Phosphorous Diffusion in Partially Crystallized Films of SiO_2," to be published.

B. PHOSPHORUS DIFFUSION IN PARTIALLY CRYSTALLIZED FILMS OF SiO_2

D. R. Campbell, E. I. Alessandrini
K. N. Tu and J. E. Lewis

A study of the diffusion of P into thin SiO_2 films on Si was undertaken in order to assess both the fundamental and technological significance of an anomolous, rapid diffusion mode reported by Li et al..[1] Diffusions were performed over a wide range of temperature (1100°C - 300°C) and time (1 hr. - 21 days) using diffusion sources prepared from neutron-activated red phosphorus powders (P^{32} radioisotope). It was found that diffusion anneals in P vapors catallyzed a localized amorphous-to-crystalline transformation in the initially amorphous films thereby creating rapid diffusion paths at the interfaces between the crystalline islands and the surrounding amorphous matrix. The composite nature of the experimentally determined P^{32} penetration profiles confirmed that structural defects (i.e., crystallites) were contributing to the flux of P through SiO_2 films in addition to that anticipated from ordinary diffusion in the amorphous matrix. The diffusion parameters for both processes have been determined and interpreted using a combination of reaction-rate and free volume theories after Macedo and Litovitz.[2]

1. Li Ke-Chang, Xue Shin-Yin, Zhu Shong-de and Huang Yun, Acta Physica Sinica 20, 496 (1965).

2. P. B. Macedo and T. A. Litovitz, J. Chem. Phys. 42, 245 (1965).

I. INTRODUCTION

Although the diffusion of P in amorphous SiO_2 films has frequently been investigated[1-5], there has been considerable discrepancy in the measured values of diffusivity and fundamental uncertainty concerning the nature of the diffusion process[3]. In view of the widespread use of P in Si device technology, we felt it imperative to clarify the question of P diffusion in amorphous SiO_2 films by undertaking a further study. Our results provide new and more readily interpretable parameters for diffusion in the amorphous matrix and identify a hitherto unrecognized diffusion process in "amorphous" films involving migration along the interface between crystallized islands and the amorphous matrix which surrounds them. The localized crystallization of the film is, itself, attributed to a catallytic influence of the diffusant.

II. EXPERIMENTAL

Our study of the diffusion of P into thin (.5 μ) amorphous films of SiO_2 (steam grown) on (100) Si wafers (B-doped, 2 Ω-cm) was performed over a wide range of temperature (1100°C - 300°C) and time (1 hr.-21 days) using P^{32} isotope. The source of the radioisotope was neutron-activated, red phosphorus powder which was encapsulated, together with the SiO_2/Si samples in evacuated silica ampoules. At diffusion temperatures the phosphorus source was completely vaporized. Serial sectioning (∿ 50 - 200 A°/ section) was performed by timed etching of the amorphous SiO_2/Si with a diluted "P"-etch[6], the rate for which was established with the aid of ellipsometry measurements of thicknesses successively removed. The activity of each section so taken was determined by liquid scintillation methods.

III. RESULTS AND DISCUSSION

A. Evidence of Crystallization

The resulting diffusion profiles exhibited a composite shape as illustrated in Fig. 1 which suggested that structural defects (i.e., crystallites) were contributing to the flux of P through the SiO_2 films in addition to that anticipated from ordinary diffusion in the amorphous matrix. The existence of structural defects was further suggested by the appearance of numerous, small areas of high P concentration on autoradiographs of the diffused films (Fig. 2). Reflection electron diffraction from the surface of the same films showed the presence of a crystalline phase (α-crystobalite) which apparently resulted from a catalytic influence of P, as samples given simulated diffusion anneals without P showed no evidence of crystallization (Fig. 3). Subsequently, some diffused wafers were diced and portions with structural defects, as determined from the autoradiograph, were back-etched and examined by electron tranmission and diffraction microscopy techniques. It was determined that the defects were crystallized islands, surrounded by amorphous material[7]. In fact, many were large enough (several microns in diameter) to be easily seen by optical microscopy (Fig. 4).

The density of crystallites necessary to account for the level of P activity seen in the tailing regions of our profiles is approximately $10^4/cm^2$ assuming the individual crystals are a few microns in diameter. Confirmation of the above density and size of defects by optical microscopy is possible for samples diffused at 700°C and above. At lower temperatures, the presumed smaller size of the crystallites (i.e., submicron) precluded observation by optical means.

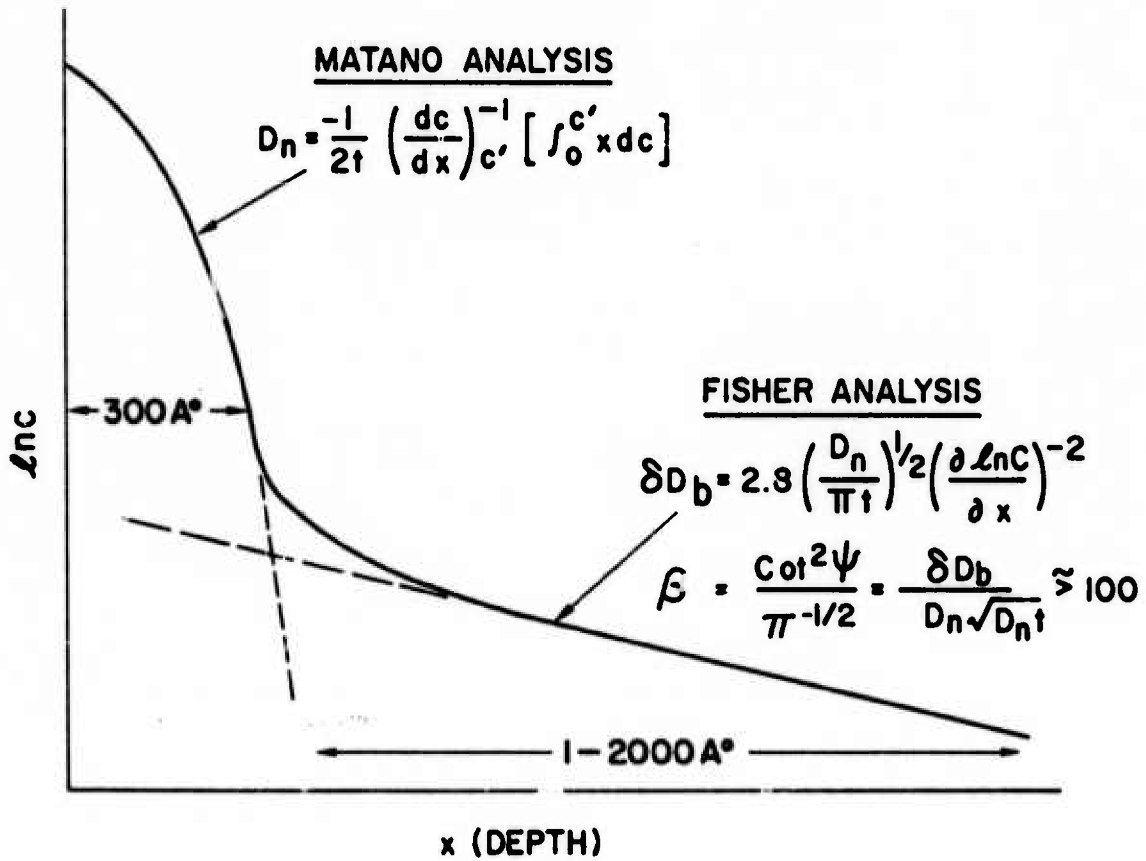

Fig. 1. Composite penetration profile illustrating the influence of both network (D_n) and boundary (D_b) diffusivity.

AUTORADIOGRAPHS

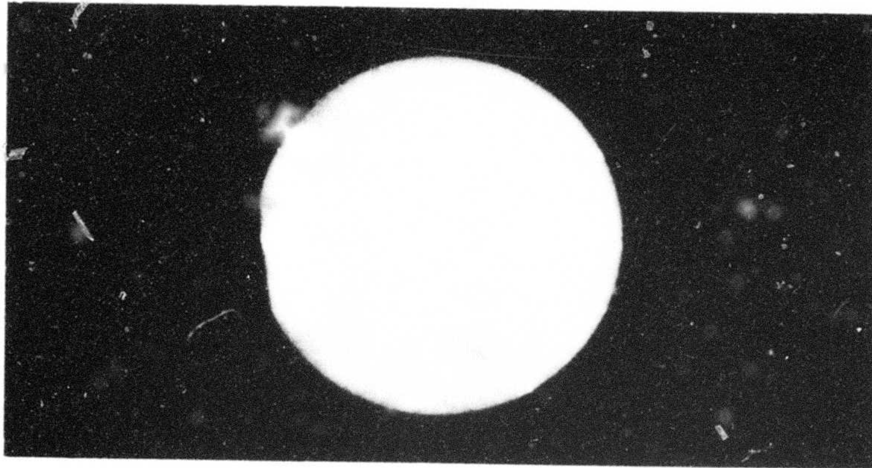

P^{32} DIFFUSED SiO_2 WAFER

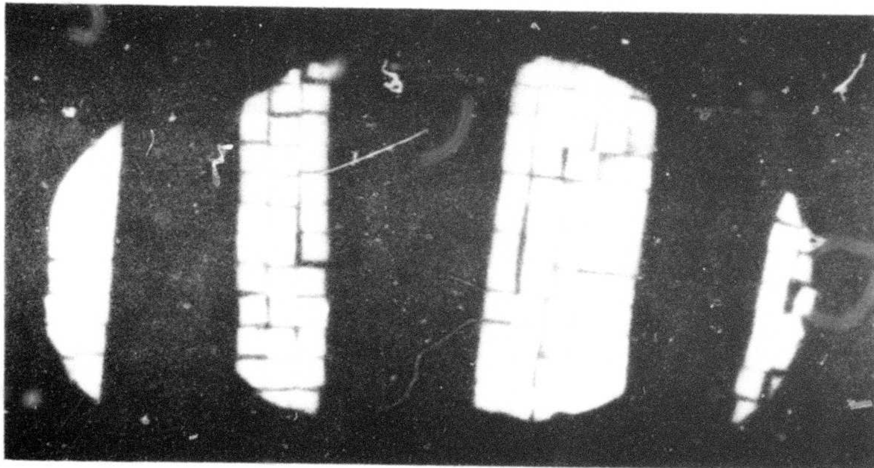

WAFER DICED

Fig. 2. Autoradiograph of SiO_2 film on Si diffused with radioactive P.

REFLECTION ELECTRON DIFFRACTION

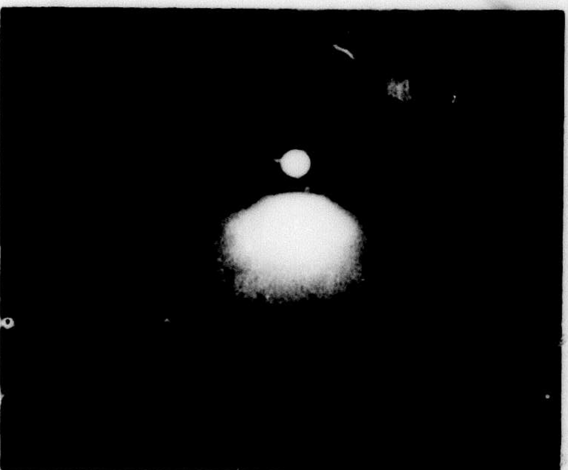

SiO_2 FILM ON (100) Si
UNDIFFUSED
700°C 92 HRS.

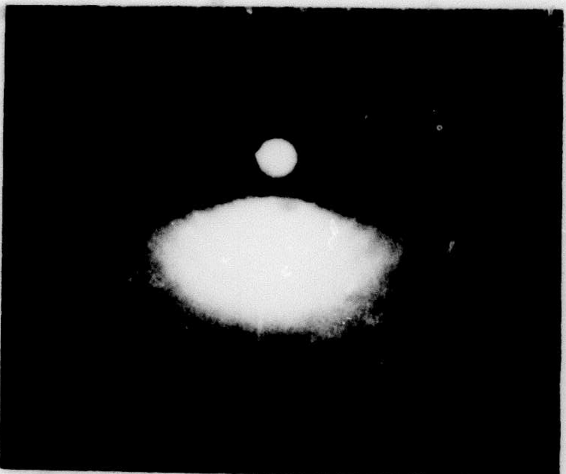

SiO_2 FILM ON (100) Si
P^{32} DIFFUSED
700°C 92 HRS

Fig. 3. Reflection electron diffraction patterns from undiffused and diffused films. The presence of α-crystobolite is indicated in the pattern for the diffused film.

Fig. 4. Crystalline island seen in a P-diffused SiO_2 film.

P. Penetration Profiles

On the basis of these experimental evidences, and with the aid of Fig. 5, we can explain the results of our profiling as follows: In the vicinity of a crystallized island a potentially rapid diffusion path exists at the interface between crystalline and amorphous regions. The diffusivity in this boundary (D_b) may be several orders greater than the diffusivity in the undisturbed amorphous network (D_n). Therefore, depending where on the film surface the P^{32} vapors impinge, there will occur different modes of diffusion. One mode is diffusion directly into the amorphous matrix giving rise to the first portion of our profile (i.e., nearest the surface) where the concentration falls smoothly from its high initial value until it intercepts the linear portion at a depth of a few hundred Å. In Fig. 5 this diffusion is responsible for the iso-concentration contours that are parallel to the specimen surface as occur at some distance from the crystalline region. A typical experimental profile is shown in Fig. 6 where D_n has been determined by the Matano method, (see Fig. 1), in order to test for a possible concentration dependence. (Indications are that D_n is not appreciably concentration-dependent at concentrations $< 10^{20}/cm^3$; however, more extensive data would be needed before rigorous conclusions could be drawn.) In Fig. 7 we show the values of D_n corresponding to a phosphorus concentration [P] of $\sim 10^{19}/cm^3$ plotted against 1/T together with data from two other investigations[2,3]. The second diffusion mode, as evidenced by the linear portion of the profile (Fig. 1), is due to a combination of rapid diffusion down the crystalline-amorphous boundary with eventual lateral migration into

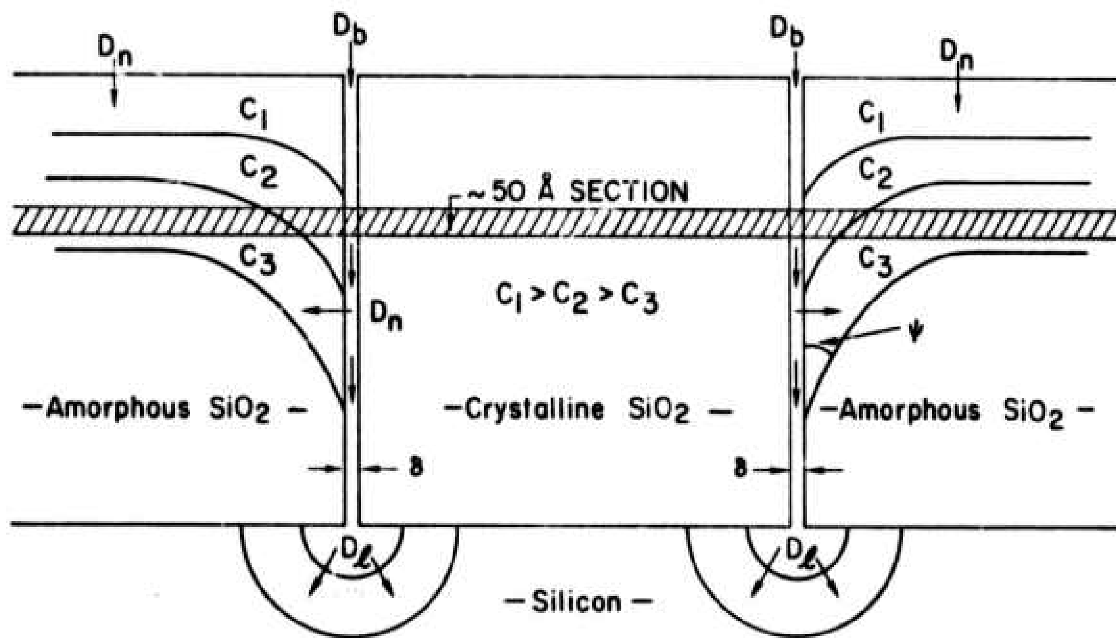

Fig. 5. Isoconcentration contours for P in SiO_2 film in the vicinity of a crystallized island.

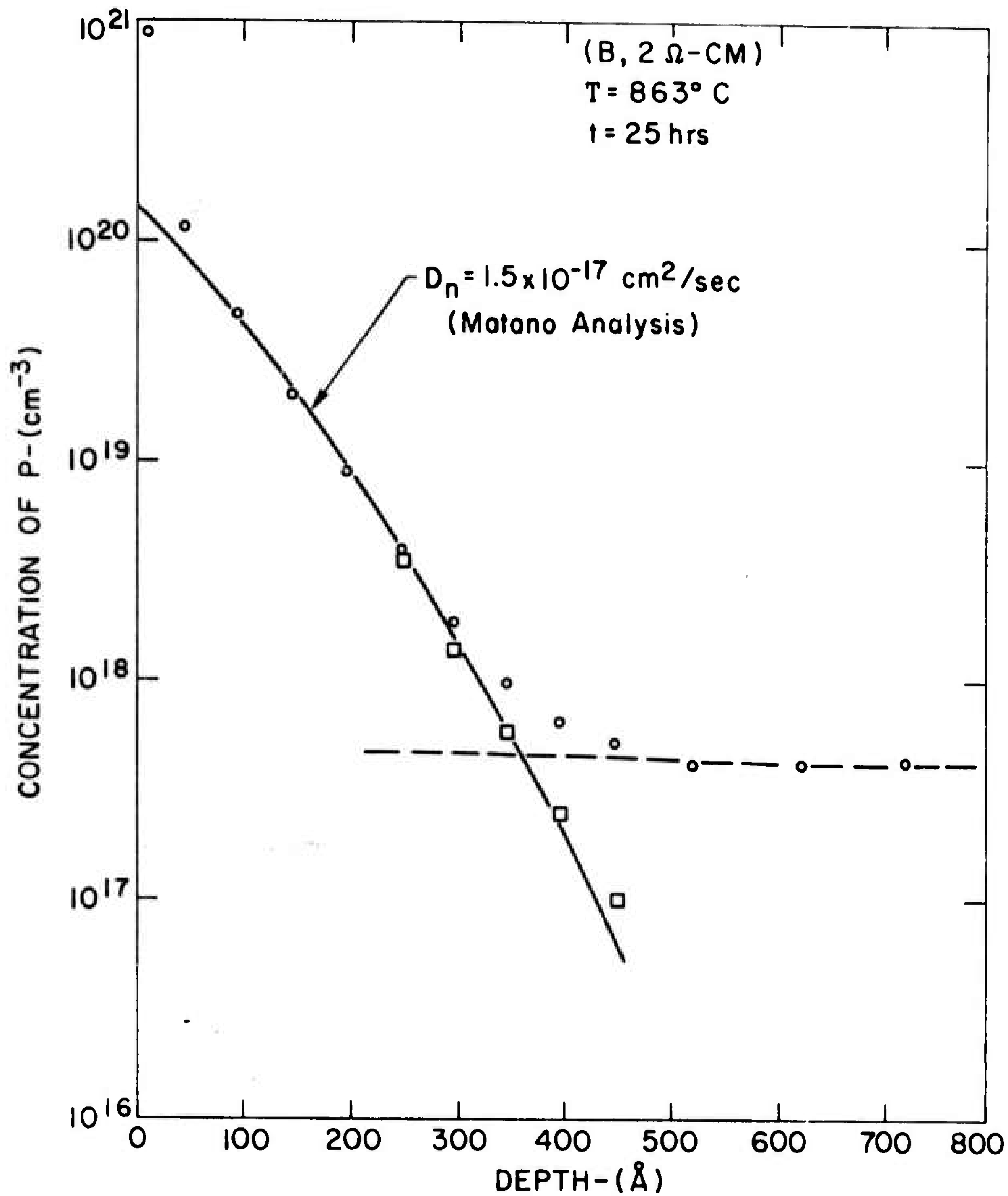

Fig. 6. Phosphorus penetration profile due to diffusion in the amorphous network.

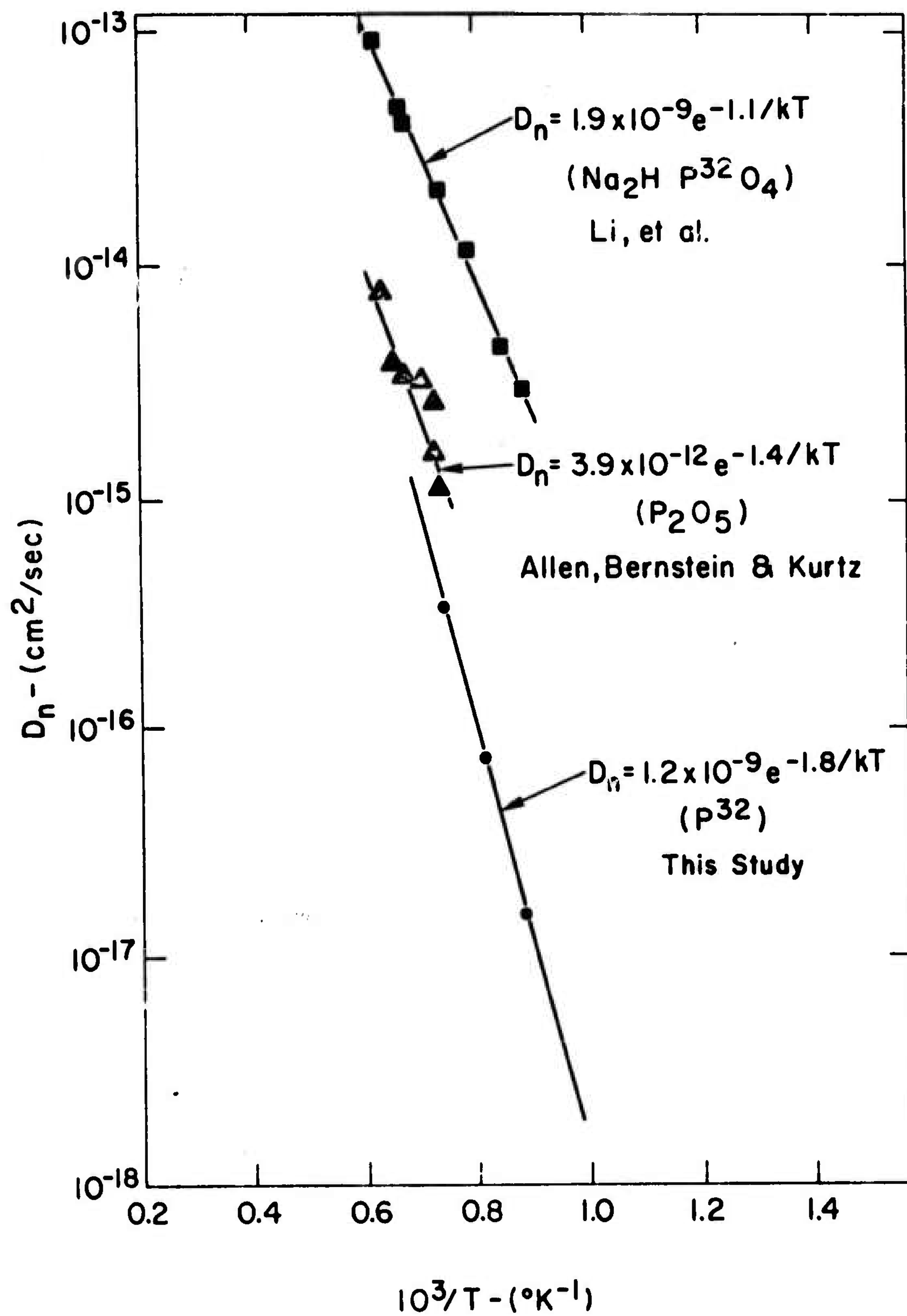

Fig. 7. log D_n vs. 1/T for diffusion of P^{32} in SiO_2 films.

the amorphous network and away from the boundary. (We are neglecting the lateral migration into the crystallized region which should not appreciably affect our results owing to the anticipated lower diffusivity of P in this region.) For our purposes, an approximate analysis of boundary diffusion by Fisher[8] is adequate for analyzing profiles such as those shown in Fig. 8 and the measured values δD_b are shown plotted vs. 1/T in Fig. 9. (The width of the boundary is designated by δ.) In Fig. 5 this second diffusion mode is responsible for the bending of the isoconcentration contours down at the boundary which they all intercept at some finite angle ψ, depending on the diffusion conditions (Fig. 1). As an added note, some of the P atoms starting out in the boundaries travel directly down to, and become incorporated in, the underlying Si where their accumulation is sufficient to noticeably enhance the exposure of the autoradiograph in places corresponding to the defect locations (Fig. 5 and Fig. 2).

C. Diffusion Mechanisms

Basically, two distinctly different types of diffusion behavior are expected for dilute impurities in directionally bonded, amorphous materials. The first and typically more rapid mechanism involves migration through the interstices of the structure while the second and slower mechanism involves migration along the structure itself. Examples of the former are the diffusion of inert gases[9,10] and alkali and noble metal impurities[11,12] in SiO_2 and possibly noble metal impurities[13,14] in chalcoginide glass films. Examples of the latter are the diffusion of various network forming ions in SiO_2 films - for which there exists a

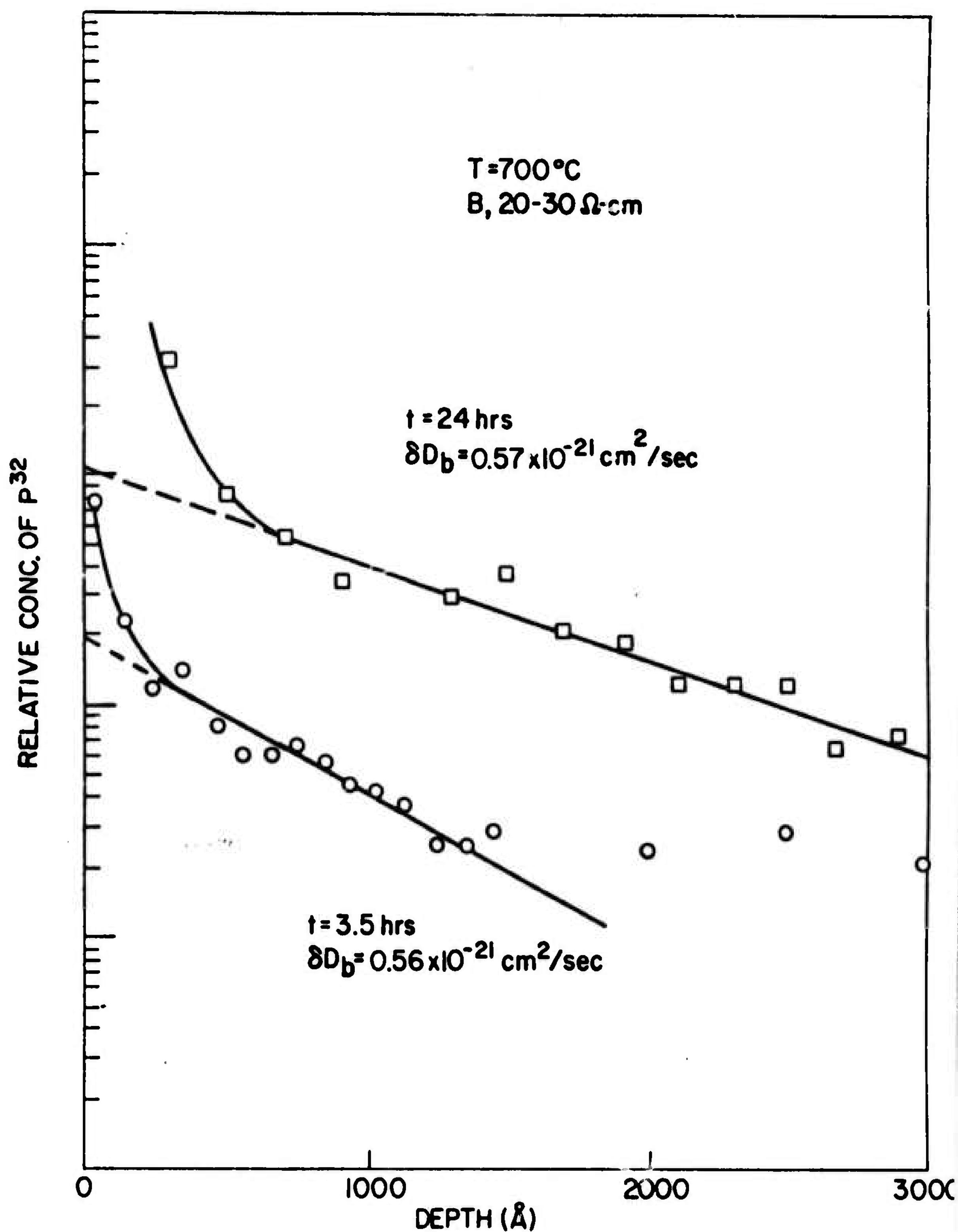

Fig. 8. Phosphorus penetration profiles due to diffusion along the crystalline-amorphous boundary. The close agreement between δD_b values for two different times substantiates the boundary diffusion model (Ref. 7).

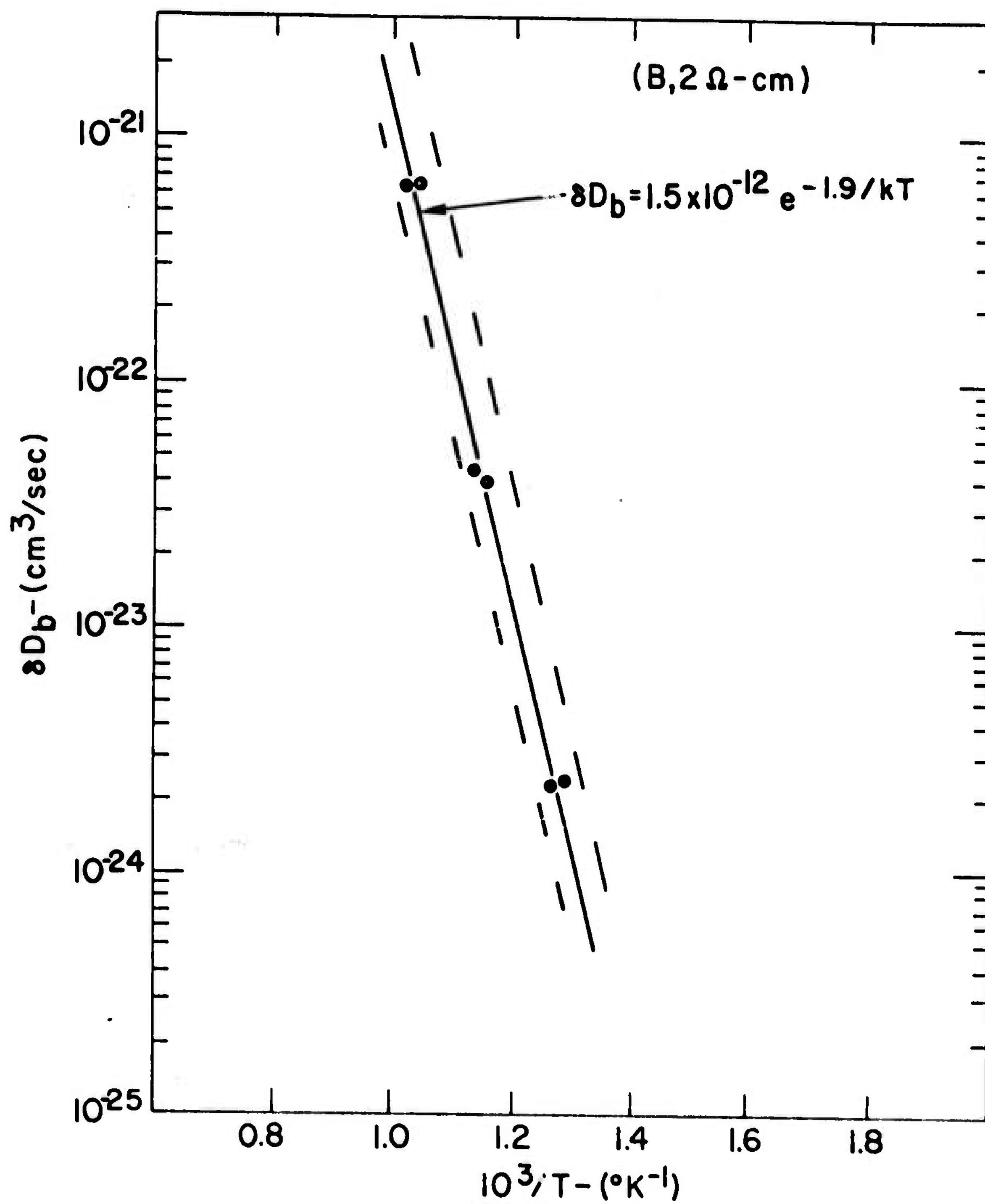

Fig. 9 log δD_b vs. $1/T$ for diffusion of P^{32} in SiO_2 films.

a considerable amount of data[15] as many of these ions are also common dopants for Si (e.g., Al, B, P. As, Sb).

As the motion of ions within the structure is analogous to self diffusion, atomic models proposed for viscosity in liquids and glasses should be applicable. Microscopic models of atomic mobility in liquids around or above the glass transition temperature[16-19] usually emphasize the free-volume concept which says that the chance of a net displacement of an atomic species will be related to the probability that an opening of sufficient size is near it. However, the free volume model by itself is inadequate to describe diffusion in some liquids[19] and in glasses well below the glass transition temperature, since no provision is made for an energy barrier in the atomic jump process. (By definition, "free-volume" can be rearranged without incurring any change of enthalpy of the system.) In contrast, an Arrhenius behavior for diffusion in glasses, including amorphous SiO_2 films, is typically observed[15]. Macedo and Litovitz[20] have proposed an expression for viscosity which combines both the free-volume and rate-reaction approaches and demonstrated the ability of such an expression to describe viscosity in many types of liquids and notably in the network liquid SiO_2. This hybrid equation of Macedo and Litovitz was subsequently placed on a more firm, statistical mechanical basis by H. S. Chung[21]. Using the Stokes-Einstein equation, Macedo and Litovitz then gave an expression for diffusivity which is,

$$D = D_o e^{-(\gamma V_o/V_f + E/kT)}$$

where γ is a numerical factor ($.5 \leq \gamma \leq 1$) which corrects for overlap in the summation of free-volume, V_o is the atomic volume associated with the diffusing specie (or complex) and V_f is the average atomic free volume. The second exponential term is the usual Boltzman factor occurring in a diffusion coefficient where E is the activation enthalpy for motion and the other terms have their usual meaning. In the context of the Macedo-Litovitz model, the pre-exponential term, D_o, can be expressed in terms of temperature independent parameters appropriate to the liquid state. However, in view of the "solid-like" nature of SiO_2 at the relatively low temperatures of our diffusions, we choose to express D_o in a manner appropriate for diffusion in an isotropic solid, i.e.,

$$D_o = 1/6\ \nu\ a^2\ f\ C_v\ e^{\Delta S_m/k}$$

where ν and a are vibration frequency and jump distance respectively, f is the correlation factor, C_v is the concentration of oxygen vacancies and ΔS_m the entropy of motion of a PO_4 complex. Obviously, the inclusion and definition of certain terms above depends on our idea of how diffusion proceeds which we will now describe:

When a P atom is incorporated into a tetrahedrally coordinated oxide glass, it is thought[22] to form bonds with at most 3 bridging oxygen ions, leaving its remaining 2 valence electrons to be associated with one non-bridging oxygen, which results in a PO_4 complex that is electrically neutral. When an oxygen vacancy occurs on a site immediately adjoining the complex, diffusive transport can occur, in part, by a sequence of bond breaking and remaking steps such as is shown schematically

below:

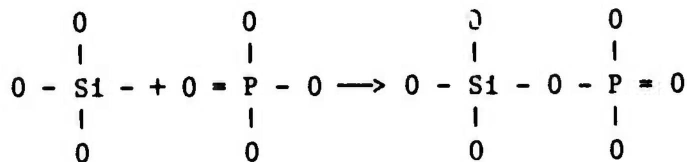

In this picture, the required activation energy for diffusion will be approximately ~ 2 eV,[23] (we observe E = 1.8 eV, see Fig. 7) since each step in the sequence requires the breaking of only one Si-O bond. (Here we are assuming that the concentration of oxygen vacancies is largely determined by the presence of structural discontinuities (or impurities) which are not thermally equilibrated and that C_v is, therefore, independent of temperature.) It is easy to envision, from the above schematic, that merely relocating one bond will not result in a significant amount of translation of the center of gravity of the impurity complex unless there is also a concomitant, liquid-like motion throughout a small region surrounding, and including, the complex. This motion would be limited largely by the availability of free volume and the degree to which the otherwise "intact" bonds can be bent or stretched throughout the activated region. What is not so clear, however, is that breaking of only one bond suffices to initiate such diffusive transport - rather, this is an assumption which is compatible with the experimental findings.

Another simplifying assumption is to set $\Delta S_m \simeq 0$. Owing to the rather loose structure of the SiO_2 network, any change of vibration frequency about the saddle point may not be as important here for describing the motion process as it is for "interstitial" inert gas atoms in SiO_2.[9,10] (In this latter case, the experimental evidence suggests that diffusing

atoms must squeeze through a relatively small opening when passing from one "interstitial" site to the next.) Since our complex is assumed to be electrically neutral, we will exclude the possibility of binding between an impurity complex and an oxygen vacancy, which eliminates the need to consider the complex and temperature dependent correlation effects which characterize impurity diffusions in materials where such binding occurs. Unfortunately, a correlation factor for network diffusion in amorphous oxides has not been determined but we may take it as unity without introducing serious error. The quantities ν and a^2 are estimated at 10^{-12}/sec and 10^{-15} cm^2 respectively and the ratio V_o/V_f can be taken as 6.3 if we allow the use of a molecular-to-free volume ratio derived fron densification measurements[24]. We also assume that V_f is independent of temperature, following the treatment of Macedo and Litovitz[20] for liquid SiO_2. Finally, the overlap parameter, γ, is taken as unity. With the aid of the above mentioned values and our experimentally determined value for $D_o e^{-\gamma V_o/V_f}$, (1.2×10^{-9} cm^2/sec), we calculate C_v to be roughly 4×10^{-3} cm^{-3}. This density appears reasonable considering both the amorphous structure and the low oxygen pressure in our diffusion capsules ($\sim 10^{-3}$ mm Hg).

In comparison with other works[2,3], our values of D_n appear to be the lowest reported (See Fig. 7) which we explain as follows: The data of Allen, Bernstein and Kurtz[2] is close, but distinctly higher, than the extrapolated fit through our own data points. These authors did not profile their SiO_2/Si specimens, but instead deduced D_n from profile measurements of the underlying Si, with the aid of a two-phase diffusion model. A consequence of this is that their diffusivities are characteristic of

P concentrations which excede $10^{20}/cm^3$ whereas our measurements are at substantially lower concentrations ($\sim 10^{19}/cm^3$). This may be an indication of a concentration dependence in D_n, which, in a macroscopic sense, can arise from a decrease in viscosity accompanying high P concentrations. However, concentration effects are probably not the only reason for the very large discrepancy between our data and that of Li _et al_.[3]. The introduction of net-work modifying Na^+ ions from their disodiumphosphate source is more likely the cause. The well-known affinity of Na^+ ions for P in phosphosilicate glasses, for example, suggests that the high diffusivity they see is due to some enhancement effect of Na on P movements.

Diffusion down the crystalline-amorphous interface is characterized by an activation energy (1.9 eV) which is very close to the 1.8 eV found for the amorphous network. This suggests that migration along the interface may be due to a similar bond breaking process as in the network. When, δ, the boundary width ($\delta \sim 10^{-7}$cm) is factored out of the combined pre-exponential factor ($\delta\ D_b^{\circ} \sim 1.5 \times 10^{-12} cm^3/sec$) we obtain D_b° of $\sim 1.5 \times 10^{-5}\ cm^2/sec$. One interpretation of this 4 order increase in pre-exponential factor for boundary diffusion is that both the oxygen vacancy concentrations and the average free volume in the boundary are increased substantially over that in the network. Although obviously speculative, this interpretation is qualitatively compatible with the customary notion that interface regions are loosely structured. Of course, we recognize that considerable error may occur in δD_b due to scatter in the measurement and possibly to the continued nucleation and growth of crystallites during diffusion. (The latter situation would invalidate Fisher's analysis which presumes stable boundaries.) Fortunately, the change in the slope of our

profiles with time follows Fisher's kinetics (Fig. 8) which implies that the extent of crystallization of our films becomes stabilized in times which are short compared with the durations of our diffusions.

IV. CONCLUSIONS

The application of the combined reaction-rate and free volume theories of atomic motion[20] to the diffusivity of P in the amorphous SiO_2 network has provided for a reasonable explanation of both the experimentally determined "pre-exponential" factor (i.e., $D_o e^{-\gamma V_o/V_f}$) and the activation energy (E) as derived from our Arrhenius plot (Fig. 7). On the strength of this, we feel there is good reason for assuming that P diffuses through the amorphous SiO_2 network not as an individual atom or ion but instead as a complex of P surrounded by a tetrahedra of O atoms. We realize, however, that before a critical evaluation of our model can be made, some additional experimental evidence would be necessary. For example, the effects of stress (or variation in density) and stoichiometry on the diffusivity of network forming ions in SiO_2 films would yield important information on the roles of free-volume and oxygen vacancies, respectively, in the diffusion process but unfortunately such measurements present formidable experimental difficulties. Also, refinements in the model such as allowing for some energy to rearrange neighboring SiO_4 tetrahedra during the diffusive motion of a PO_4 complex or to redistribute "free-volume"[19] would be desirable but the overall precision of our experimental data and that of others[15] for the very slowly diffusing network forming ions does not warrant the incorporation of further refinements at present.

Finally, from a practical standpoint, the formation of crystallites such as we have seen in a diffusion mask during P diffusion (or in an SiO_2 layer during PSG deposition) will leave the underlying Si susceptible to P penetrations in localized areas[25] where such unintentional doping may be undesirable. At first sight, it seems unlikely that a network forming ion like phosphorus should catalyze crystallization especially in view of the negative results of Sugano et al. who looked for evidence of crystallization in P-doped oxides[26]. However, analogous crystallization effects have been attributed to the presence of As (also a network forming ion) in arsinosilicate glasses[27] and the reason cited was that As_2O_5 formed distinct compounds with SiO_2 which may have provided nuclei for the subsequent growth of crystalline SiO_2. In our case, compounds such as $P_2O_5 \cdot SiO_2$ or $P_2O_5 \cdot 2\,SiO_2$, which are known to occur from phase segregation in phosphosilicate glass films[28], are possible candidates for such nuclei[7]. It seems likely that crystalline areas in films may also act as sites for accumulation of undesirable metallic ions such as Na, but unfortunately our efforts to see such an effect using Na^{22} tracer and autoradiography techniques were inconclusive due to sensitivity problems.

ACKNOWLEDGMENT

The authors are particularly indebted to R. MacInnes for diffusing and profiling the specimens and to R. Robinson for autoradiography with tagged Na. The authors wish also to extend their appreciation to Dr. E. Bassous, Mrs. D. Bauer and Mr. J. A. Kucza for advice and assistance in sample preparation, and to Drs. D. Gupta, A. Mayadas and R. Rosenberg

for many helpful discussions.

This work is supported in part by ARPA Contract No. F19628-73-C-006 administered by AFCRL.

References

1. C. T. Sah, H. Sello and D. A. Tremere, J. Phys. Chem. Solids 11 288 (1959).

2. R. B. Allen, H. Bernstein and A. D. Kurtz, J. Appl. Phys. 31 334 (1960).

3. Li Ke-Cheng, Xue Shin-Yin, Zhu Shong-de and Huang Yun, Acta Physica Sinica 20 496 (1965).

4. Y. Watanabe and M. Yoshida, Jap. J. Appl. Phys. 6 410 (1967).

5. M. L. Barry, J. Electrochem. Soc. 117 1405 (1970).

6. After W. Pliskin, IBM, GPD, East Fishkill.
The etch was prepared as follows, 15 ml HF, 10 ml HNO_3, 3 ℓ H_2O.

7. E. I. Alessandrini and D. R. Campbell (next paper, this journal).

8. J. C. Fisher, J. Appl. Phys. 22 74 (1951).
Fisher's method is considered accurate provided the parameter β (Fig. 1) is $\sim$ 100 or greater, which was the case for our diffusions. Our expressions for δD_b and β differ by factors of 2 and 1/2, respectively, from their usual forms since we can have leakage from the interface in only one direction, i.e., into the amorphous material. The correction factor 2.8 is taken from N. A. Gjostein, in Techniques of Metals Research edited by R. A. Rapp (Interscience, N. Y. 1970, p. 447).

9. W. G. Perkins and D. R. Begeal, J. Chem. Physics 54 1683 (1971).

10. K. N. Woods and R. H. Doremus, Phys. Chem. Glasses 12 69 (1971).

11. G. H. Frischat, J. Am. Ceram. Soc. 51 528 (1968).

12. R. H. Doremus, Phys. Chem. Glasses 10 28 (1969).

13. L. A. Freeman, R. F. Shaw and A. D. Yoffe, Thin Solid Films 3 367 (1969).

14. S. Maruno, T. Yamada, M. Noda and Y. Kondo, Japan J. Appl. Phys. 10, 653 (1971).

15. A recent summary of diffusion in SiO_2 films has been given by M. Ghezzo and D. M. Brown, J. Electrochem. Soc. 120, 146 (1973).

16. M. H. Cohen and D. Turnbull, J. Chem. Phys. 31 1164 (1959).

17. D. Turnbull and M. H. Cohen, J. Chem. Phys. 34 120 (1961).

18. D. Turnbull and M. H. Cohen, J. Chem. Phys. 52 3038 (1970).

19. J. Naghizadeh, J. Appl. Phys., 35 1162 (1964).

20. P. B. Macedo and T. A. Litovitz, J. Chem. Phys. 42 245 (1965).

21. H. S. Chung, J. Chem. Phys. 44 1362 (1966).

22. For a discussion of the structure of phosphorous based glasses see J. M. Stevels, The Structure and Physical Properties of Glass, Handbuch Der Physik XIII, p 534 (S. Flügge, 1962).

23. E. W. Sucov, J. Amer. Ceram. Soc. 46 14 (1963).

24. J. D. Mackenzie, J. Amer. Ceram. Soc. 46, 461 (1963).

25. The inhomogeneities seen in the diffusion masking properties of SiO_2 films for P by Fränz and Langheinrich could well be due to crystallization. (I. Fränz and W. Langheinrich, Solid State Electronics, 14 835 (1971).

26. T. Sugano, K. Hoh, K. Kudo and N. Hishinuma, Jap. J. Appl. Phys. 7 715 (1968).

27. M. Ghezzc and D. M. Brown, J. Electrochem Soc. 120 110 (1973).

28. P. F. Schmidt, W. van Gelder and J. Drobek, J. Electrochem. Soc. 115 79 (1968).

C. INTERACTION OF V WITH BARE AND OXIDIZED Si WAFERS*

by

K. N. Tu
J. F. Ziegler
C. J. Kircher

IBM Thomas J. Watson Research Center
Yorktown Heights, New York 10598

ABSTRACT: Formation of vanadium silicides by the interactions of vanadium with bare and oxidized Si wafers have been studied by both x-ray diffraction and He ion backscattering techniques. X-ray diffraction was used to identify phases and ion backscattering to profile compositional changes. In the case of V on Si, the silicide VSi_2, which is a silicon-rich phase, was found to form at temperatures from 600°C to 1000°C. In the case of V on SiO_2, reactions took place only at temperatures above 800°C and the reaction products were identified to be V_3Si, V_5Si_3 and V_2O_5. Both V_3Si and V_5Si_3 are vanadium-rich phases and the V_3Si that we found was a continuous layer between the substrate and the other two phases, and became superconducting at about 15°K.

*This work was supported in part by ARPA Contract No. F19628-73-C-0006 administered by AFCRL.

Recently, there were two reports[1,2] on the interaction of vanadium with vycor silica for the purpose of fabricating the superconducting phase V_3Si (Tc = 17°K) in a wire form that can be used to transmit power. High transition temperture superconductors are also important for cryogenic electronic circuitry, for example, as ground planes for Josephson junction circuitry. For these applications it is necessary to have the superconductor in the form of planar thin films. We have studied the reaction of V thin films on Si and SiO_2 surfaces in an attempt to make V_3Si in a planar film. In this letter we present our preliminary results of the interactions of V with bare and oxidized Si wafers. We find the V_3Si phase by reacting V with SiO_2, yet the reaction of V with the bare Si produced only the VSi_2 phase.

In addition to the above application, this work introduces new information relating to several recent studies of metal/silicon[3-5] and metal/oxide[1,2] interactions and rates of new compound formation.

Vanadium films of 3200 Å thickness were deposited at a rate of about 300 Å/min by electron gun evaporation onto bare and oxidized silicon wafers maintained at room temperature. Before the deposition, the vacuum evaporation chamber was about 10^{-7} torr. The bare silicon wafers were (100) oriented. The oxidized Si wafers had an oxide thickness of 5400 Å. The surface of the wafers was carefully cleaned before the deposition.

After the V deposition the samples were heat treated in a resistance furnace contained a He atmosphere in the temperature range from 600 to 1000°C for various periods of time, from 15 minutes to several hours. The He was filtered for oxygen by passing it through a 900°C Ti bed before it

entered into the furnace. The oxygen partial pressure in the furnace is estimated to be only about 10^{-9} torr. Both Seemann-Bohlin x-ray diffraction[6] and 2 MeV He ion backscattering[7] techniques were used to analyze the heat treated samples. The diffraction was used to identify phases and to characterize their structures. The backscattering was used to profile compositional change and to measure reaction rates.

The interaction of V and Si was found to be much simpler than that of V and SiO_2, and will be presented first. For samples of V on Si, we found the formation of VSi_2 phase in all heat treatments above 600°C. Figure 1 shows superimposed ^4He backscattering partial spectra from V on Si samples after various anneals. To first order, the spectra show a concentration versus depth profile of the V layer, with the film surface lying on the right. The spectra show how the lower V concentration, corresponding to V in VSi_2, starts at the back edge of the film and proceeds towards the surface. This diffusion limited reaction is similar to that found previously for Pd, Ti[3], and Hf[8] on silicon. The X-ray diffraction pattern of the reacted sample showed 12 reflections and all of them can be indexed in accord with ASTM diffraction cards #13-260 as reflections from the phase VSi_2. No preferred orientation is indicated by their relative intensity ratios.

Analysis of the backscattering spectra was carried out in a manner described in Ref. 8. We find that the compound phase VSi_2 forms with an activation energy of 2.9eV and a diffusion constant of 2.9×10^{-15}, 1.9×10^{-14} and 1.3×10^{-13} cm^2/sec at 600, 650 and 700°C, respectively.

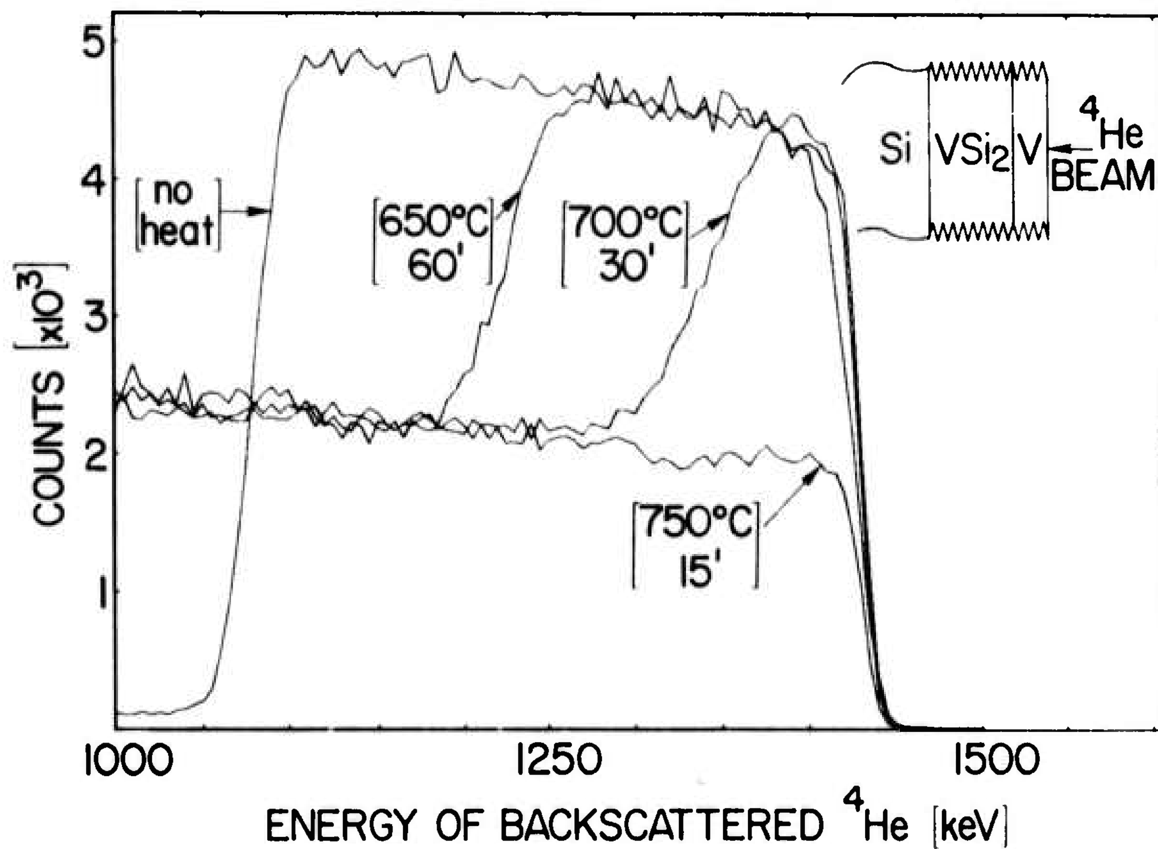

Figure 1

A portion of the ^{4}He backscattering spectra from heat treated samples of V on Si. Shown is the V peak, and its alteration during various anneal cycles. The lowest level, (700°C - 15 minutes) indicates a V concentration corresponding to VSi_2. This compound was verified from x-ray spectra. The intermediate anneal spectra show how the compound VSi_2 forms first at the V/Si interface and expands towards the surface. The kinetics of the formation are discussed in the text.

For samples of V on SiO_2, we found no changes in V and in SiO_2 after 15 minutes at 600 and 700°C. Because the vanadium has a high affinity for oxygen at high temperatures, this is a very good indication of a low oxygen partial pressure in the He ambiant that was used in this study. Indeed we found that similar heat treatments that were carried out in poor vacuum (10^{-6} torr) resulted in the formation of vanadium oxides. However, above 800°C interaction occurred, and in a sample that had been treated at 900°C for 1 hour, both x-ray and backscattering showed the formation of V_3Si, V_5Si_3 and an oxide phase of V_2O_5. The backscattering spectra are shown in Figure 2 for three samples (from top to bottom): pure V on Si; V on SiO_2 annealed at 900°C - 30 min; and V on Si annealed at 900°C - 30 min. The schematic representatives on the right of the figure indicate the positions of the various layers. The x-ray pattern is shown in Fig. 3 where seven reflections have been indexed in accord with ASTM Diffraction Cards #19-1405 as V_3Si which has a β-tungsten structure with a lattice parameter of 4.725 Å. Reflections of V_5Si_3 and V_2O_5 have also been indexed. The backscattering spectra show the reacted sample to be a layered structure as shown in the upper corner of Fig. 3. The V_3Si layer forms next to the SiO_2, and the surface layer is a mixture of V_2O_5 and V_5Si_3. The spectra of the reacted V clearly shows two plateaus. The one occuring at low energy belongs to V_3Si; the other one to mixed V_2O_5 and V_5Si_3. The spectra of silicon and oxygen showed that both of them had reached the free surface. However, the most outstanding feature that we found from the backscattering is a reduction in the width of the oxygen spectrum of the SiO_2 layer after the reaction. It indicated

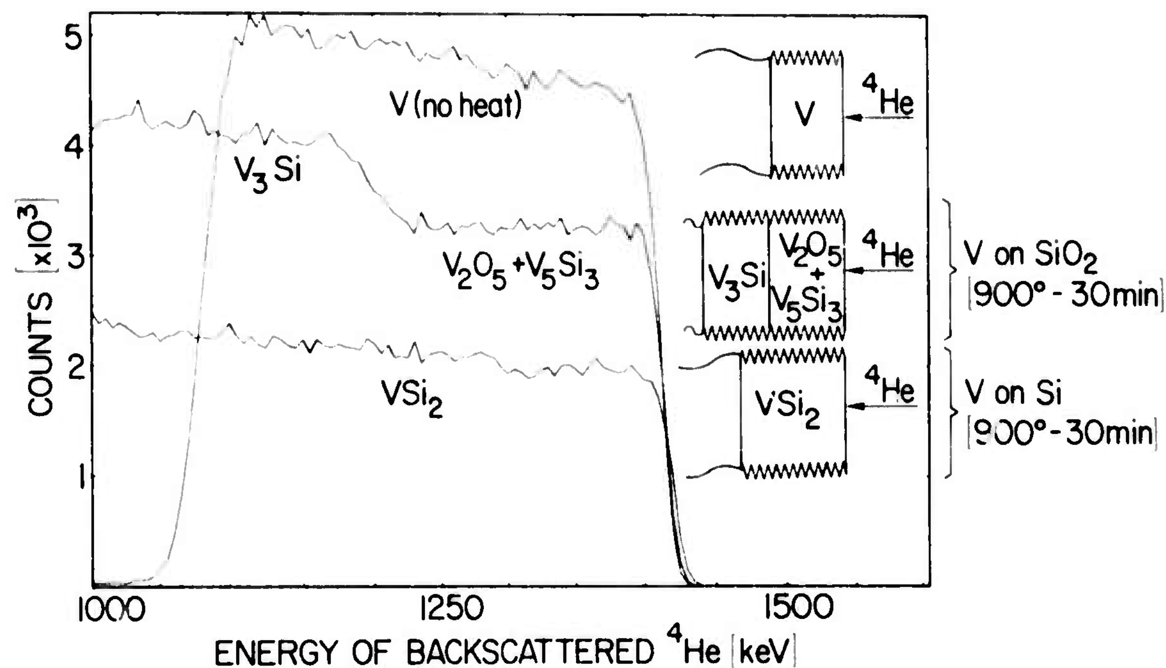

Figure 2

The central spectra shows the complex layer formation obtained after heat treatment of V on SiO_2. The upper curve shows a pure V peak for reference, and the lower curve indicates the level of VSi_2 shown also in Figure 1. The continuous superconducting layer of V_3Si was verified by x-ray analysis and transition temperature measurements as discussed in the text.

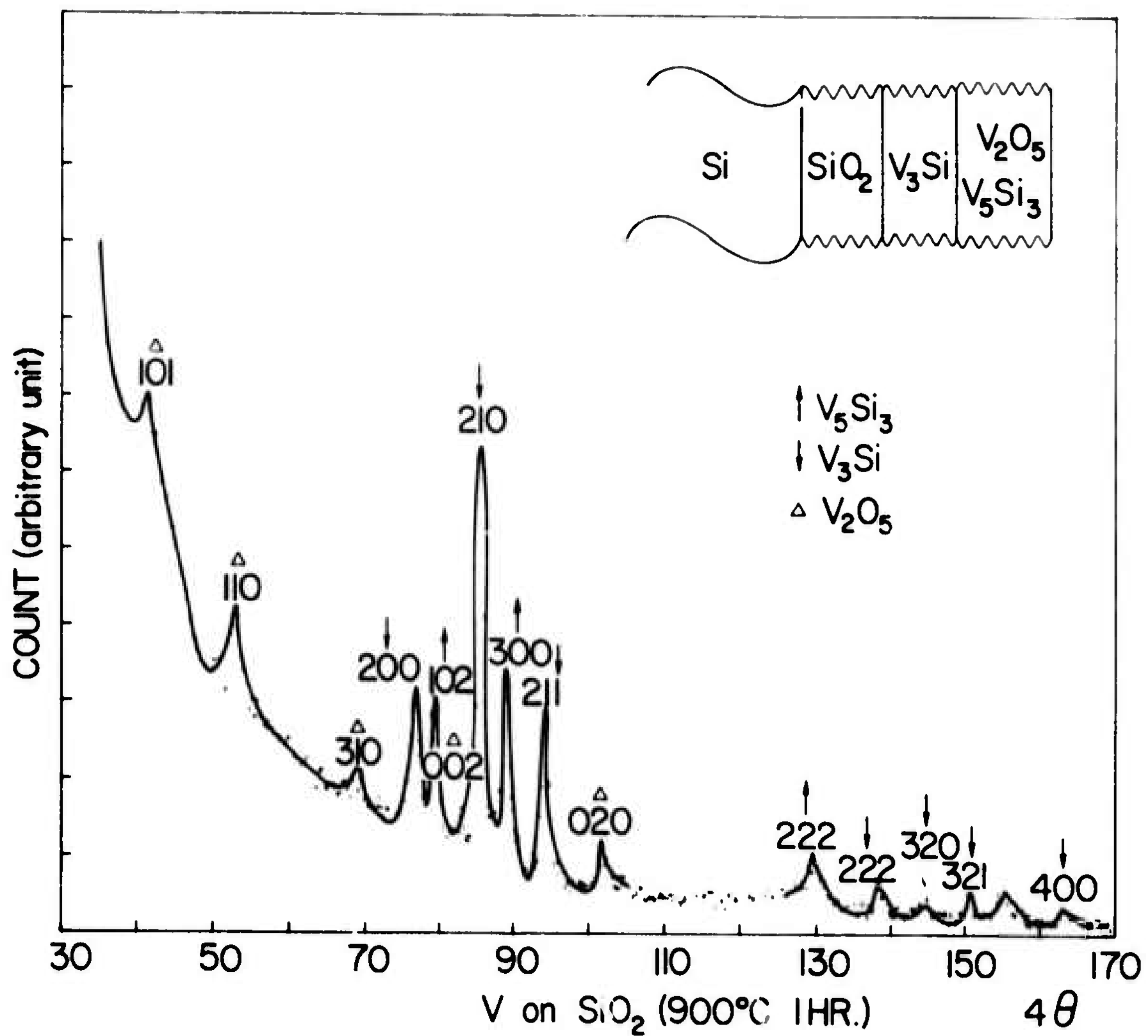

Figure 3
X-ray diffraction patterns of V/SiO_2 heat treated at 900°C for 60 minutes in an oxygen free furnace. Reflections of V_3Si, V_5Si_3 and V_2O_5 are observed.

that a portion of the SiO_2 layer has been decomposed and reacted with vanadium to form the oxide and silicides.

Besides x-ray and backscattering results, the formation V_3Si superconducting phase is also supported by the superconducting transition measurement. To obtain a transition temperature measurement of the V_3Si layer we found that the surface layer of mixed V_2O_5 and V_5Si_3 which cracked quite often can easily be peeled off by an adhesive tape to expose the V_3Si. A transition temperature of 13 to 15.2°K has been obtained from our samples using a two-point probe resistance measurement. The measured value compares favorably to that reported.[1]

There are three stable silicides in the V-Si system: VSi_2, V_5Si_3 and V_3Si. Even though we have observed all of them, they do not appear together in the same reactions. Our results show that the formation of a vanadium silicide whether it is silicon-rich or vanadium-rich seems to depend on whether we use a bare or oxidized wafer. With vanadium on a bare wafer, the silicon-rich silicide VSi_2 is produced. The formation of VSi_2 occurs alone and is stable without the companion of, or the conversion from, other silicides. According to Gibbs phase rule, we would expect at thermodynamic equilibrium state the coexistence of Si and VSi_2 in our samples of V on Si wafers. On the other hand, in order to reach the end state of VSi_2, the reaction may have recourse to the formation of other silicides if this happens to be energetically favorable. We recall that the formation of both PtSi and $HfSi_2$ by interdiffusion are good examples of having intermediate states.[4,5] Thus, depending on the nucleation and diffusion kinetics one silicide or another may form. In the present case, the VSi_2 alone seems

to form at a temperature above 600°C, nevertheless, whether the reaction at lower temperatures which is very slow, will be the same is not clear yet.

With V on an oxidized Si wafer, the vanadium-rich silicides V_3Si and V_5Si_3 are produced. It is possible that the Si needed to form the silicides can be depleted from the Si wafer by diffusion through the SiO_2 layer, however, we have found that the Si wafer remained unchanged after the reaction. Also it is possible that the oxygen needed to form the V_2O_5 can be supplied from the ambient rather than from decomposing SiO_2. However, we have shown that our furnace was almost oxygen free. Then because of the reduction of SiO_2 layer thickness, we conclude that the formation of the vanadium oxide and silicides is due to the interaction between the metal and the silica glass. The occurrance of the interaction requires that its total free energy change must be negative. A detailed calculation of the free energy change, for the present case, is not yet possible because we do not know the formation energy of the silicides. However, it is worthwhile pointing out that V_2O_5 is a more stable oxide than SiO_2, and this can be shown by comparing their formation energies.[9] Obviously, if a metal whose oxide is not as stable as SiO_2, most likely it will not be able to decompose SiO_2. So it seems that a metal which has high affinity to oxygen will be an essential criterian for it to react with silica. Furthermore, it helps if the metal also forms silicides.

Finally, the earlier work[1,2] of vanadium on vycor has reported a much lower temperature of forming V_3Si. This is probably due to the fact that thermally-grown SiO_2 film is a more pure and denser glassy material than

vycor silica, so that higher thermal energy is required in order to break the bonds in the film. To enhance the bond-breaking, besides the supply of thermal energy, the function of V or other impurities to act as a catalyst may be required. The details of the metal-glass interaction is far from understood yet. More work on phase identification, structural and morphological analyses, reaction rate and in particular the atomic motions of all elements involved are needed.

The authors are grateful to W. C. Kateley for the thin film deposition, H. F. Lazzari for heat treatment, W. Hammer for supervising the backscattering experiments, J. M. Viggiano and R. B. Laibowitz for critical temperature measurements, and J. W. Mayer for his stimulating and helpful discussions.

REFERENCES

1. F. J. Cadieu, G. R. Johnson and D. H. Douglass, J. of Low Temp. Phys., 6, 529 (1972).
2. J. H. P. Watson, P. A. Tick, R. M. Hawk and L. J. Neuringer, Bulletin of the Am. Phys. Soc., Ser. II, 18, 77 (1973).
3. R. W. Bower and J. W. Mayer, Appl. Phys. Letters, 20, 359 (1972).
4. H. Muta and D. Shinoda, J. Appl. PHys. 43, 2913 (1972).
5. C. J. Kircher, J. W. Mayer, K. N. Tu and J. F. Ziegler, Appl. Phys. Letters, 22, 81 (1973).
6. K. N. Tu and B. S. Berry, J. Appl. Phys. 43, 3283 (1972).
7. M-A. Nicolet, J. W. Mayer, and I. V. Mitchell, Science, 177, 841 (1972).
8. J. F. Ziegler, J. W. Mayer, C. J. Kircher and K. N. Tu (to be published in J. of Appl. Physics, Sep. 1973).
9. Handbook of Chemistry and Physics, 48th Edition (1967-1968), The Chemical Rubber Co.